UNDERSTANDING FORMATION AND EVOLUTION OF DUNE FIELDS BY SPATIAL MAPPING AND ANALYSIS: UPPER MUSKEGON RIVER VALLEY, MICHIGAN

Paul W. O'Malley

A Thesis

Submitted to the Graduate College of Bowling Green
State University in partial fulfillment of
the requirements for the degree of

MASTER OF SCIENCE

August 2019

Committee:

Peter Gorsevski, Advisor

James Evans

Jeffrey Snyder

ABSTRACT

Peter Gorsevski, Advisor

The morphology of vegetation-stabilized parabolic dunes has been seen as a source of climate information from their periods of stabilization. Several dune fields in the upper Muskegon River Valley in central Michigan, including fields not previously described in the literature, were mapped using Geographic Information System (GIS) based techniques. The mapping used terrain analyses, derived from a digital elevation model (DEM) and a Light Detection and Ranging (LiDAR) based terrain model in tandem with semi-automated based extraction followed by manual refinement of delineation and visualization techniques (VT). Terrain parameters and VT also guided digitization of dune crestlines. The morphology of the mapped dunes was characterized in terms of slope and aspect relationships, and comparisons were evaluated. Directional statistics were used to describe crestline orientations and circular variance. The morphology of these dune fields likely reflects a climate having an unequal bimodal wind regime, the dominant regime being northwesterly and the secondary regime being southerly or southwesterly. Based on visual interpretations, the location of downwind, compound parabolic forms are linked to locations likely to have had shallow groundwater, or to possibly suitable locations for parkland that could have induced precipitation ridges marking downwind dune field margins. Elongated dune forms are linked to rising terrain. Exploratory data analysis (EDA), primarily based on slope and aspect correlations, revealed a strongly asymmetric distribution in slopes of the fields, indicating the potential that a bimodal wind regime was present when the dunes stabilized. Cross-cutting relationships between dunes and terraces of the Muskegon River were observed which place formation of the dunes before the formation of

paleo-meanders by a forerunner to that stream. The planform and distribution of the dunes in the dune fields also appear closely tied to the changing groundwater availability.

TABLE OF CONTENTS

CHAPTER 1. INTRODUCTION

Parabolic aeolian dunes may be considered phenomena of margins which occur in two contexts, coastal and inland, when predominantly unidirectional wind regimes prevail (Anthonsen et al., 1996; Yan and Baas, 2015; Colgan et al., 2017). In the coastal context the margin is the water-to-land border where wave action is a control on the sediment supply required for the presence of dunes. Blowouts are the primary mode of dune formation (Yan and Baas, 2015). However, the focus in this study is inland dunes. An inland area with the potential for dune formation is one with a sediment source, persistent strong winds and a lack of vegetation (Greeley and Iversen, 1987). Sediment sources may be associated rivers which can deliver sediment, or they may be tied to glaciated terrain where sediment has been deposited, although other contexts are known (Rawling et al., 2008; Hugenholtz et al., 2009; Ewing and Kocurek, 2010; Warren, 2013; Fisher et al., 2019). The formation and reorganization of dunes and dune fields can occur in response to movement of the margins of climatic zones across the area (Barchyn and Hugenholtz, 2012a). For example, a change in moisture availability can affect the extent of vegetation cover on de-glaciated terrain. During dry periods sediment is exposed and barchan dunes can form from the now available sediment (Barchyn and Hugenholtz, 2013). The transition from barchan to parabolic types occurs as vegetation establishes itself on the barchan forms. This can occur with increases in moisture availability (Hugenholtz, 2010; Barchyn and Hugenholtz, 2012b).

The evolution of inland parabolic dunes from predecessor types is closely linked to the presence, character and growth rate of vegetation, the availability of sediment, the wind regime, and precipitation or water table levels relating to the availability of moisture (Barchyn and Hugenholtz, 2012c). In other words, a spectrum of climate-related factors and the responses thereto control change in a dune field (Yan and Baas, 2015). As a consequence, inland dunes are highly sensitive to changing climate conditions (Yan and Baas, 2015). Evidence recording the transition of inland dune fields from active to inactive states serves as an important proxy for the study of the character and timing of changes in regional climate (Campbell et al., 2011; Kilibarda and Blockland, 2011).

In the inland context, dominance by barchan and parabolic dune types may be considered the morphological end points of a dune field in active and stabilized states (Barchyn and Hugenholtz, 2012a). Barchan dunes have a crescentic planform with a slip face on the inside of the crescent. The dune apex is blunt and points upwind while the horns are relatively short and point downwind (Warren, 2013). Parabolic dunes have a planform with upwind pointing arms which extend from a downwind mound or apex (Hugenholtz et al., 2009). The transition from barchan to parabolic results from inversion of the barchan form forced by spreading vegetation (Fig. 1). This may start on the lee face of the outward tips of the horns of a barchan dune, with vegetation gradually extending inwardly along the lee side of the arms (Barchyn and Hugenholtz, 2012b). Because the center of the dune is migrating faster downwind than the ends of the horns, and because the wind regime is substantially unidirectional, or acute bimodal, the center of the dune continues to move downwind as the horns progressively stabilize, then become re-oriented into upwind pointing arms (Durán and Herrmann, 2006; Reitz et al., 2010; Goudie, 2011; Barchyn and Hugenholtz, 2012b; Yan and Baas, 2017). As a consequence of the reversal in horn orientation, steepened faces are left on the outside of the parabola. These faces are rotated both clockwise and counter clockwise relative to the predominant wind regime up to, and including, orientations orthogonal to the wind direction. The outward slopes are steepened with the initial slope gradient approaching or equaling slip face angles (Barchyn and Hugenholtz, 2012b).

Contemporary evidence, developed from areas such as the North American Great Plains, has tracked the transition of dunes of a dune field between active states characterized by dominance of barchan types (or barchanoid ridges) to stable states where the dune fields are dominated by parabolic types. The change between active and stable can occur on a decadal scale (Halfen and Johnson, 2013). Models developed from these fields may serve to inform evaluation of the fields which stabilized in earlier periods.

Several populations of inland dunes which have long been stable are located in the western Great Lakes Basin (Fisher et al., 2019). These fields tend to be comparatively low relief fields (< 10 m), often located near or on glacial outwash or glaciolacustrine plains inland from the modern Great Lakes (Rawling et al., 2008; Campbell et al., 2011; Kilibarda and Blockland, 2011; Arbogast et al., 2015). These dunes have some resemblance to the Great Plain dunes, including the presence of parabolic dunes, but have largely been dated to the late Pleistocene or early Holocene, leading to speculation about a possible association of their stabilization with the end of Younger Dryas (YD) cold reversal (Campbell et al., 2011; Arbogast et al., 2015; Colgan et al., 2017).

An important step to extracting information about the conditions under which inland parabolic dunes evolved is the quantitative characterization of the dunes in three dimensions (Hugenholtz and Barchyn, 2010). Geographic Information Systems (GIS) allows the convenient extension of analysis to expand to three dimensional models, primarily raster based elevation models (Mitasova et al., 2012; Miyasaka et al., 2016).

Dunes are a type of landform which, in the context of a GIS, consist of characteristic array of pattern, forms, size, scale, and shape of features (MacMillan and Shary, 2009; Warren, 2013). Defining various types of landforms in operational terms is essential to geomorphological mapping. Marking the limits of a landform is necessary for measurement of area or mean slope of the landform (Evans, 2012). An example of a landform definition was given by Evans (2012), who defined a mountain as a landform that exhibited a boundary of uniform altitude enclosing terrain having a highest point inclined by at least 10 degrees above every boundary point and exceeding twenty degrees for at least some boundary points. The highest elevation point must also exceed the boundary elevation by one thousand feet. A dune may be defined in an analogous fashion.

The recognition of aeolian dunes and their landform elements in a GIS requires a definition for the pertinent type of dune and enumeration of its land form elements which can be recognized from visualization techniques (VT) applied to an elevation model or terrain parameters derived from the elevation model (MacMillan and Shary, 2009; Wernette et al., 2018). A parabolic dune is defined in this study as a landform, usually characterized by the presence of a pair of elongated, upwardly-convex arms, which tend toward a mutually sub-parallel orientation and with slip faces rotated to the outside (Barchyn and Hugenholtz, 2012b). If one of the dune arms is not fully developed the dune may take on a hook-like planform. The area between the arms is a topographically lower zone, often open at the upwind end (Pye and Tsoar, 2009). An apex, if present, is a downwind mound marking a common junction of the arms (Pye, 1993). A crestline extends along the dunes arms and apex marking local points of maximum elevation across the arms and apex (Warren, 2013). The dune brinklines are a distinct slope break occurring at an elevation just below the crestline and located between the crestline and the slip faces of the dune (Warren, 2013). The arms tend to exhibit different slopes from the inside of the parabola compared to the outside of the parabola below the brinkline (Barchyn and Hugenholtz, 2012b). Toward the inside of the parabola, dune crests blend into relatively shallow slopes. As seen in Figure 1, the steeper, outwardly oriented slopes tend to be planar and to be set off by the brinkline from the ridge crests and a continuous base.

Some additional definitions specific to particular dunes include transgressive dunes, which are defined as dunes which form from sand sheets (Parteli et al., 2006). Simple parabolic dunes include lunate or hemicyclic, lobate, hairpin and highly elongate or windrift types (Pye, 1993). Lunate dunes are those with a length to width ration of less than 0.4. For hemicyclic types the same ratio falls between 0.4 and 1.0. In a lobate dune the arm length to width ratio ranges from 1 to 3. For elongate or hairpin type dunes the ratio exceeds 3 (Fig. 2). Windrift dunes may involve exceptionally elongated hairpin dunes where breached apices result in linear parallel or converging dunes. Some modifying terms specific to individual dunes are used in this study. One such term is a long-walled transgressive ridge. This refers to situations where sediment crosses pre-existing, typically partially-vegetated terrain (Pye, 1993). A precipitation ridge is a type of depositional ridge, one having a laterally extensive slip face associated with encounter with a forested area (Pye, 1993; Baas and Nield, 2007; Hesp, 2013). Elongated trailing ridges and precipitation ridges have been observed together in the Taranaki dunes of New Zealand (Hesp, 2013). Highly digitate and crenate morphology have been observed along active precipitation ridges (Hesp, 2013). Compound and complex dunes involve the coalescence of superimposition of two or more dunes (Kocurek and Ewing, 2005; Pye and Tsoar, 2009). Compound dunes incorporate dunes of the same type while complex dunes allow diverse types (Wolfe and David, 1997; Pye and Tsoar, 2009; Goudie, 2011). Once a field, or portion of a field, is largely stabilized complex swarms of dunes may occur including development of a crenate precipitation ridge which may be broken by sporadically spaced blowouts (Hesp, 2013). Complex dunes may exhibit evidence of interference between dunes and a variety of dune variants are described in the literature such as nested, en-echelon and digitate (Pye, 1993; Barchyn and Hugenholtz, 2012a).

In order to extract information from the geomorphologic features for the detection and delineation of dunes and dune fields, this research implements a set of techniques including VT, derivation of topographic parameters, and statistical analyses. There are several landform elements which can be tested for to confirm the character of dune fields. These include, a brinkline which exhibits a strong convex upward curvature; the orientation of the crest zone or brinkline; the dominant orientations of slopes as a function of slope angle; and, dune bases which exhibit a strong concave upward curvature along the outward face of the dunes and a weaker concave upward curvature along inward faces. VT should image the parabolic planforms and parallelism of the dune arms. Basic landform parameters should enable tighter identification of actual dunes. Exploratory data analysis (EDA) is used to understand different characteristics and relationships between geomorphologic features that describe dunes and dune fields. Classification is supported using VT.

This study applies a GIS approach, coupled with remote sensing (RS) derived data, to the study of the geomorphologic features of dunes from several dune fields in the upper Muskegon River Valley and the contexts in which the dunes stabilized. It is my contention that the dune types and the morphology of the dunes records effects from relative ground water levels and temporal variability in wind regimes. The study intends to accomplish the following objectives: (1) to identify the extent of the dune fields and to delineate individual dunes using digital elevation models; (2) to extract terrain parameters from inland dune fields and to compare the fields for similarities and dissimilarities using EDA; (3) to suggest the processes which acted on the dunes and controlled their evolution.

The first objective uses two different elevation models including a fine resolution 1 m model based on light detection and ranging (LiDAR) data and a coarser resolution 10 m digital elevation model (DEM) data from which terrain parameters are extracted. The elevation models are used to generate analytical hillshades, wind exposure index maps and normalized height index maps. The second objective is based primarily upon differentiation of the terrain parameters and association of the parameters with land form elements including graphical comparisons of topological parameter populations using EDA techniques. The parameter populations are primarily derived from the delineated dunes. The third objective will be addressed using a combination of VT, EDA and continuous wavelet analysis.

CHAPTER 2. STUDY AREA

The study area includes vegetation stabilized inland dunes and dune fields in to the Houghton Lake Basin (HLB) in north central Michigan (Schaetzl et al., 2013). The HLB lies within the Michigan High Plains. The Michigan High Plains are a relatively elevated, glacial interlobate area in the north central portion of Michigan's Lower Peninsula (Fig. 3). The Michigan High Plains are characterized by deep glacial deposits exceeding 200 m in depth and orgainized into moraines of thick sandy drift (Schaetzl et al., 2017). The HLB is dominated by a glaciolacustrine plain which lies between two of the moraines, the Cadillac Moraine to the west and the West Branch Moraine to the southeast. The HLB is likely the former lake bed of glacial Lake Roscommon. The HLB includes outwash surfaces, scattered relict deltas along former shorelines, swamps and modern Houghton Lake. It also includes a series of roughly parallel ridges, interpreted as ice contact ridges, which extend across the basin (Schaetzl et al., 2017). Among these ridges are the Lake City-Harrison Ridges (LHR). The ice contact ridges have northwesterly strikes and are broken in places by outwash gaps. The HLB is believed to become deglaciated relatively soon after the last glacial maximum (LGM) with the bordering moraines marking the margins of re-advances of the Laurentide Ice Sheet (LIS) which occurred to either side of the basin (Arbogast et al., 2015; Schaetzl et al., 2017).

The HLB is drained by the Muskegon River which originates at Houghton Lake and follows a generally southwesterly course to Lake Michigan. The portions of the HLB relevant to the dune fields are likely influenced by the history of the Muskegon River, particularly during the late Pleistocene and early Holocene (Arbogast et al., 2015). Four terraces (Fig. 4) have been identified in the shallow river valley of the upper reach of the river (Arbogast et al., 2008). Two of these (T-3 and T-4) form the outer valley. The T-4 terrace, which extends up to 1 km from the east side of the river underlies portions of the Rosco and Clare Dune Fields and thus predates the dunes (Arbogast et al., 2015). The T-3 terrace corresponds to paleomeanders which incised the T-4 surface. The T-3 terrace has been dated by radiocarbon means to 12,360 to 9500 calibrated ^{14}C YBP. The T-1 and T-2 terraces correspond to the modern river valley (Arbogast et al., 2008).

The study focuses on the Rosco Wolf (RW) complex, the Rosco Main (RM) complex and the Clare Dune Field (CDF). These dunes lie in the southwestern portion of the HLB or on the LHR. Grouping dunes as fields or complexes was based on several factors. Arbogast et al (2015) identified the Rosco Dune Field, describing it as being bisected by Wolf Creek. These two sections have been treated as distinct complexes in this study due to the systematically smaller size of the dunes north of Wolf Creek (the RW complex) and the distinctive morphology of the southern section (the RM complex). In addition, the two complexes are, at their closest points, at least 1 km displaced from one another, although this gap could the result of destruction of connecting dunes with the formation of Wolf Creek.

The CDF is not known to this researcher to have been previously described in the literature. Its dunes are tightly grouped and exhibit a largely coherent morphology. In this study the CDF is occasionally broken out into two sub-units. The northern part of the complex (Lower Clare) is located on the T-4 terrace while the dunes in the southern quarter of the field (Upper Clare) are located on the higher ground of the LHR. The LHR has a rugged surface with relief reaching tens of meters. In this study it was felt that the varying topography underlying Upper Clare might affect some morphological analyses.

Relatively scattered individual and small groups of dunes are located downstream from the study area dunes. These are referred to here as the Muskegon River Dunes (MRD) and are treated as a group here only as a matter of convenience. Some of the MRD are located on the T-4 terrace, but, more typically, they are located on higher ground well to the east of the Muskegon River. The dunes are located at distances from the modern river valley ranging from approximately 1 - 7.5 km. No reference to the MRD was found in the literature, and the full extent of the MRD was not determined. This study does not use these dunes for EDA, though some comparisons are drawn between these dunes and the primary fields on the basis of visual attributes of the dunes and comparisons of locations relative to the Muskegon River.

The combined RW and RM complexes cover about 10 km^2 and overlie the surface of the HLB. The HLB underlying the dunes consists primarily glacial outwash and postglacial alluvium (Arbogast et al., 2015; Luehmann, 2015). The CDF covers about 6 km^2 with Lower Clare overlying glacial outwash or wetlands, and Upper Clare overlying a mixture of coarse sand and cobble.

Arbogast et al. (2015) used optically stimulated luminescence (OSL) dating of samples taken from seven locations in RW and RM to determine ages ranging from 9700 - 13000 years for the field (Table 1, Fig. 5). On the basis of the OSL dates and substantially coeval dates from the previously mentioned ^{14}C dating, Arbogast et al., (2015) suggested the dunes and T-3 terraces were formed at the same time and, consequently, that it was unlikely that groundwater levels were a control on dune formation. The CDF has not been dated but is believed by one researcher to be similar in age to the broader Rosco Dune Field (personal communication – Arbogast, 16 October 2017). The dates are similar to dates attributed to other stabilized inland dune fields in Wisconsin (Rawling et al., 2008), northwest Indiana (Kilibarda and Blockland, 2011) and northwest Ohio (Campbell et al., 2011). Generally, the possible age range stretches from the Younger Dryas to 1500 years following the Younger Dryas (YD) (Fisher et al., 2019).

The ages of the dunes of the MRD are not known and linking any of them to the YD would be speculative.

CHAPTER 3. DATASETS AND METHODS

The methodology presented in this research employs two digital elevation models for generating topographic derivatives which are then used for the identification, characterization, analysis and comparison of likely dunes and dune fields. Targets are then qualified, or rejected, based on the definition. Initially, GIS based VT are used to locate targets. The VT are further applied to determine the extent of the prospective dune fields, to assess intra-field dune relationships and to evaluate dune field context presented by underlying and adjacent terrain. A blend of semi-automated and manual techniques are used to delineate of individual dunes. This involves using threshold qualification of landforms against normalized height or wind exposure indices, followed by visualization to evaluate those landforms against the definition set out above. Delineation of dunes from the landforms is refined using visualizations of curvature parameters, normalized height indices and topographical position indices. Lastly, the terrain parameters within the delineated dunes are generated and sampled for statistical analyses of the dune fields. EDA extends the study to the comparison of landform elements between and within the fields. The methodology workflow is shown in Figure 6.

3.1 DEM and LiDAR Datasets

The digital elevation models included one based on light detection and ranging data (the LiDAR dataset), and a second derived primarily from contour maps (the DEM dataset). The datasets are raster data structures. Raster data structures are two-dimensional, square-grid models where the cells of the grid are uniformly sized and are spatially-indexed along georeferenced *x*- and *y*-axes (Pike et al., 2009). The resolution is given in terms of the surface angle transected by a cell, or by the length measurement for a side of the cell (Pike et al., 2009). The z-value of each cell is an elevation referenced to mean sea level (Hengl and Evans, 2009; Pike et al., 2009).

The spatial resolutions of the datasets differ. The DEM dataset has a resolution of 1/3rd arc second (10 m) and a relative vertical accuracy of 1.6 m (Gesch et al., 2006). The resolution of the LiDAR dataset is 1 m with a vertical accuracy of 0.070 m with 95 % confidence. Both are referenced to the North American Vertical Datum of 1988. The datasets were constructed from tiles obtained from the National Elevation Dataset of the United States Geological Survey (USGS) (Table 2). Projection was based on the Universal Transverse Mercator (UTM) (Zone 16N) with horizontal coordinate information referenced to the North American Datum (NAD) of 1983. The datasets were pre-processed to remove sinks and peaks.

3.2 Terrain Derivatives

There are a number of terrain derivatives relating to the land surface morphology which can be generated from georeferenced land surface models without any additional knowledge of the area represented (Olaya, 2009). These include various terrain parameter models used to describe the surface geometries and other features of land surface forms or elements (Wilson, 2012). Other topographic indices that can be used to detect discrete land surface objects at different spatial scales (Weiss, 2001).

Basic terrain parameters for geomorphometric analysis such as slope, aspect and curvatures are the fundamental derivatives used in landform classification procedures (Olaya, 2009). The derivation of the basic terrain parameters is local, being based on a neighborhood around target cells, typically using a three-by-three moving window (Olaya, 2009; Gorsevski et al., 2016).

Landform classification is extended by generation of topographic indices such as the topographic position index (TPI), the multi-scale topographic position index (MSTPI) and the normalized height index (NHI). The TPI and NHI, as classes, broadly relate to terrain roughness. In this research, visualizations of derivatives including index rasters aided in the location of dune boundaries and in locating dune landform elements where determination of their location was obscured by other landforms such as moraines. The convergence index (CI) relates to relative flow convergence or divergence from a cell.

3.2.1 Basic Land-Surface Parameters

Slope is the maximum rate of change in elevation on a surface. It is expressed as an angle or as percent rise. Slope is directional, that is, it has an aspect. Aspect is the compass direction in which a slope faces. More technically, aspect is the flow line direction of a fluid moving under the influence of gravity over a surface (Olaya, 2009). Slope and aspect are first derivatives. They are estimated using algebraic functions applied to a neighborhood around an area of interest (Olaya, 2009; Wilson, 2012). The functions are applied over a window of cells, centered on a target cell in the raster. For slope and aspect, and most other local parameters, the window size is 3 x 3 cells (Olaya, 2009). Excluding border cells, the window is moved to successive target cells to generate a raster for each parameter of interest (Olaya, 2009; Wilson, 2012).

In relation to a land surface, curvatures are functions of the second derivative. They are continuous variables and, among other features, can represent rate of change in slope or aspect. The two most frequently used curvatures, plan and profile, are surface curvatures in planes perpendicular to and aligned with the direction of gravity, respectively (Olaya, 2009; Wilson, 2012). Curvatures may be convex or concave relative to a defined orientation of its plane. The meaning of these curvatures with respect to a raster cell is primarily related to fluid flow behavior through the cell. Convex and concave plan curvature indicates diverging or converging flow, respectively (Olaya, 2009).

Dune landform elements tend to exhibit particular profile curvatures (Smith and Clark, 2005). Crests and brinklines exhibit convex-upward profile, with brinklines tending to exhibit stronger convexity than dune crests. Brinklines mark upward bounds of slip faces. Dune bases, such as toes, are concave upward. Dune slip faces should exhibit a neutral profile curvature. Visualization of profile curvatures was used in refining the boundaries of dunes. Profile curvature was used to manually adjust dune boundaries, to digitize crests and, in combination with slopes, to identify slip faces. Profile curvature was also used to evaluate slip faces.

3.2.2 Topographic Indices

The CI relates to the degree of convergence or divergence of fluid flow over a surface. Slope, aspect and curvature terrain parameters are used for calculation of the CI which is also a basis of wetness indices. The usual scale is in radians/100m with ranges from -100 to 100 with -100 corresponding to a divergent area such as a ridge. A visualization of the CI was used in identifying dune crests (Olaya and Conrad, 2009).

The NHI relates to surface hydrology, it is an indicator of the relative slope position of a cell in a catchment (Böhner and Selige, 2006). It is similar to a wetness index. Use of the tool tends to smooth out highly local roughness. The primary use of the NHI in this study was to delineate dunes.

TPIs compare the elevation of a central cell to the average elevation for a neighborhood around the cell to produce an index value (Weiss, 2001). Positive index values indicate a cell elevation exceeds the mean elevation and negative values indicate the opposite (De Reu et al., 2013). TPIs are inherently scale dependent in that the index value for a cell depends upon the size of the neighborhood used for the calculation. Changes in neighborhood size reveal topographic features of different sizes (Weiss, 2001). MSTIPs combine TPIs calculated using different neighborhood sizes. The combination of indices allows for the better detection of nested landforms (Weiss, 2001). MSTIPs are an approach to dealing with the observation that no parameter generated using a moving window of a single fixed size will perfectly capture the wavelength of all landform features of interest (MacMillan and Shary, 2009)**.**

TPIs and MSTIPs have been commonly applied to landform classification, particularly in respect to measuring the sheltering effects of landscape, and have been used by biologists to identify habitats (Lindsay et al., 2015). They have been used for slope position classification among other applications (De Reu et al., 2013). MSTPIs are of interest here because changes in the scale of measurement reveal topographic features of different sizes (Weiss, 2001). In this study, an MSTPI was generated using three size scales, a minimum scale setting of 1 (i.e. a 1-cell radius around the target cell), a maximum scale setting of 8 (i.e. an 8-cell radius around the target cell) and a scale of intermediate size, in this study a 2-cell radius. The MSTPI served as an analogue to an adjustable band pass filter, mitigating noise at short landform spatial wavelengths and muting long spatial wavelengths in underlying terrain landforms. So applied, MSTPIs were effective in bringing out dune margins for a variety of dune sizes.

Land-surface parameters related to topo-climatology describe the influence of topography on climate. Topo-climatology parameters include wind exposition indices (WEI) and solar radiation indices (Böhner and Antonić, 2009). The WEI, used here for dune extraction, is based on terrain parameters including aspect, horizon angle and sky view factor, and indicates an average wind effect for all directions to generate a dimensionless index (Böhner and Antonić, 2009). The index is centered on 1, which is neutral, with smaller values indicating sheltered areas and larger values indicating exposure.

Statistical indices are used to measure surface roughness (Olaya, 2009). Among these, anisotropy indices such as the anisotropic coefficient of variation (ACV), indicate directionality of surface variation. In their stricter forms they are defined as the ratio of the minimum and maximum range parameter of spatial dependence. The index describes the general geometry of a local surface and can be useful in distinguishing elongated from relatively more oval land forms, for example ridges and hills (Olaya, 2009). In the present study, the ACV tool from the GRAS GIS was used to locate crestlines.

3.3 Visualizations

GIS provides a variety of VTs which may be applied to raster. This involves binning the attributes by using gray- or color-scale indices, and imaging the result for each location. Images for multiple DEMs may be combined by generating a raster with different gray- or color-scale index attributes and varying the weight assigned to each of the multiple attribute classes. Examples are given in Figure 7. In the first example the elevation data attributes are linked to a grayscale in a logical progression and imaging the result (Fig. 7A). In this grayscale image the darkest shade of gray is assigned to the lowest elevation attribute values and successively lighter gray colors are assigned to increasing elevations.

Another VT is the analytical-hillshades (Fig. 7B). Analytical-hillshades are a particularly common VT because they produce relief map like images of terrain that may be interpreted in the same manner as aerial photographs (Gorsevski et al., 2016; Bonaventura et al., 2017). The technique simulates light reflection and shading along landforms based on cell elevation, slope and aspect relative to the altitude and azimuth of a point light source (Horn, 1981). The altitude and azimuth from this light source are adjustable at the preference of the investigator, to differently highlight detail (Bonaventura et al., 2017). As intermediate steps in generating an analytical-hillshade, the slope and aspect for each cell must be derived from the DEM in order to determine the amount of reflectance from the cell and whether the cell is in shadow. Albedo is treated as a constant. The relative "sunniness" or “shadiness” for a cell is usually based on a scale of 1 to 100 (Olaya, 2009). Analytical-hillshades are commonly blended with other images. For example, color tinting is often used to enhance visualization of attributes, such as slope gradient. It is also commonly applied to images as an alternative to contour lines. When so used it is referred to as hypsometric tinting. An example of a hypsometric tinting blended with analytical-hillshading is shown in Figure 7(C).

An issue with analytical-hillshade images linked to the observer flexibility it provides is azimuth biasing. Azimuth biasing is the variation in detail revealed with changes in position of the illumination source. Choice of illumination source position is illustrated in Figure 8. In Figures 8A and 8B the illumination source is positioned first at an azimuth of 315° followed by placement at 45°. The subject is a barchan dune located west of the CDF. The northern horn of the dune appears to vary in length depending upon the choice of azimuth, even with elevation and exaggeration left unchanged. Such changes in perception make the use of at least two azimuths for the illumination source a recommended practice (Smith and Clark, 2005).

Pseudo 3-D visualizations are an enhancement of analytical-hillshades based on orthographic projections of the hillshades. This allows for changes in the viewer’s observational position relative to the imaged surface. A local relief model (LRM) is a VT which provides for removing potentially obscuring effects of a base land surface layer from elements characterized by more abrupt shifts in elevation. Its usual application is to bring out archeological sites in an analytical-hillshade relative to background terrain (Novák, 2014). In its simplest form, an LRM is implemented by applying a low pass filter to a raster-based elevation model to produce a smoothed elevation model. The smoothed elevation model is then subtracted from the original model to produce a difference model. The difference model is visualized using an analytical-hillshade to produce an image which emphasizes fine detail relative to the original model. The variant implemented in the LRM Toolbox for ArcGIS refines the process with additional steps. These include generation of a “flat terrain” digital elevation model where cell attributes are the difference between an expected terrain elevation and the real elevation (Novák, 2014). The tool was used in an attempt to subdue the LHR in imaging the Upper Clare unit.

3.4 Extraction of Dunes and their Elements

The delineation of dunes and dune crestlines included semi-automated extraction of possible dune forms using terrain indices followed by boundary refinement based on manual digitization guided by VT applied to terrain indices and analytical hillshades. Visualization of basic terrain parameters was particularly applied to identify crests and to locate lee slopes (Evans, 2012; Bernhardson and Alexanderson, 2017).

The preliminary extraction of prospective dunes was partly based on automated thresholding. The WEI was used for delineating potential dunes from the DEM dataset. After generation of a WEI raster, a threshold value of 1.01 was used to generate a bifurcated categorization of the raster. The value was selected based on trial-and-error and on the need for dunes to correspond to closed polygons. Areas meeting the threshold were converted to polygons. Polygons too small to check for conformance to the planform parts of the GIS oriented dune definition were then eliminated. The remaining polygons were manually inspected for shape and orientation. Once a polygon was accepted as corresponding to a dune, it was superimposed as a bounded transparent image on visualizations of analytical-hillshades, and other terrain parameters, for manual re-digitization of its boundaries.

A similar approach was used with the LiDAR dataset. Here a NHI was used, as computing an NHI was less computationally intensive. The NHI was selected as it should be sensitive to upward convexity. In an NHI raster the attribute values are scale values from 0 to 1. Minimum index threshold values of 0.52 to 0.60 were used to divide the raster between cells potentially corresponding to dunes, and those which did not. A minimum value of 0.51 was required to produce closed polygons in the upper part of the scale. The precise threshold was adjusted by trial-and-error to produce polygons reflecting parabolic shapes. Again areas meeting the threshold were converted to polygons that corresponded to possible dunes. To validate and improve delineated dune boundaries, the polygons were manually adjusted using VT for better correspondence to dune landforms. The adjustment of dune boundaries included different VT including hillshades and various terrain parameters such as curvatures, an MSTPI and an NHI. For example, imaging the MSTPI raster produced moat like zones (areas of negative index values) that bordered dunes. Refinement of dune shapefile boundaries almost invariably resulted in their outward displacement, and the delineation of additional dunes.

The delineation of crestlines as polylines used manual digitization based on visualization of analytical-hillshades, hypsometrically-tinted elevation maps, profile curvatures, ACV indices, and proximity to slopes exceeding minimum gradients based on the LiDAR dataset. Profile curvatures are strongly convex along brinklines which parallel dune crests and separate the crests from steep slip faces. Elevations are at a maximum along the crestline. The orientation of crestlines is used to identify the principal direction of the wind. A high proportion of crestlines for parabolic dunes are aligned with the wind which predominates at the time of stabilization. Identification of a brinkline was usually required before a crestline was drawn. This requirement was relaxed in a few cases of small dunes in the RW complex. Crestlines were drawn to parallel the line of maximum convex profile curvature.

3.5 Applications of Terrain Parameters

Terrain parameters were generated from the raster-based DEM and LiDAR datasets using SAGA, ArcGIS, and GRASS GIS software. The terrain parameters included, aspect, slope, convergence index, cross sectional curvature, longitudinal curvature, plan curvature, profile curvature, normalized height index, topological position index, multi-scale topological position index, topological wetness index, and wind exposure index. Random sampling for the statistical analysis was implemented only on the LiDAR dataset, while whole populations were used with respect to the DEM dataset. From the LiDAR dataset a total of 34,275 sample points were taken from the CDF, RM and RW using stratified sampling. For this purpose, the divisions of the study area were RM, RW with the CDF being divided into two complexes, Lower and Upper Clare, based on whether a dune was on the LHR or not. The same percentage of points (0.5 %) was sampled within each division resulting in the number of points sampled being 5,262 for Lower Clare, 3,903 for Upper Clare, 19,942 for RM and 5,168 for RW.

Analysis and comparisons of dune fields were extended using EDA implemented in R-CRAN software. The EDA implemented with elevation model derivatives for the DEM dataset included probability density plots by field for elevation, slope, vertical distance to channel network among other parameters; density plots for the same variables by aspect and field; elevation and slope histograms by field; scatterplots comparing various combinations of parameters within fields; and rose diagrams for evaluating aspects of different slope categories. For the LiDAR dataset, EDA was substantially limited to slope and aspect relationships. Rose diagrams were plotted for exploration of the relationship between slopes and aspects.

Additionally, wavelet analysis and scatterplots were used to investigate the possibility that bedform wavelengths were present in the dune fields or landform elements recurred periodically. Wavelet analysis allows the identification of underlying spatial frequency information (cycles/meter), even where this spatial signal has a short length (Torrence and Compo, 1998; Wu et al., 2018). Such would be the case in a small dune field. Terrain parameter and elevation profiles were sampled systematically at 1 m or 10 m intervals, depending upon the resolution of the dataset. The Morlet wavelet was used as the wavelet input. Among the possible signals recovered involved elevation and terrain parameter change along transects in the RM complex. These transects were orthogonal to the direction of elongation of several sub-parallel dunes. Another possible signal involved changes in aspect along a dune slip face in the CDF. The output of the analyses is graphical, with distance displayed along the horizontal axis and period/wavelength displayed along the vertical axis. Wavelet coherence occurs where two distance series co-vary.

3.6 Ground Reconnaissance

The CDF, RW and RM complexes were physically scouted to evaluate that landforms identified as dunes from the DEM dataset. Evaluation included determination of the constituent material of the candidate landforms and comparison of the constituent material with the material of the underlying layers. The CDF and RM complex were observed to have been impacted by recreational use with numerous trails for dune vehicles and snow mobiles being present, although portions of the Lower Clare, particularly its eastern parts, were undisturbed, particularly where the dunes overlay wetlands. The small portion of the RW complex visited was less impacted by these activities than the other fields. At no location visited were candidate dunes found to be made of anything other than sorted sand. The terrain underlying the Upper Clare was found to consist of a mixture of cobble and sand.

CHAPTER 4. RESULTS

The study evaluates the various visualizations, the results of ground reconnaissance, and the characteristics of the terrain parameters to, among other things, isolate dunes from other possible landforms, as might be present in a de-glaciated area. For example, ridges can be formed by eskers or moraines (Sjogren et al., 2002). These features can usually be distinguished by observation of the sediment constituting the landform. Other, sandy formations, such as beach ridges, could be left along strand lines of pro-glacial lakes (Fisher, 2005; Fisher et al., 2015). Shore line features can be expected exhibit smooth planforms and to roughly follow elevation contours. The possible existence of a pro-glacial lake in the HLB raised the possibility of relic deltas in the area (Evans and Clark, 2011; Schaetzl et al., 2017).

4.1 Descriptions of the Dune Fields

Descriptions of the RW complex, the RM complex, the CDF and the MRD are based on visualization. The images are primarily blends of analytical-hillshades and hypsometrically-tinted elevation images derived from the LiDAR dataset.

4.1.1 Visualization of the Rosco-Wolf Complex

Visualizations of the RW complex are reproduced in plan view in Figure 9. The eastern portion of the complex overlays a wetland “A”, which has an elevation of just under 340 m. The wetland is visible in recent aerial views (Google Earth image date 6 May 2018), with the southern portion of the wetland being substantially open, with sparse bushes and exposed mud with mudcracks. The northern portion is more densely bush covered. A ridge like form “B”, which may be combination of a windrift dune (forming the western and center portions) and an arm of a parabolic dune (forming the eastern end), extends approximately 1200 m from the

WNW to the ESE through the center of Fig. 9. The easternmost portion of the ridge rests on the western portion of the wetland “A”. Relief along the ridge generally ranges from about 2 - 4 m.

Ridge “B” separates terrain to its south, which has a base elevation of approximately 340 m, from terrain to the north which, excluding the wetland and small dunes, has an elevation of about 341 m. Likely parabolic dunes “C” to the south of the eastern half of the ridge “B” include several well-formed V-shaped hairpin types which are among the largest dunes of the RW complex as seen in Fig. 9. The arms of these dunes are on the scale of 100s of meters. Mean relief, based on sampling of 22 points, is 3.1 +/- 0.6 m. Arm to arm widths of dunes approach 100 m, making most of the dunes hairpin parabolas. Apices of the easternmost dunes “C” are superimposed on wetland “A”. A stream course “D”, which borders the southeast margin of the parabolic dune group “C” appears to have been bisected “E” by one dune of this group. Lobate type dunes, and possible lunate and hemicyclic dunes, occur at the western margin of group “C” adjacent a possible deflation plain “F”. The areas between the arms of the larger dunes of group “C” are depressed relative to prevailing terrain elevations. At their deepest, the elevations are about 1.5 m below prevailing basal terrain to the east and west. These are likely intra-dune deflation zones.

The RW complex includes other, less prominent dunes. There is a likely dune formation “I” to the southeast of stream “D”. In addition, possible dunes “G” are located to the northwest of the central ridge “B” (Fig. 9A). These dunes are comparatively small, with the dominant dune type being a simple lobate parabolic form. The dunes range from about 60 -160 m in length and from 20 – 40 m in width qualifying the dunes as hairpin types. Dune relief averages 1.2 +/- 0.4 m based on eight samples. These dunes rest on the relatively higher ground compared with other dunes in the RW complex and are fairly densely packed across as area extending about 800 m northward from the ridge “B”. The northwest margin of these dunes terminates along a contour having an elevation of approximately 339.8 m, an elevation which the bases of the dunes never fall below. This contour marks a smooth, shallow indentation in the dunes and corresponds to an abrupt drop in prevailing terrain elevation from approximately 341 m to 338.5 m. This feature is interpreted as a beach ridge. Contemporary aerial photography (Google Earth image, 6 May 2018) suggests the low lying area, designated “H” in Fig. 9A, may be a contemporary wetland. The surface of area “H” likely marks or is near the position of the water table.

4.1.2 Visualization of the Rosco-Main Complex

Most dunes of the RM complex (Fig. 10) are located in two major lobes, a more northerly lobe “B” and a southwesterly lobe “C”. There are a handful of small, possible dunes “G” located about 1 km to the east of the extreme eastern margin of lobe “B”. Some relation between these dunes and the rest of the RM complex is suggested by their orientation and likely downwind location relative to the main body of the RM complex.

Lobe “B” covers a generally crescentic area and lies to the east of a plain “A”. Lobe “B” is open to the west and has an eastern margin following a nearly continuous, irregular, semi-circular ridge “H”. Ridge “H” appears, in places, to comprise parabolic dune apices, dune arms and possible precipitation ridges based on its crenulated character. The breadth of lobe “B”, measured along strikes parallel to dune arms, ranges from 1.2 km in the north, to 2.2 km in the center, and back to 1.5 km in the south. The western portion of lobe “B” is located on the T-4 terrace, the eastern portion extends onto uplands “E” above the terrace. Plain “A”, which is adjacent the eastern margin of the modern Muskegon River Valley, is the location of a possible deflation plain and source of sediment for the formation of lobe “B”. Generally, terrain elevation underneath lobe “B” rises from west to east, with the net increase being about 2 m. However, increases in elevation are uneven from east to west. Most of the increase in base elevation occurs in the western part of lobe “B”, but ceases from between 500 to 1000 m west of ridge “H”. Lobe “B” seems comprised of dunes which climbed the transition from the T-4 terrace to surrounding uplands. A trend toward increasing elevation resumes about 500 m west of the onset of the “G” dunes, which lie on terrain approximately 0.5 - 1.0 m higher than the elevation of land at the base of ridge “H”.

Visually, lobe “B” is dominated by elongated ridges “F”. These ridges generally exceed 1 km in length. They extend from the hypothesized deflation plain A to ridge “H”. The elongated ridges “F” have a roughly WNW strike, with the more northerly ridges being noticeably parallel and exhibiting fairly even ridge-to-ridge (150 to 190 m) spacing. To the south, the ridges are less regularly spaced and less obviously parallel. Relief along the elongated ridges “F” can vary from about 1.0 - 6.0 m and the ridges resemble windrift dunes. At their western ends, the elongated ridges “F” tend to terminate along the western margin of a shallow depression, which lies between the deflation plain “A” and uplands “E”. From west to east the ridges extend through the depression, which varies between about 250 to 350 m in width and which has a maximum depth of about 1.5 m. The depressed area may correspond to deflation basins which formed between the arms of dunes in transition from barchan to parabolic forms. The depths exhibited of these possible deflation basins might then have been limited by the water table. The western ends of some of the elongated dunes are tapered, while others appear to be sequences of small parabolic dunes. Relief in the RM complex averages 3.5 +/- 0.5 m, based on 43 samples.

Lobe “C” of the RM complex is more compact than lobe “B” and includes a possible complex dune. Lobe “C” is located on the T-4 terrace and is bounded roughly between the modern Muskegon River Valley on the west, wetlands to the south and southeast, deflation plain

"A" to the north, and lobe "B" to the northeast. A few apices of lobe "C" extend onto the wetland "D". Much of the lobe may be characterized as compound and includes several instances of recognizably parabolic forms superimposed on one another. The western ends "I" of several dune arms appear to have been crosscut during formation of the T-2 and T-3 terraces, suggesting the field once extended farther to the west. This strongly suggests that the paleomeanders of the T-3 terrace postdate formation of this lobe and open the possibility that the sediment source for the lobe, another deflation plain, was destroyed by later evolution of the Muskegon River.

4.1.3 Visualization of the Clare Dune Field

In Figure 11, the CDF is identified as including two sub-units, a Lower Clare sub-unit "B" which rests on the T-4 terrace, and an Upper Clare sub-unit "C", which overlays the LHR "D". The Lower Clare sub-unit is generally to the east or north of a possible deflation plain "A". Base elevations for the Upper Clare dunes are up to 20 m higher than for dunes on the T-4 terrace. The CDF superficially appears to be organized in a dendritic-like pattern, balanced across an east-west axis. Several features can be interpreted as instances of dunes superimposed on other dunes. This results in a series of possible compound dunes arranged across the field's east-west axis. The field as a whole covers an area having the shape of a rough half-oval, pointing to the east and open to the west. Relief for the dunes of the CDF averages 4.3 +/- 0.7 m based on 37 samples. Maximum relief reaches 10.4 m.

In general, the Lower Clare sub-unit is comprised of U-shaped parabolic dunes. Although dune lengths often exceed 0.5 km, widths are on often of a scale of 200-300 m. The dunes are mostly lobate types rather than hairpin types. The northern, eastern and southern margins of the CDF are marked by a continuous line of dune ridges, similar to the margin of the RM Complex but more continuous and regular. The north-eastern and eastern margins of the Lower Clare sub-unit of the CDF is a generally continuous ridge, comprising arms and apices of distinguishable parabolic dunes. The northwest margin of the CDF appears to have been crosscut by T-3 terraces of the Muskegon River although, in contrast to the RM complex, only one or two dune arms are crosscut by the terraces. Still, unlike the rest of the CDF, nothing of the T-4 terrace is available as a deflation plain to supply sediment for this portion of the CDF.

An isolated barchan dune “G” is located 2 km to the west of these crosscuts, across the modern river valley. This dune was imaged in two analytical-hillshade images previously introduced in Figure 8. The barchan dune is a possible remnant of CDF from an earlier state. The presence of a broad plain to the west of the barchan dune (3.8 km) could have been part of the sediment source for the CDF. It is likely that portions of the T-4 terrace were once located between this dune and the lower Clare sub-unit. The morphology of the barchan dune may support the existence of a bimodal wind regime in the area. The northern horn of this dune is distinctly longer than the southern horn (Fig. 8A), a development which has been linked to bi-modal wind regimes. Models suggest that the side of the barchan dune opposite to the secondary wind elongates. However, such an elongated horn can also result from an off-center collision of two barchan dunes (Parteli et al., 2013). Any significance of asymmetry in the barchan dune, in so far as it relates to the wind regime, also depends on the dune having been active at the same time that the CDF was active.

The southern quarter or Upper Clare sub-unit “E” of the CDF has climbed onto the LHR and includes dune ridges extending up to 3 km across the area. Base elevations for the Upper Clare dunes are up to 20 m higher than on the T-4 terrace underlying the Lower Clare sub-unit. The specific forms of the dunes are not as readily distinguishable here as in the lower sub-unit, though parabolic dunes are still recognizable.

4.1.4 Possible Residual Dune Ridges of the Clare Dune Field

Residual dune ridges (RDRs) mark the former back base lines of dune stoss slopes, as shown in the cartoon in Fig. 12A, and can be used to track progressive locations of a migrating dune (Wolfe and Hugenholtz, 2009). They tend to be straight or concave downwind, and to exhibit an even height along their crests of 0.3-1.0 m. (David et al., 1999; Wolfe and Hugenholtz, 2009). They develop when dune migration is interrupted by ground water levels rising to, or above, the surface (Levin et al., 2009). They are thought to reflect brief climate fluctuations and to track interruptions in the advance of a dune downwind (David et al., 1999). A ridge “I”, possibly part of one extant dune, or formed from one or more former parabolic dune arms, crosses wetlands “E” in the vicinity of Rice Pond and marks the northeast margin of the CDF (Fig. 12B). Visible to the southwest of this feature are a series of low relief landforms “H” suggestive of RDRs. Identification of the low relief features “H” as RDRs is supported by the base elevation to the southwest of ridge “I” being the same as it is in the wetlands to the northeast. Any temporary increase in groundwater level within the present area of the CDF during its formation would have appeared first here. Most of the features identified as prospective RDRs are approximately 0.4 m in height, which is fairly consistent along their lengths. However, the features do not unambiguously connect arms across a parabolic dunes, but appear to roughly conform to the interior shape of ridge “I”.

4.1.5 Visualization of the Muskegon River Dunes

The MRD were observed using an analytical-hillshade developed from the LiDAR dataset. These landforms were not visited and their identification as dunes is tentative. The numerous parabolic and elongate forms observed in the MRD resemble the Fair Oaks Dunes of northwest Indiana (Kilibarda and Blockland, 2011) although there is a seeming tendency for landform shape to vary with elevation. The landforms of the MRD are imaged in Figure 13 in a blending of hypsometric tinting and analytical-hillshade visualizations. Although the MRD fall outside the study area, and outside the area covered by the DEM dataset, some association of these dunes with the Muskegon River seems likely. The MRD are scattered in distribution, compared to the RW complex, the RM complex and the CDF. Relief for the MRD, based on haphazard sampling, generally ranges from 2-3 m, making them more subdued than the RM complex and the CDF and only about one-half to one-third the height of the Fair Oaks Dunes (Kilibarda and Blockland, 2011). The landform group labeled “A”, those closest to the river, include several lunate and hemicyclic parabolas, with some superimposition of dunes. Moving inland, the landforms trend toward lobate forms in Group “B”, and finally elongate forms in Group “C” at the highest elevations. At least one elongate form from Group “C” is 2 km in length. The dunes of groups “B” and “C” are located in a band ranging from 2.0-7.5 km from the modern river valley. The band parallels the river, extending southwesterly from the CDF to at least the limit of the LiDAR dataset coverage, a distance of over 10 km.

4.2 Characteristics of and Comparisons between the Dune Fields

4.2.1 Differences in Dune Delineation based on Dataset

The spatial differences in dune delineation for RM, RW and the CDF, resulting from the two datasets, are illustrated in Figures 14, 15 and 16. Here the polygons developed from the LiDAR and DEM datasets have been overlayed. It was expected that polygons derived from the DEM dataset would be largely contained within polygons derived from the LiDAR dataset. This appears to be the case with the RM and RW complexes. For the CDF, the dunes delineated using the DEM dataset appear shifted to the west relative to dunes delineated from the LiDAR dataset.

Road cuts through the RM complex are seen as aligned breaks in the dune polygons running north to south.

4.2.2 Descriptive Statistics

The dune areas extracted from the CDF, RW, and RM complexes were estimated from the areas of the polygons (Table 3). For the DEM dataset, the dune areas in the RW complex, the RM complex and the CDF were approximately 482,000 m^2, 1,417,000 m^2 and 1,893,000 m^2, respectively. For the LiDAR dataset, the comparable values were 1,031,500 m^2, 2,966,100 m^2 and 1,907,700 m^2, respectively. The areas generated using the LiDAR dataset increased substantially for the RW and RM complexes. However, the change in measured areas for the dunes of the CDF is almost negligible. The polygons developed from the LiDAR dataset overlapped 70.9 %, 64.3 % and 54.3 %, respectively, of the RW, RM and CDF dune polygons developed from the DEM dataset. The areas measured for the RW and RM complexes using the LiDAR dataset are almost certainly more accurate. Visualizations based on the finer on the finer data clearly revealed dunes in the RW and RM complexes not visible from visualization of the coarser dataset. Accordingly, the discussion of analyses of the fields based on terrain parameters is presented with reference to the LiDAR dataset. A comparison of results from the two datasets is set aside in a separate section.

The data of Table 3 shows that the RM complex exhibits somewhat greater relief and steeper slopes than the RW complex. This result may be attributable, in whole or in part, to the influence of the dunes of group “G” in the RW complex (Fig. 9). The CDF, though, exhibited much greater relief than the other two fields, and both average and median slopes of the CDF were steeper.

4.2.3 Crestlines

The main characteristics of the crestlines delineated from the LiDAR dataset are shown in Table 4. The measured lengths of the crests total over 25 km for each of the CDF and RM complex and close to 17 km for RW complex. For the RM complex, the mean and median lengths of crest segments, as well as the 25^{th} and 75^{th} percentile cutoffs, are noticeably longer than for the other two fields. Figure 17 illustrates crestlines for the RW complex, RM complex, and the CDF using density heat maps to show inter-crestline proximity. Density is calculated in units of length per unit of area. The RW complex and the CDF have substantially higher densities than the RM complex. This is consistent with the relative compactness of the RW complex and the CDF compared to the extended, sub-parallel ridges of the RM complex. The RW complex also has a number of small, simple parabolic dunes which are fairly tightly packed (Fig. 17A). Mean and median orientations fall in the east-south-east sector for all three fields. For the RM complex, essentially half the crest orientations fall in the range of 90° - 160° range, and there is less variance than for the CDF or RW complex.

4.2.4 Exploratory Data Analysis

Further characterization of the dune fields is based on terrain derivatives. The Table 3 data shows that slopes in the CDF are steeper than for other fields. The table also points to a broader distribution of slopes in the CDF, particularly of steeper slopes. Boxplot analyses of the distribution of dune slopes by aspect category produced distinctly asymmetric results for all four divisions of the study area (Fig. 18). For all four divisions, slopes with northeasterly aspects were, on average, steeper than slopes having other aspects. These slopes also tended to exhibit a broader range of values. Excluding the RM complex, slopes with easterly aspects also tended to be relatively steep and the range of slopes exhibited tended to be broad. The RM complex may have lacked differentiation in slopes with easterly aspects due to the prevalence of elongated dune forms oriented along east-southeasterly strikes and a relative lack of parabolic dune apices. For all four divisions, slope steepness distribution was, for northwesterly, westerly, and southwesterly aspects, relatively tight and the median steepness tended to be relatively shallow. Based on the expectation that upwind slopes would tend to be shallow, this is consistent with a prior assessment that the prevailing winds at the time the dunes stabilized were westerlies (Arbogast et al., 2015).

Slope/aspect relationships are further explored in Figure 19, which are rose diagrams allowing analysis of the number of slope sample points falling into each of 36 aspect categories. The slopes are categorized into four classes by steepness including: (1) < 50th percentile; (2) the 50 - 75th percentile; (3) the 75 - 90th percentile; and (4) > 90th percentile. For the RW complex (A) the slope percent rise thresholds were set to 7.35 %, 11.98 % and 17.69 %. For the RM complex (B) the slope percent rise thresholds were set to 8.41 %, 12.86 % and 18.74 % for the LiDAR dataset. For the CDF (C) the slope rise percent thresholds were set to 10.58 %, 15.75 % and 22.98 %. The slope percent rise, or angle of repose, for slip faces on active dune generally exceed 57 % (34°), though slip face percentage rise may be somewhat shallower under certain wind conditions (Mitasova et al., 2005; Pelletier et al., 2015). The thresholds used in this study allow for the shallowing of the dune faces due to weathering (Hansen et al., 2009), while covering an extent of the dunes that should approximate slip face area as a percentage of total dune area. This study treats the steepest category of slopes as former avalanche or slip faces.

In general, slopes tended to have southwesterly or northeasterly aspects, with southwesterly aspects being the more dominant. With increasing slope steepness, aspect trends to shift to northeast. For the steepest 10 % of slopes, aspect is almost exclusively northeasterly. The distribution of slopes by aspect were comparable for the RW and RM complexes. However, the CDF exhibited a stronger tendency for slopes of the two steepest categories to have northeast aspects than reflected in the RW and RM complexes. The tendency of slopes of parabolic dunes to be oriented to the southwest or northeast is consistent with an assessment that the primary wind regime was west northwesterly. Most slopes are located along the arms of the dunes and have orientations orthogonal to the primary wind direction. However, the bias in the orientation of the steepest slopes toward the northeast is not explained by this observation. A unidirectional wind regime should produce an equal distribution of rotated slip faces in the two orthogonal directions.

There are other differences between the fields. For example, the distribution of the steepest category of slopes is rotated to the northeast for the CDF, compared to the RM and RW complexes. In the CDF, virtually all of the slopes of the steepest category have northerly or northeasterly aspects. The RW complex exhibits a larger proportion of southerly aspects among the steepest slopes than the other fields.

The spatial placement of the slopes in the dune fields is considered in Figures 20, 21 and 22. The steepest slopes (shown in red) tend to be located on the northern faces of northern arms of parabolic dunes, on the eastern faces of parabolic dune apices, or on the northerly faces of the elongated ridges of the RW complex. The mean aspect of the steepest class of slopes in the RW complex is 62° with a circular variance of 0.62. The mean aspect of the steepest class of slopes in the RM complex is 48° with a circular variance of 0.49. The mean aspect of the steepest class of slopes in the CDF is 41° with a circular variance of 0.30. The relatively tight variance for the CDF compared to the RM and RW complexes is a product of the absence of steep slopes with southerly and southwesterly aspects.

Rotated slip faces should exhibit a planar slope unless eroded. This was evaluated in Figure 23 by filtering the steepest slope category for each field for profile curvature. A profile curvature index value of between -0.02 and +0.02 was taken as a proxy for a constant or planar slope. The CDF was broken into its Lower and Upper Clare components. A higher slope threshold was used for Upper Clare than with Lower Clare to allow for the possibility that the rougher terrain had distorted the profile of the steepest slopes.

For the RW (Fig. 23A) and RM complexes (Fig. 23B), the steepest category of slopes have a mixture of profile curvature indices. The proportion of constant slopes increased for the slopes with northeast aspects compared with other directions, particularly for the RW complex. The steepest slopes in the component units of the CDF exhibited overwhelmingly constant slopes (Figs. 23C and 23D). In the Upper Clare the slopes were almost exclusively constant. These results may suggest stronger erosional effects on the slopes of the RW and RM complexes.

4.2.5 Evidence for Bedform Wavelengths and other Periodicities

The elongated ridges of the northern RM complex suggested parallelism and some degree of regular spacing (Fig. 24). This raised some question as to whether the dunes were evolving into longitudinal dunes (Lancaster, 2009; Goudie, 2011). Under arid conditions longitudinal dunes can develop, given uniform conditions, an adequate sediment supply and a bimodal wind regime with a minimum 45° divergence in wind direction (Reffet et al., 2010; Warren, 2013). Alternatives to this possibility exist. Seif-like dunes have been associated with the extension of barchan dune horns (Warren, 2013). Sand ridges have been linked to elongated arms of parabolic dunes, again where a bimodal wind regime was present (Warren, 2013). If the dunes were developing characteristics of longitudinal dunes, a characteristic bedform wavelength should exist orthogonal to the direction of dune elongation. The transect of Figure 24A was constructed on a strike of 30°. This was selected to be orthogonal to dominant orientation of the ridge crests. The transect extends 1.9 km, with distances being measured from the southwest end. Elevation along the transect was sampled every meter. Peaks corresponding to ridge crests occurred at locations “A” through “F”, “K” and “L” (Figs. 24A and 24B). The ridge to ridge spacing varies from a minimum of 100 m to a maximum of 380 m. However, a road cut is located in the middle of the maximum gap. It appears that a ridge would have occurred but for a road in the vicinity of three very low, false peaks “G”, “H” and “M”. Another false peak corresponding to road work occurs works at “N”. A peak “O” occurs at approximately the 820 m mark along the transect. Peak “O” is part of the base terrain. Another substantial gap of about 360 m occurs between ridges “C” and “D”.

Wavelength in ridge spacing for the RM complex was tested for using a univariate wavelet analysis on elevation based on a Morlet wavelet input (Fig. 25). Figure 25A is a spectrum analysis in which increasingly warm colors indicate correlation. In this figure transect distance is displayed along the horizontal axis and spatial wavelength is displayed along the vertical axis. From the power to wavelet (Fig. 25B), correlation appears strongest at about 70, 200, and 600 m, however correlation at 70 m is intermittent, corresponding to elevation peaks along the transect. Thus the 70 m signal is likely an indication of ridge widths. The 600 m signal is discounted as being a multiple of the 200 m signal. This leaves the 200 m wavelength as the most likely candidate for a bedform wavelength. This is due to correlation being continuous along the length of the transect.

Longitudinal dunes should exhibit a ratio of ridge to ridge spacing over dune width of about two (Greeley and Iversen, 1987). Here the ratio is 200 m to 70 m, or close to three. On the basis of width to wavelength ratios, the possibility that regular spacing between ridges is present remains open, but questionable. However, the underlying elevation data includes peaks which are easily identifiable as false positives. These include point “O”, and an unlabeled peak occurring between “O” and “D”. The portion of the transect from “D” to “L” may exhibit shorter wavelengths, but this section of the transect includes still more false peaks “G”, “H” and “N”. On the basis of the somewhat wide spacing between the dunes, and problems with using elevation data, it is concluded that the elevation data do not demonstrate that the dunes were evolving into longitudinal dunes.

There are other data other which may be more reliable indicators of wavelength than changes in elevation. Referring back to Figure 21, there is an obvious correlation of steep slopes with ridges, particularly. The aspects of these slopes should roughly align with the transect. Figure 26 reflects the results of a wavelet analysis of aspect over slope versus transect distance. The choice of aspect over slope was made in preference to other combinations, (1) based on its having the highest power level, and (2) based on the observation that while aspect and slope were correlated across ridges, they were unlikely to be correlated across the underlying terrain. The axes of Figure 26A are the same as in Figure 25A, with warm colors indicating correlation. The direction of the arrows indicates whether correlation is positive or negative, with right oriented arrows indicating the former and left oriented arrows indicated the latter. Here, whether correlation is negative or positive is unimportant as long as it is consistent across ridges. From Figure 26B, signal peaks of about 40, 80 and 120 m are observed. Coherence at 40 and 80 m tend to be intermittent and localized around ridge locations (Fig. 26A). The 120 m signal has some continuity along the entire transect, but coherence is still variable. In my view, the detected wavelengths again only reflect ridge widths.

A Morlet wavelet was used in the slope over aspect analysis, but this choice may not have been ideal here. Ignoring the gaps between the ridges, following a transect across a series of un-eroded ridges should produce a slope signal comprising constant values with reversing polarity. In other words, the signal would resemble a square wave. A non-sinusoidal wavelet, one combined with allowing for negative slopes along the directional transect, may be a better choice for slope analysis than the Morlet wavelet.

The possible RDRs found in the Lower Clare sub-unit were examined for evidence of wavelength (Fig. 12B). Due to the low relief of the landforms in context this analysis was limited to consideration of elevation change. The elevation profile appeared noisy, and was limited to maximum possible count of four ridges. The minimum spacing between features was approximately 30 m and the maximum gap was on the order of 80 to 100 m. No evidence was seen of the presence of a regular wavelength.

Wavelet analysis was also used to explore the possibility that periodicity might appear on outward facing slopes of the parabolic dune arms in terms of varying aspect. Figures 27-29 reflect the results of this inquiry. The dune marking the NE margin of the CDF and facing Rice Pond was viewed as a favorable test location. The dune has a rotated slip face slope facing to the NE for almost 1 km (Fig. 27), providing a large sample size. The level underlying terrain limited the possibilities that slope orientation would be altered by terrain.

A 900 m trace was manually digitized along the slope (Fig. 27). Aspect along the trace (Fig. 28), was found to vary through a counter-clockwise arc from 74° to 350°. The results of a univariate wavelet analysis on aspect along the trace are presented in Figure 29. Two significant signals (wavelengths) appear, a continuous one of 64 m and an intermittent signal at 128 m signal (Fig. 29A). The longer wavelength may be an echo of the shorter wavelength. A nonsignificant signal in the range of approximately 5 m is also present. The possible 5 m signal is highly intermittent (Fig. 29A) and suggests subtle crenulation along the dune arm. These may be occurrences of the dune having encountered scattered obstacles such as trees or brush in its direction of migration. The 64 m wavelength signal has the most power (Fig. 29B).

4.3 Comparison of DEM and LiDAR Datasets

The mean dune elevations from Table 3 for the dune polygons are comparable across the datasets. Dune elevation range was expected to be greater for the finer resolution LiDAR dataset than for the coarser resolution DEM, particularly given the wider coverage of polygons derived from the LiDAR dataset. Except for the RW complex this was not the case. The largest change in median elevation between the two datasets was an increase by 0.6 m from the DEM to the LiDAR dataset for the CDF. Elevation distribution of the dunes by field is characterized by dune bases (taken as the 10th percentile) of approximately 338 - 339 m for all three dune fields. Typical crest elevations associated with the 75th to 90th percentiles for the RW and RM complexes range were about 342 m for the RW and from 343 - 345 m for the RM complex, regardless of the dataset used. There was a wide gap between the 75th and 90th percentile elevations for the CDF for both datasets, reflective of the presence of the LHR. Based on the dune elevation quantiles for either dataset relief in the RW complex was approximately 2 - 4 m and 2 - 5 m in the RM complex. Taking the same approach to the CDF produces a much larger gap, on the order of 9 - 20 m, however these numbers are inflated by a substantial number of dunes being located on the LHR.

Figure 30 adds insight into differences in elevation attributes provided by the datasets by graphing elevation density for the field polygons. The RW and RM DEM datasets exhibit two distinct peaks in elevation density occurring at approximately 339 m and 342 m. A third, weaker peak occurs for the RM complex at just under 345 m. No such peaks occur for the complexes from the LiDAR data which peak at about 340 m and then taper off. In contrast, the CDF elevation densities generated from the two datasets track one another fairly well. Relief in the RW and RM complexes may have been too small to be consistently picked up during generation of the elevation model, resulting in binning of elevations for areas actually covered by dunes into either base terrain or a second bin. The difference in elevation between the two bins reflects average relief. These results suggest that relief in the CDF passed a minimum threshold at which point the precision of the DEM dataset allowed a major improvement in congruency with the LiDAR dataset results. In terms of slopes, the binning of elevations may have resulted in the high density of near zero slopes in the RW and RM complexes (Fig. 31).

Figures 32, 33 and 34 are analytical-hillshade visualizations of the three study area dunes fields. Images generated from the DEM dataset from the LiDAR dataset are shown in each figure. The hillshades cover identical areas at identical scales and are illustrated with the light source positioned at azimuth 45° and an altitude of 45°. Vertical exaggeration is 4X.

Comparing the DEM dataset and LiDAR dataset derived hillshades (Figs. 32A and 32B) for the RW complex, the sparse appearance of the DEM dataset image is immediately apparent. It is difficult to recognize the RW complex in the DEM dataset. A significant number of very low relief dunes in the north central portion of the field are visible only in the LiDAR based view. The presence of superimposed forms is also only visible using the LiDAR dataset. Generally, only dune apices and the central windrift dune were imaged for the RW complex using the DEM dataset.

Hillshades for the RM complex generated from the DEM and LiDAR datasets are illustrated in Figures 33(A and B). Unlike the RW complex, similarities in the visualization of the RM complex from the two datasets are more readily seen. Differences of note are still present, but tend to be reflected in artifacts in the DEM based hillshade. Among these were rayed areas, which appear in the LiDAR based DEM to have been parts of dunes or islands. There are also occurrences of infilling of intra-dune zones in the DEM dataset image.

In contrast to the first two fields, the similarities between the hillshades for the CDF based on the two datasets are strong (Figs 34A and 34B). Occurrences of superimposition are clear, as are the general shapes of the dunes. There are instances of infilling of intra-dune zones.

CHAPTER 5. DISCUSSION

5.*1 Characteristics of the Dunes*

For the RW complex, visualizations revealed the presence of at least two distinct dune morphologies, a group of more northerly, smaller-scale dunes with simple parabolic planforms, and other, larger dunes the southeast of the first group. The northerly dunes (labeled "G" in Fig. 9) are primarily lobate and lie in relatively close proximity to one another, but with few, if any, instances of superimposition. The occurrence of these dunes terminates fairly abruptly along a modern wetland to their northwest. The margin between the dunes and the wetland corresponds to an approximately 2.0 - 2.5 m drop in elevation across a space spanning about 20 m. This zone may be a beach ridge formed along a former strandline.

The "G" dunes resemble closely packed parabolic dunes such as found in the Jafurah Desert and coastal sabkhas of eastern Saudi Arabia (Goudie, 2011; Yan and Baas, 2015). The Jafurah Desert dunes have been linked to an arid climate and ubiquitous shallow groundwater. The proximity of the group "G" dunes to a possible paleo-lake, and their similarity in appearance to the Arabian peninsula dunes, point to shallow ground water availability. The dunes may also have been low fore dunes which have undergone extensive reworking, or a simple lake-plain complex dunes (Hansen et al., 2010). Any of these cases suggests the presence of open water to the northwest, and a different age for these dunes that the other dunes of the Rosco Field then late Younger Dryas (Arbogast et al., 2015). The development of a lake covering the modern wetland to the northwest of these dunes, followed by its retreat and pro-gradation of the shore line would place the age of these dunes later than the other dunes in the area.

Among the larger parabolic dunes of the RW complex, those in the central portion of the field (Group “C”-Fig. 9) include occurrences of superimposition of open dunes on other open dunes, resulting in compound forms (Wolfe and David, 1997). Individual dunes remain distinctive. This suggests that the dunes formed successively, and that the field has been reworked (Wolfe and David, 1997). The western tips of arms of this group tend to be located in a shallow depression. The depression, which is roughly orthogonal to the orientation of the parabolic dune arms, is interpreted as a merger of deflation basins which formed between the dunes arms. The eastern margin of this group is marked by a more frequent occurrence of superimposition of dunes.

The northern portion of the RM complex is dominated by ridges ranging from about 1 - 2 km (“F” in Fig. 10), extending from the west-northwest to the east-southeast. The ridges terminate against another ridge (“H” in Fig. 10) which forms a rough half circle or crescent around the elongated ridges, closed to the east around the presumably downwind margin, and open to the west. This crescentic resembles an eastward pointing, crescent-like ridge formed from nested compound and lobate parabolic dunes in the central Fair Oaks Dunes (FOD) of NW Indiana. The FOD system however lacks the elongated interior ridges of the RM complex (Kilibarda and Blockland, 2011). The authors suggested that the FOD crescent may have formed from an oppositely oriented megabarchan. The northern portion of the RM complex also resembles parabolic dunes located along the eastern margin of the Defiance Moraine in NW Ohio, just to the west of Winameg Ridge, although the RM complex is not as large (Fisher et al., 2015). The NW Ohio dunes also terminate along a continuous ridge.

The elevation of the terrain underlying the elongated ridges in the RM complex rises from west to east, which is presumably the direction of dune extension, until a subtle flattening of the underlying terrain occurs. It is here that the downwind marginal ridge “H” is located. The cessation in the rise of terrain would have resulted in a reduction in sediment flux. It could also mark the onset of a line of vegetation, which could have produced a precipitation ridge (Hesp, 2013). The eastern most portion of the ridge “H” is marked by compound forms, crenulation and possible infilling. All of these may be taken as a stalling in the migration of the system to the east which is consistent with both a drop off in sediment flux or development of a precipitation ridge.

The southwestern portion of the RM complex (dune group “C” of Fig. 10) are located on generally lower elevation terrain than the rest of the complex. The area is dominated by parabolic dunes superimposed on other parabolic dunes. Crosscutting relationships are prominent, with the western ends of several dunes arms terminating abruptly along paleomeanders of the Muskegon River. A few dune arms are cross-cut by modern meanders. Relative dating places the formation of the dunes before formation of the paleomeanders, an assessment which conflicts with the appraisal of Arbogast et al. (2015). In their research, based on the statistically coeval ^{14}C dating of the paleomeanders and OSL dating of the dunes, suggested that the dunes and meanders formed at the same time. The cross-cutting also indicates that this portion of the RM complex extended further west than it does presently, possibly placing portions of a lost deflation plain for the area to west of the modern Muskegon River.

The Lower Clare sub-unit comprises numerous nested and superimposed dunes which form compound parabolic dunes. The entire sub-unit is located on the relatively low, flat terrain of the T-4 terrace. Taken together with the Upper Clare sub-unit, the field covers a crescent shaped area, closed along the presumed downwind margin by a nearly continuous ridge comprising arms and apices of parabolic dunes. Unlike the RM complex, the component parts of the ridge are, for the most part, distinguishable. The crescent includes nested and compound dunes. The dunes of the Upper Clare sub-unit are more difficult to categorize, although there appear to be fewer instances of dunes superimposed on other dunes. The roughness of the underlying terrain likely redirected and reshaped the dunes.

The pattern of dunes in the CDF is seen as evolving from repeated instances of reworking. This could imply sporadic increases in moisture availability in the course of a longer term dry period. The CDF is seen as having undergone several instances of activation and stabilization.

The MRD are diverse dunes which occur in a variety of contexts. Some are on relatively low terrain within 1.5 km of the modern T-1 and T-2 terraces. Most of the dunes are at least 2 km from the river valley and some of these extend up to 7.5 km inland. At distances closer to the river lobate parabolic dune forms appear more common, while extended parabolic forms appear at middle distances. At the greatest distances the dunes are situated on higher elevation and generally have evolved into elongated windrift forms. Similar to the ridges of the RM complex, the elongated forms appear associated with increasing elevation along their length. The changes in form suggests a role for groundwater depth as control on field activity. However, linking the dates of formation of these diverse dunes to the period in which the dunes of the study field formed is problematical.

5.2 Sources of Sand

The RW complex, RM complex the CDF and MRD are located to the east of the modern Muskegon River, and downstream from a blend of outwash surfaces, glaciofluivial sediment and paleo-lacustrine plains drained by the river (Schaetzl and Weisenborn, 2004; Arbogast et al., 2008; Schaetzl et al., 2017). The dunes of the RW complex, the southwestern portion of the RM complex, and the Lower sub-unit of the CDF lie of the T-4 terrace. The western margin of the northern portion of the RM complex is also located on the terrace. Most of the northern RM complex, the Upper Clare sub-unit of the CDF and almost all of the observed portion of the MRD are located on uplands to the east of the T-4 terrace.

The terrace, supplemented by the predecessors to the modern river, are potential sources of sediment. In the case of the central portion of the RW complex and the northern portion of the RM complex, plains are located on the T-4 terrace between the dunes and the modern river valley. These plains are well located, and are constituted of appropriate material, to be deflation plains. Possible supplementary sources of sediment for the central portion of the RW complex and the northern RM complex are depressions collocated with the distal ends of parabolic dune arms in these fields. Portions of the southwestern part of the RM complex appears crosscut by other terraces. Similarly, the western most margin of the lower sub-unit of the CDF lies essentially adjacent to the modern river valley. The immediate source of sediment for these dunes was likely deflation plain on a portion of the T-4 terrace eroded by later evolution of the Muskegon River.

Other potential sources of sediment, general to all of the fields, include Cadillac Morainic Uplands to the west of the study area fields. Substantial amounts of sand are available here (Schaetzl et al., 2017). The presence of the dunes in a basin adjacent these uplands makes the area a potential sediment trap (Hansen et al., 2009).

5.3 Wind Regimes

The only prior study of the Rosco Dune Field known to this researcher was directed to determination of two things, the age of the field and the dominant wind regime at the time the field assumed its present configuration (Arbogast et al., 2015). Based in part on dune orientations, it was concluded that westerlies were the dominant wind regime. In this study, the orientation of the crestlines broadly supports the earlier work regarding the dominant wind regime. In addition, the absence of steeper slopes with northwesterly, westerly and southwesterly aspects points to these slopes being stoss slopes.

However, a secondary wind regime could have influenced sediment transport, deposition or vegetation growth (Hansen et al., 2009). Any of these could influence parabolic dune morphology where the dune was undergoing progressive, vegetation–mediated stabilization. The steepest slopes in all three study fields are strongly biased toward northerly and northeasterly aspects. The near absence of slopes of the steepest category having southerly aspects in the CDF, and low frequency in the occurrence of such slopes in the RW and RM complexes, point to a secondary southwesterly wind regime. It may not have been necessary that these winds have been strong enough to transport sand. If the winds served to accelerate drying of southerly slopes, or otherwise acted to prevent vegetation from taking hold, a difference in slope stability would have been present. Southwesterly winds strong enough to transport sediment would have made northeasterly facing slopes into occasional lee slopes. This too would contribute to steepening the slopes. It remains a possibility that slopes with northern aspects, because they received less insolation, would hold snow or remain frozen by water ice later into the spring than slopes having southern aspects, and thus been stabilized by factors other than the wind. On balance, I conclude that the slopes point to a bimodal wind regime.

Possibly relating to this point is the tendency of the steepest slopes in the CDF to be planar in comparison to the steepest slopes of the RM complex. A possible explanation for this may be that the RM complex is dominated by elongated ridges. Wind steering effects along the longitudinal dunes may have caused erosion along the faces of the dunes (Hansen et al., 2009).

5.4 Groundwater Influence on Dune Stabilization

Modern wetlands border the RW and RM complexes. In the case of the RW complex, these are located to the east and northwest. In the case of the RM complex, they are to the south. Wetlands, and open water, are present along the northeast margin of the CDF. In some locations dunes appear to be superimposed on present or former wetlands. These wetlands are likely to have been recurring phenomena, and they are surficial evidence of past levels of the water table.

Direct evidence of groundwater influence on dune stabilization are the low relief ridges, interpreted as RDRs, within the lower Clare dunes. RDRs are dune remnants, linked to periodic flooding at the base of a dune. The possible RDRs appear on the lowest basal terrain on which dunes are located. They are close to modern day Rice Pond and adjacent wetlands, which suggest that the area has periodically been a wetland in the past. It is also a strong argument for at least sporadic near surface availability of ground water under the lower Clare sub-unit, particularly along its northeast margin, at the time the dune stabilized.

All three fields support compound parabolic dunes which overlay essentially flat terrain. This can be seen at the eastern margin of the dunes of groups “C” in the RW and RM complexes and possible wetlands “A” and “D” (Figs. 9 and 10). In the case of the RM complex, area “D” is approximately 3 m lower than upwind terrain. The northeastern portion of the Lower Clare dunes include compound forms on wetlands. These are modern wetlands and it is likely that the surfaces here have, at times in the past, been coeval with, or below, water table levels. Except in the case of the CDF, the failure of dunes to progress much past the apparent margins of these areas supports the conclusion that increased groundwater availability contributed to dune stabilization. The southern portion of the ridge “H” in the RM complex (Fig. 10) lies roughly parallel to wetland “D”. Groundwater influence here could take two forms, either supporting vegetation growth on the extending ridge, or in supporting parkland which could give rise to a precipitation ridge.

Areas were identified in both the RW and RM complexes which could intra-parabolic arm deflation basins. Both areas exhibit fairly consistent depths of approximately 1.5 m compared to surrounding terrain. It is possible that deflation was limited by encountering groundwater at that depth. This would limit sediment supply to the dunes.

The elongated ridges in the RM complex lie on terrain which rises in the downwind direction. Dune ridges extending downwind here could have become relatively elevated relative to groundwater compared to the dune arms in the RW complex or Lower Clare sub-unit. Lack of access to water would have been a factor retarding stabilization. This would allow for longer periods of activity. There are several examples of elongated ridges (“C” in Fig. 13) among the MRD. These too occur in areas where base terrain elevation rises downwind.

The limit of the ridges extension to the east corresponds to a cessation in increasing elevation. The change in slope here would contribute to a decrease in sediment flux, and could correspond to a shallowing of groundwater levels. The northern and eastern parts of the crescentic ridge marking the downwind margin of the RM complex is attributed to development of a precipitation ridge parallel to and downwind from the contour where elevation stabilized.

Given the location of the upper sub-unit of the CDF on the LHR, which is deep, cobble based material exhibiting local relief of up to 20 m, it is difficult to see how groundwater would have been the readily available to support vegetation growth. It is more likely here that sediment flux starvation played the more important role in stabilization.

5.5 Dune Field History

The beginnings of the study area dune fields likely began with formation of the T-4 terrace, which supplied the bulk of the sediment for the dune fields. Arbogast et al. (2008) estimated this occurred 12,500 calendar YBP. Following construction of the T-4 terrace, a series of fields dominated by barchans formed. These fields may in places have extended west of the modern Muskegon River. These fields migrated eastward under the influence of prevailing westerlies. Possibly excluding the smaller dunes of the northwest RW complex, the barchans inverted into parabolic forms toward the end or after the Younger Dryas as moisture availability and groundwater levels began to increase. Some of the elongated dunes of the RM complex, and the dunes of the upper CDF, remained active longer, climbing out of greater Muskegon River onto uplands to the east.

The dunes in the northern portion of the RW complex differ from other parabolic dunes in the study area in terms of relief, and in lack of compound forms. Consequently, these dunes may have a different history than those dunes. It is possible they either postdate or predate the other dune fields, with their formation could be tied to their location on very well drained soil, with a shallow groundwater level. The possibility that a lake existed their northwest is consistent with this hypothesis. Shallow groundwater could have prevented the growth of boreal forest common to the area during the early Holocene (Hupy, 2012).

CHAPTER 6. CONCLUSIONS

Results from this study demonstrate that the dune fields of the upper Muskegon River Valley are much more extensive than previously believed. One field not previously discussed in the literature, referred to here as the Clare Dune Field, was revealed by the generation of a wind exposure index from a 10 m resolution digital elevation model, and applying landform definitions to zones qualified using the index. Additional dunes (the MRD) were revealed using analytical-hillshade visualizations generated from the LiDAR dataset.

Known dune orientation was seen as evidence that both sections of the Rosco Dune Field were formed under the influence of westerly winds. Terrain analysis implemented using GIS and based on slope and aspects strongly suggests that the wind regime was an unequal bimodal regime, with west-north-westerlies being the predominant regime, but with a secondary, possibly seasonal, south or southwesterly wind regime. This result supports the conclusion that winds off the Laurentide Ice Sheet did not influence dune morphology, at least in its last stages.

The study partially conflicts with earlier conclusions regarding timing of events in the fields based on absolute dating methods. Formation of the Rosco Dune Field had been seen as contemporaneous with the down cutting that produced the T-3 terraces of the Muskegon River. Margins of error in those studies allow for relative dating placing that down cutting after the dunes formed. Portions of the fields almost certainly extended further west than is now seen, into areas now lost due to formation of the T-1, T-2 and T-3 terraces.

Arbogast et al., (2015) argued that the groundwater table level was unlikely to have been a control on the Rosco Dune Field. That argument was based on the appraisal that the paleomeanders and dunes were coeval in age. In addition to the cross-cutting relationships developed in this study, more can be said about the terrain underlying the dunes. The superimposition of compound parabolic dunes on what appear to be present or former wetlands, the possible presence of RDRs in the Clare Dune Field, and the differences in morphology between dunes on the T-4 terrace and dunes which climbed off the terrace point to a clear role for groundwater in stabilizing the dunes on lower terrain.

The dune fields examined in this study also exhibited a heterogeneity in morphology not previously suspected. The fields are not simply a collection of simple inland parabolic dunes. A portion of the RW complex suggests the possibility origination and evolution as a small coastal field. The RM complex includes elongated, possible windrift dunes migrating off the T-4 terrace. These last dunes suggest sustained periods of activity in contrast to the other two fields. Somewhat similar dunes, even further removed from the modern river, appear among the MRD.

Suggestions for future research include strategic absolute dating of the fields guided by relative dating. With relative dating as a guide comparative OSL dating can be taken from nearby locations on arms of different parabolic dunes. Another line of research would be to evaluate the age of the barchan dune located upwind from the CDF. The shape of the barchan dune is consistent with it being composed of relatively coarse sediment, which may explain how it survived and may allow it to be of similar age to the study area fields (Warren, 2013). The possible presence of small, coastal dunes in the RW complex could aid in evaluating stages of an hypothesized Lake Roscommon or other paleo-lakes of the HLB (Schaetzl et al., 2017).

REFERENCES

Anthonsen, K.L., Clemmensen, L.B., Jensen, J.H., 1996. Evolution of a dune from crescentic to parabolic form in response to short-term climatic changes: Rabjerg Mile, Skagen Odde, Denmark. Geomorphology 17, 63–77.

Arbogast, A.F., Bookout, J.R., Schrotenboer, B.R., Lansdale, A., Rust, G.L., Bato, V.A., 2008. Post-glacial fluvial response and landform development in the upper Muskegon River valley in North-Central Lower Michigan, U.S.A. Geomorphology 102, 615–623. https://doi.org/10.1016/j.geomorph.2008.06.008

Arbogast, A.F., Luehmann, M.D., Miller, B.A., Wernette, P.A., Adams, K.M., Waha, J.D., O'Neil, G.A., Tang, Y., Boothroyd, J.J., Babcock, C.R., Hanson, P.R., Young, A.R., 2015. Late-Pleistocene paleowinds and aeolian sand mobilization in north-central Lower Michigan. Aeolian Research 16, 109–116. https://doi.org/10.1016/j.aeolia.2014.08.006

Baas, A.C.W., Nield, J.M., 2007. Modelling vegetated dune landscapes. Geophys. Res. Lett. 34, L06405. https://doi.org/10.1029/2006GL029152

Barchyn, T.E., Hugenholtz, C.H., 2013. Reactivation of supply-limited dune fields from blowouts: A conceptual framework for state characterization. Geomorphology 201, 172–182. https://doi.org/10.1016/j.geomorph.2013.06.019

Barchyn, T.E., Hugenholtz, C.H., 2012a. Aeolian dune field geomorphology modulates the stabilization rate imposed by climate: DUNE FIELD STABILIZATION RATE. Journal of Geophysical Research: Earth Surface 117, n/a-n/a. https://doi.org/10.1029/2011JF002274

Barchyn, T.E., Hugenholtz, C.H., 2012b. A process-based hypothesis for the barchan-parabolic transformation and implications for dune activity modelling. Earth Surface Processes and Landforms 37, 1456–1462. https://doi.org/10.1002/esp.3307

Barchyn, T.E., Hugenholtz, C.H., 2012c. Predicting vegetation-stabilized dune field morphology. Geophysical Research Letters 39, n/a-n/a. https://doi.org/10.1029/2012GL052905

Bernhardson, M., Alexanderson, H., 2017. Early Holocene dune field development in Dalarna, central Sweden: A geomorphological and geophysical case study: Dune field development in Sweden. Earth Surface Processes and Landforms 42, 1847–1859. https://doi.org/10.1002/esp.4141

Böhner, J., Antonić, O., 2009. Chapter 8 Land-Surface Parameters Specific to Topo-Climatology, in: Developments in Soil Science. Elsevier, pp. 195–226. https://doi.org/10.1016/S0166-2481(08)00008-1

Böhner, J., Selige, T., 2006. Spatial Prediction of Soil Attributes using Terrain Analysis and Climate Regionalisation, in: SAGA - Analysis and Modelling Applications, Goettinger Geographische Abhandlungen. pp. 13–28.

Bonaventura, X., Sima, A.A., Feixas, M., Buckley, S.J., Sbert, M., Howell, J.A., 2017. Information measures for terrain visualization. Computers & Geosciences 99, 9–18. https://doi.org/10.1016/j.cageo.2016.10.007

Campbell, M.C., Fisher, T.G., Goble, R.J., 2011. Terrestrial sensitivity to abrupt cooling recorded by aeolian activity in northwest Ohio, USA. Quaternary Research 75, 411–416. https://doi.org/10.1016/j.yqres.2011.01.009

Colgan, P.M., Amidon, W.H., Thurkettle, S.A., 2017. Inland dunes on the abandoned bed of Glacial Lake Chicago indicate eolian activity during the Pleistocene-Holocene transition, southwestern Michigan, USA. Quaternary Research 87, 66–81. https://doi.org/10.1017/qua.2016.13

David, P.P., Wolfe, S.A., Huntley, D.J., Lemmen, D.S., 1999. Acitivity cycle of parabolic dunes based on morphology and chronology from Seward sand hills, Saskatchewan, in: Holocene Climate and Environmental Change in the Palliser Triangle: A Geoscientific Context for Evaluating the Impacts of Climate Change on the Southern Canadian Praries, Geological Survey of Canada. Geological Survey of Canada, pp. 228–243.

De Reu, J., Bourgeois, J., Bats, M., Zwertvaegher, A., Gelorini, V., De Smedt, P., Chu, W., Antrop, M., De Maeyer, P., Finke, P., Van Meirvenne, M., Verniers, J., Crombé, P., 2013. Application of the topographic position index to heterogeneous landscapes. Geomorphology 186, 39–49. https://doi.org/10.1016/j.geomorph.2012.12.015

Durán, O., Herrmann, H.J., 2006. Vegetation against dune mobility. Physical review letters 97, 188001.

Evans, I.S., 2012. Geomorphometry and landform mapping: What is a landform? Geomorphology 137, 94–106. https://doi.org/10.1016/j.geomorph.2010.09.029

Evans, J.E., Clark, A., 2011. Re-interpreting Great Lakes shorelines as components of wave-influenced deltas: An example from the Portage River delta (Lake Erie). Journal of Great Lakes Research 37, 64–77. https://doi.org/10.1016/j.jglr.2010.10.002

Ewing, R.C., Kocurek, G.A., 2010. Aeolian dune interactions and dune-field pattern formation: White Sands Dune Field, New Mexico. Sedimentology. https://doi.org/10.1111/j.1365-3091.2009.01143.x

Fisher, T., Blockland, J.D., Anderson, B., Krantz, D.E., Stierman, D.J., Goble, R., 2015. Evidence of Sequence and Age of Ancestral Lake Erie Lake-Levels, Northwest Ohio. The Ohio Journal of Science 115, 62. https://doi.org/10.18061/ojs.v115i2.4614

Fisher, T., Blockland, J.D., Anderson, B., Krantz, D.E., Stierman, D.J., Goble, R., 2015. Evidence of Sequence and Age of Ancestral Lake Erie Lake-Levels, Northwest Ohio. The Ohio Journal of Science 115, 62. https://doi.org/10.18061/ojs.v115i2.4614

Fisher, T.G., 2005. Strandline analysis in the southern basin of glacial Lake Agassiz, Minnesota and North and South Dakota, USA. Geological Society of America Bulletin 117, 1481. https://doi.org/10.1130/B25752.1

Fisher, T.G., Horton, J., Lepper, K., Loope, H.M., 2019. Aeolian activity during Late Glacial time, with an example from Mongo, Indiana, USA. Canadian Journal of Earth Sciences. https://doi.org/10.1139/cjes-2018-0127

Gesch, D.B., Oimoen, M., Greenlee, S., Nelson, C., Steuck, M., Tyler, D., 2006. The National Elevation Dataset. Photogrammetric engineering and remote sensing 68, 5–32.

Gorsevski, P.V., Brown, M.K., Panter, K., Onasch, C.M., Simic, A., Snyder, J., 2016. Landslide detection and susceptibility mapping using LiDAR and an artificial neural network approach: a case study in the Cuyahoga Valley National Park, Ohio. Landslides 13, 467–484. https://doi.org/10.1007/s10346-015-0587-0

Goudie, A., 2011. Parabolic Dunes: Distribution, Form, Morphology and Change. Annals of Arid Zone 50, 1–7.

Greeley, R., Iversen, J.D., 1987. Wind as a geological process on Earth, Mars, Venus and Titan. Cambridge University Press, Cambridge.

Halfen, A.F., Johnson, W.C., 2013. A review of Great Plains dune field chronologies. Aeolian Research 10, 135–160. https://doi.org/10.1016/j.aeolia.2013.03.001

Hengl, T., Evans, I.S., 2009. Mathematical and digital models of the land surface, in: Geomorphometry: Concepts, Software, Applications, Developments in Soil Science. Elsevier, pp. 31–63.

Hesp, P.A., 2013. Conceptual models of the evolution of transgressive dune field systems. Geomorphology 199, 138–149. https://doi.org/10.1016/j.geomorph.2013.05.014

Horn, B.K.P., 1981. Hill shading and the reflectance map. Proceedings of the IEEE 69, 14–47. https://doi.org/10.1109/PROC.1981.11918

Hugenholtz, C.H., 2010. Topographic changes of a supply-limited inland parabolic sand dune during the incipient phase of stabilization. Earth Surface Processes and Landforms 35, 1674–1681. https://doi.org/10.1002/esp.2053

Hugenholtz, C.H., Barchyn, T.E., 2010. Spatial analysis of sand dunes with a new global topographic dataset: new approaches and opportunities. Earth Surface Processes and Landforms 35, 986–992. https://doi.org/10.1002/esp.2013

Hugenholtz, C.H., Wolfe, S.A., Walker, I.J., Moorman, B.J., 2009. Spatial and temporal patterns of aeolian sediment transport on an inland parabolic dune, Bigstick Sand Hills, Saskatchewan, Canada. Geomorphology 105, 158–170. https://doi.org/10.1016/j.geomorph.2007.12.017

Hupy, C.M., 2012. Mapping Ecotone Movements: Holocene Dynamics of the Forest Tension Zone in Central Lower Michigan, Usa. Physical Geography 33, 473–490. https://doi.org/10.2747/0272-3646.33.5.473

Kilibarda, Z., Blockland, J., 2011. Morphology and origin of the Fair Oaks Dunes in NW Indiana, USA. Geomorphology 125, 305–318. https://doi.org/10.1016/j.geomorph.2010.10.011

Kocurek, G., Ewing, R.C., 2005. Aeolian dune field self-organization – implications for the formation of simple versus complex dune-field patterns. Geomorphology 72, 94–105. https://doi.org/10.1016/j.geomorph.2005.05.005

Lancaster, N., 2009. Dune Morphology and Dynamics, in: Parsons, A.J., Abrahams, A.D. (Eds.), Geomorphology of Desert Environments. Springer Netherlands, Dordrecht, pp. 557–595. https://doi.org/10.1007/978-1-4020-5719-9_18

Levin, N., Tsoar, H., Herrmann, H.J., Maia, L.P., Claudino-Sales, V., 2009. Modelling the formation of residual dune ridges behind barchan dunes in North-east Brazil. Sedimentology 56, 1623–1641. https://doi.org/10.1111/j.1365-3091.2009.01048.x

Lindsay, J.B., Cockburn, J.M.H., Russell, H.A.J., 2015. An integral image approach to performing multi-scale topographic position analysis. Geomorphology 245, 51–61. https://doi.org/10.1016/j.geomorph.2015.05.025

Luehmann, M.D., 2015. Relict Pleistocene deltas in the lower peninsula of Michigan. Michigan State University.

MacMillan, R.A., Shary, P.A., 2009. Landforms and Landform Elements in Geomorphometry, in: Geomorphometry: Concepts, Software, Applications, Developments in Soil Science.

Mitasova, H., Harmon, R.S., Weaver, K.J., Lyons, N.J., Overton, M.F., 2012. Scientific visualization of landscapes and landforms. Geomorphology 137, 122–137. https://doi.org/10.1016/j.geomorph.2010.09.033

Mitasova, H., Overton, M., Harmon, R.S., 2005. Geospatial analysis of a coastal sand dune field evolution: Jockey's Ridge, North Carolina. Geomorphology 72, 204–221. https://doi.org/10.1016/j.geomorph.2005.06.001

Miyasaka, T., Okuro, T., Zhao, X., Takeuchi, K., 2016. Classification of Land Use on Sand-Dune Topography by Object-Based Analysis, Digital Photogrammetry, and GIS Analysis in the Horqin Sandy Land, China. Environments 3, 17. https://doi.org/10.3390/environments3030017

Novák, D., 2014. Local relief model (LRM) Toolbox for ArcGIS. Czech Academy of Science.

Olaya, V., 2009. Chapter 6 Basic Land-Surface Parameters, in: Geomorphometry: Concepts, Software, Application. Elsevier, pp. 141–169. https://doi.org/10.1016/S0166-2481(08)00006-8

Olaya, V., Conrad, O., 2009. Geomorphometry in SAGA, in: Geomorphometry: Concepts, Software, Applications, Developments in Soil Science.

Parteli, E.J.R., Durán, O., Bourke, M.C., Tsoar, H., Poeschel, T., Herrmann, H.J., 2013. Origins of barchan dune asymmetry: insights from numerical simulations. arXiv:1304.6573 [cond-mat, physics:physics].

Parteli, E.J.R., Schwaemmle, V., Herrmann, H.J., Monteiro, L.H.U., Maia, L.P., 2006. Profile measurement and simulation of a transverse dune field in the Lencois Maranhenses. Geomorphology 81, 29–42. https://doi.org/10.1016/j.geomorph.2006.02.015

Pelletier, J.D., Sherman, D.J., Ellis, J.T., Farrell, E.J., Jackson, N.L., Li, B., Nordstrom, K.F., Maia, L.P., Omidyeganeh, M., 2015. Dynamics of sediment storage and release on aeolian dune slip faces: A field study in Jericoacoara, Brazil: Dynamics of Dune Slip Faces. J. Geophys. Res. Earth Surf. 120, 1911–1934. https://doi.org/10.1002/2015JF003636

Pike, R.J., Evans, I.S., Hengl, T., 2009. Chapter 1 Geomorphometry: A Brief Guide, in: Developments in Soil Science. Elsevier, pp. 3–30. https://doi.org/10.1016/S0166-2481(08)00001-9

Pye, K., 1993. Late Quaternary development of coastal parabolic megadune complexes in northeastern Australia, in: Aeolian Sediments. Ancient and Modern. Blackwell Scientific Publications.

Pye, K., Tsoar, H., 2009. Aeolian sand and sand dunes. Springer, Berlin.

Rawling, J.E., Hanson, P.R., Young, A.R., Attig, J.W., 2008. Late Pleistocene dune construction in the Central Sand Plain of Wisconsin, USA. Geomorphology 100, 494–505. https://doi.org/10.1016/j.geomorph.2008.01.017

Reffet, E., Courrech du Pont, S., Hersen, P., Douady, S., 2010. Formation and stability of transverse and longitudinal sand dunes. Geology 38, 491–494. https://doi.org/10.1130/G30894.1

Reitz, M.D., Jerolmack, D.J., Ewing, R.C., Martin, R.L., 2010. Barchan-parabolic dune pattern transition from vegetation stability threshold: DUNE PATTERN TRANSITION FROM THRESHOLD. Geophysical Research Letters 37, n/a-n/a. https://doi.org/10.1029/2010GL044957

Schaetzl, R.J., Enander, H., Luehmann, M.D., Lusch, D.P., Fish, C., Bigsby, M., Steigmeyer, M., Guasco, J., Forgacs, C., Pollyea, A., 2013. Mapping the physiography of Michigan with GIS. Physical Geography 34, 2–39.

Schaetzl, R.J., Lepper, K., Thomas, S.E., Grove, L., Treiber, E., Farmer, A., Fillmore, A., Lee, J., Dickerson, B., Alme, K., 2017. Kame deltas provide evidence for a new glacial lake and suggest early glacial retreat from central Lower Michigan, USA. Geomorphology 280, 167–178. https://doi.org/10.1016/j.geomorph.2016.11.013

Schaetzl, R.J., Weisenborn, B.N., 2004. The Grayling Fingers region of Michigan: soils, sedimentology, stratigraphy and geomorphic development. Geomorphology 61, 251–274. https://doi.org/10.1016/j.geomorph.2004.01.002

Sjogren, D.B., Fisher, T.G., Taylor, L.D., Jol, H.M., Munro-Stasiuk, M.J., 2002. Incipient tunnel channels. Quaternary International 90, 41–56. https://doi.org/10.1016/S1040-6182(01)00091-X

Smith, M.J., Clark, C.D., 2005. Methods for the visualization of digital elevation models for landform mapping. Earth Surface Processes and Landforms 30, 885–900. https://doi.org/10.1002/esp.1210

Torrence, C., Compo, G.P., 1998. A Practical Guide to Wavelet Analysis. Bulletin of the American Meteorological Society 79, 61–78. https://doi.org/10.1175/1520-0477(1998)079<0061:APGTWA>2.0.CO;2

Warren, A., 2013. Dunes: dynamics, morphology, history, RGS-IBG book series. John Wiley & Sons Inc, Chichester, West Sussex.

Weiss, A., 2001. Topographic position and landforms analysis. Presented at the ESRI user conference, San Diego, CA.

Wernette, P., Thompson, S., Eyler, R., Taylor, H., Taube, C., Medlin, A., Decuir, C., Houser, C., 2018. Defining Dunes: Evaluating How Dune Feature Definitions Affect Dune Interpretations from Remote Sensing. Journal of Coastal Research 34, 1460. https://doi.org/10.2112/JCOASTRES-D-17-00082.1

Wilson, J.P., 2012. Digital terrain modeling. Geomorphology 137, 107–121. https://doi.org/10.1016/j.geomorph.2011.03.012

Wolfe, S.A., David, P.P., 1997. Parabolic Dunes: Examples from the Great Sand Hills, southwestern Saskatchewan. Canadian Geographer, Canadian Landfrom Examples 41, 207–213.

Wolfe, S.A., Hugenholtz, C.H., 2009. Barchan dunes stabilized under recent climate warming on the northern Great Plains. Geology 37, 1039–1042.

Wu, Q., Guo, F., Li, H., 2018. Wavelet-Based Correlation Identification of Scales and Locations between Landscape Patterns and Topography in Urban-Rural Profiles: Case of the Jilin City, China. Remote Sensing 10, 1653. https://doi.org/10.3390/rs10101653

Yan, N., Baas, A.C.W., 2017. Environmental controls, morphodynamic processes, and ecogeomorphic interactions of barchan to parabolic dune transformations. Geomorphology 278, 209–237. https://doi.org/10.1016/j.geomorph.2016.10.033

Yan, N., Baas, A.C.W., 2015. Parabolic dunes and their transformations under environmental and climatic changes: Towards a conceptual framework for understanding and prediction. Global and Planetary Change 124, 123–148. https://doi.org/10.1016/j.gloplacha.2014.11.010

APPENDIX A. FIGURES

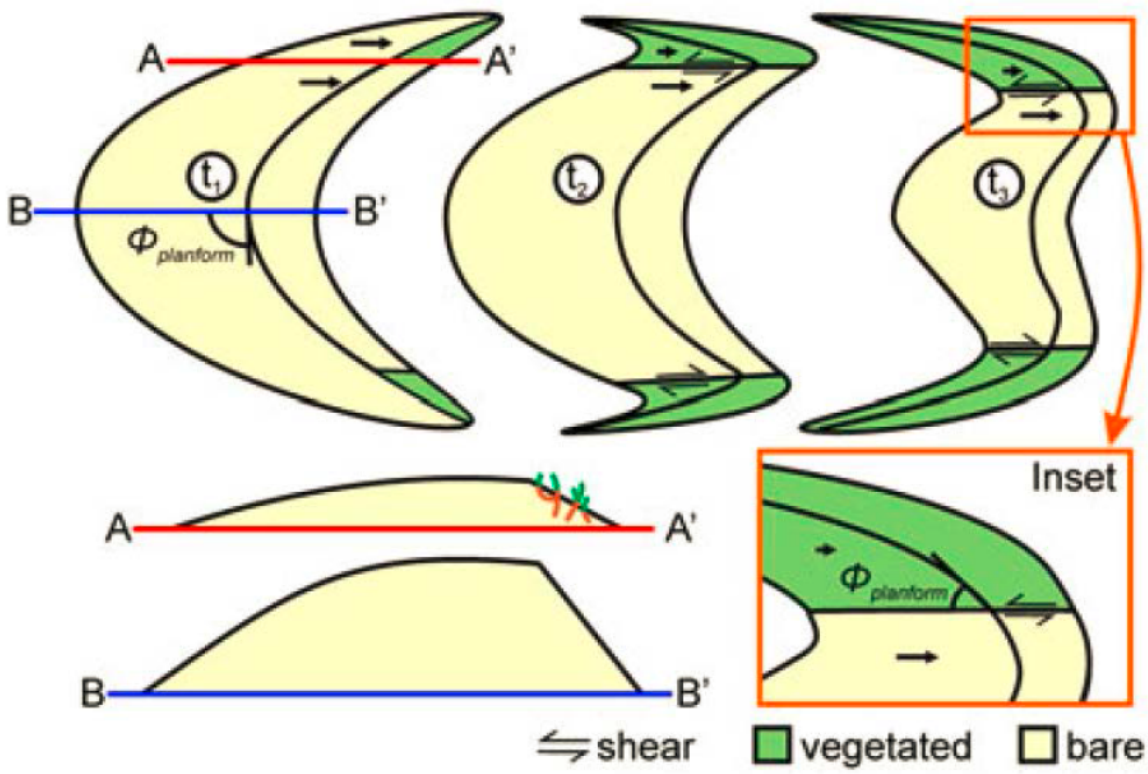

Figure 1 - Is a model of vegetation mediated transition of a dune from a barchan state to an idealized parabolic state in three time steps t_1, t_2 and t_3. Winds are predominantly from left to right. Brinkline angles Ø relate to changes in deposition rates along the developing, upwind pointing arms. Cross sections A and B of the barchan state illustrate pioneering vegetation on the lee slope of the dune horns and the dune slip face. Dune elements from left to right include the stoss slope, the crest, the brinkline and the steeper and straight lee or slip face. (Figure Credit – Barchyn and Hugenholtz, 2012b).

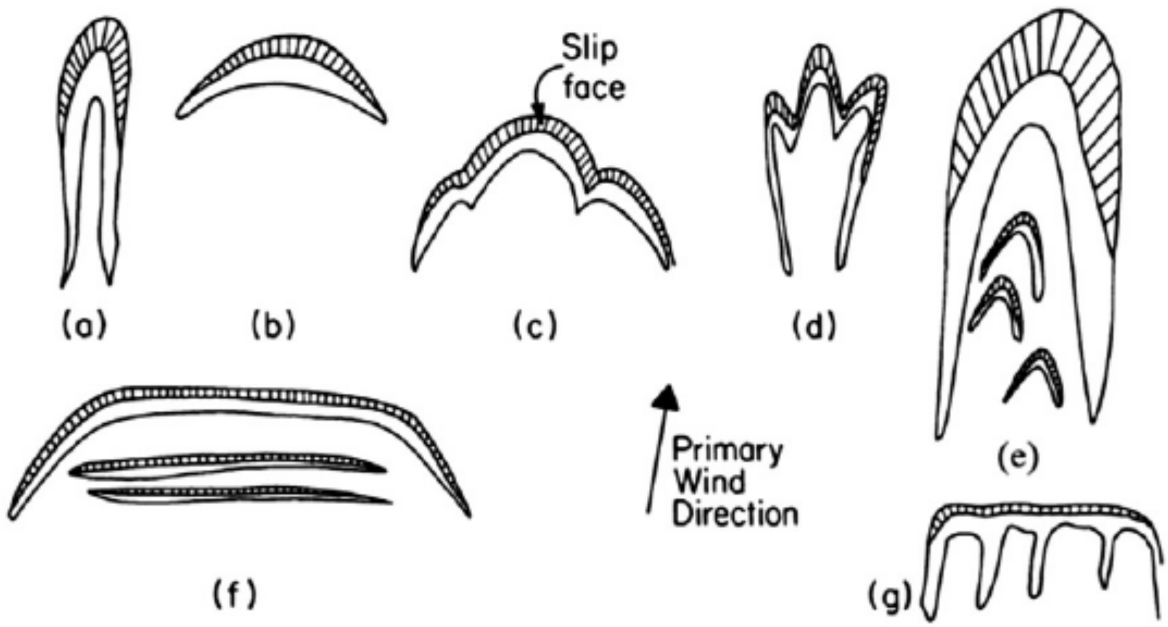

Figure 2 – Parabolic dune pattern classifications including: (a) hairpin; (b) lunate; (c) hemicyclic; (d) digitate; (e) nested; (f) long-walled transgressive ridge; and (g) rake-like. The hemicyclic, lunate, nested and rake-like dunes are examples of complex dunes. The transgressive ridge is a compound dune. (Source: Pye and Tsoar, 2009). A windrift form would follow elongation of a hairpin form followed by a blowout of the downwind apex.

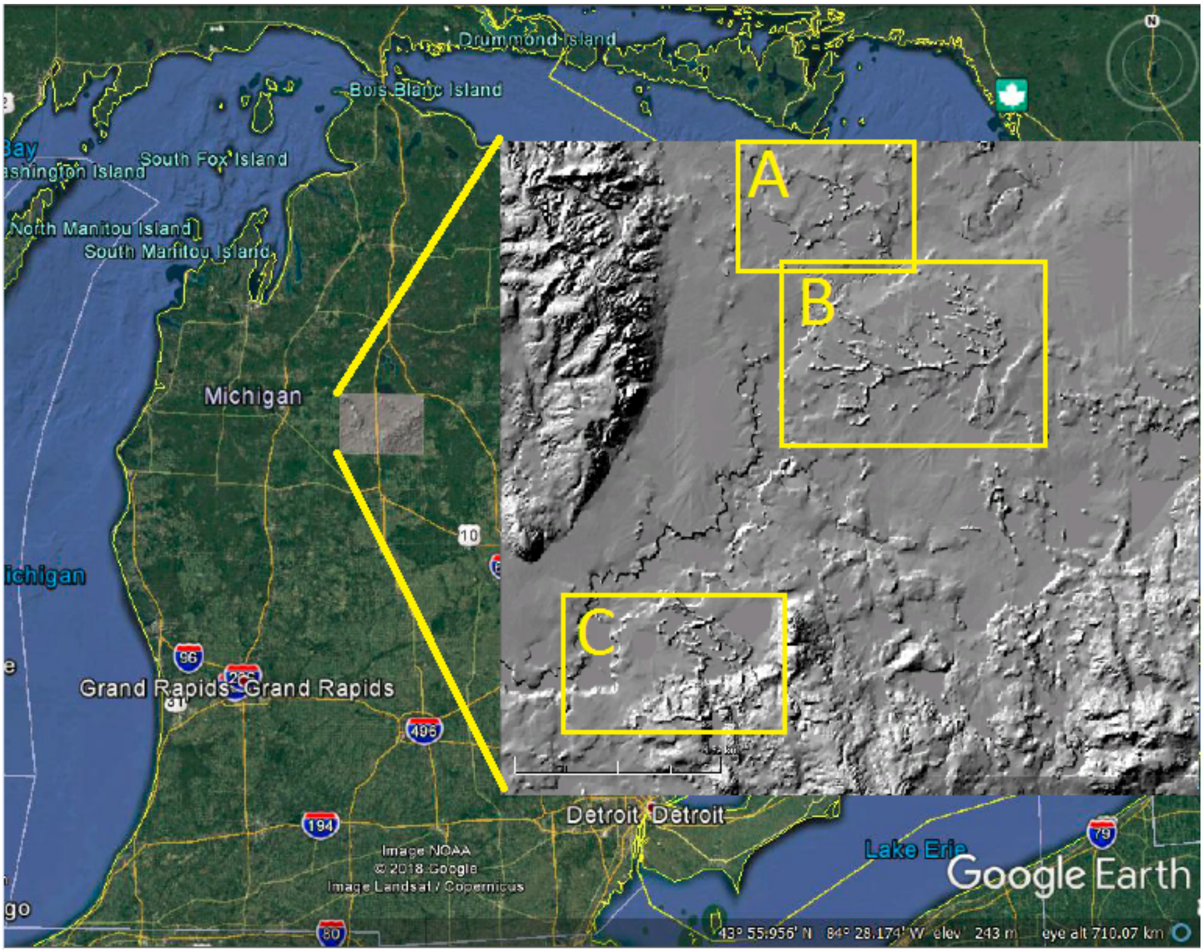

Figure 3 – The study areas are located in north central Michigan and include portions of the Houghton Lake Basin, the Harrison-Lake City Ridges and the Muskegon River valley. The Houghton Lake Basin is a glacio-lacustrine plain in the northeast quarter of the inset. The Harrison-Lake City Ridges, an ice contact ridge, extend across the basin from the southeast to the northwest. The study areas are: (A) the Rosco Wolf Dune Complex; (B) the Rosco Main Dune Complex; and (C) the Clare Dune Field.

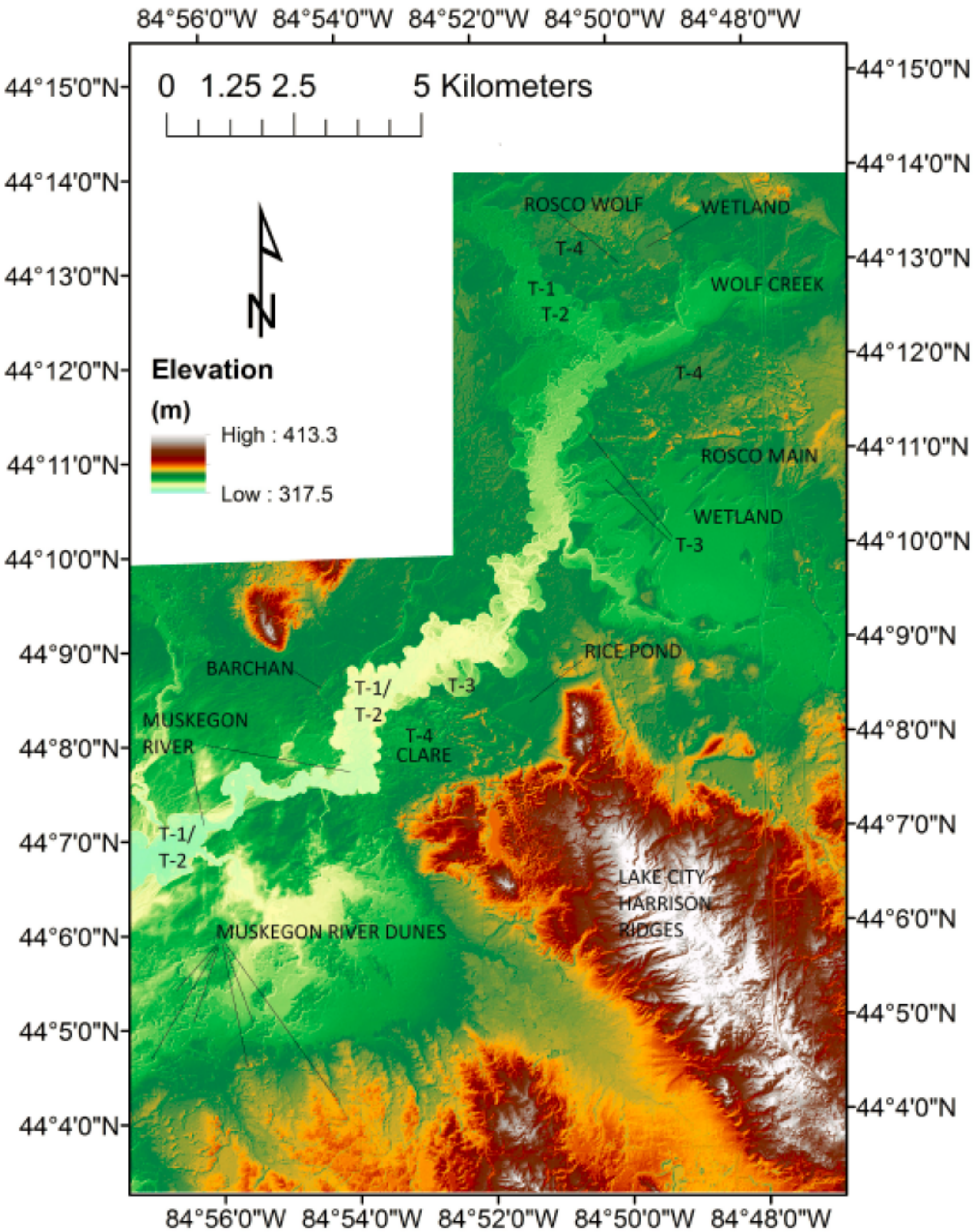

Figure 4 - Terraces of the Muskegon River Valley per Arbogast et al., 2008 and other terrain features of the study area. The Rosco Main, Rosco Wolf and Clare Dune Fields lie above and to the east of the modern river valley (T-1 and T-2 terraces) on the T-4 terrace and higher ground. The T-3 terrace corresponds to relic oxbows cut into the T-4 terrace and postdates the dunes. The Muskegon River Dunes are scattered dunes near the study area fields.

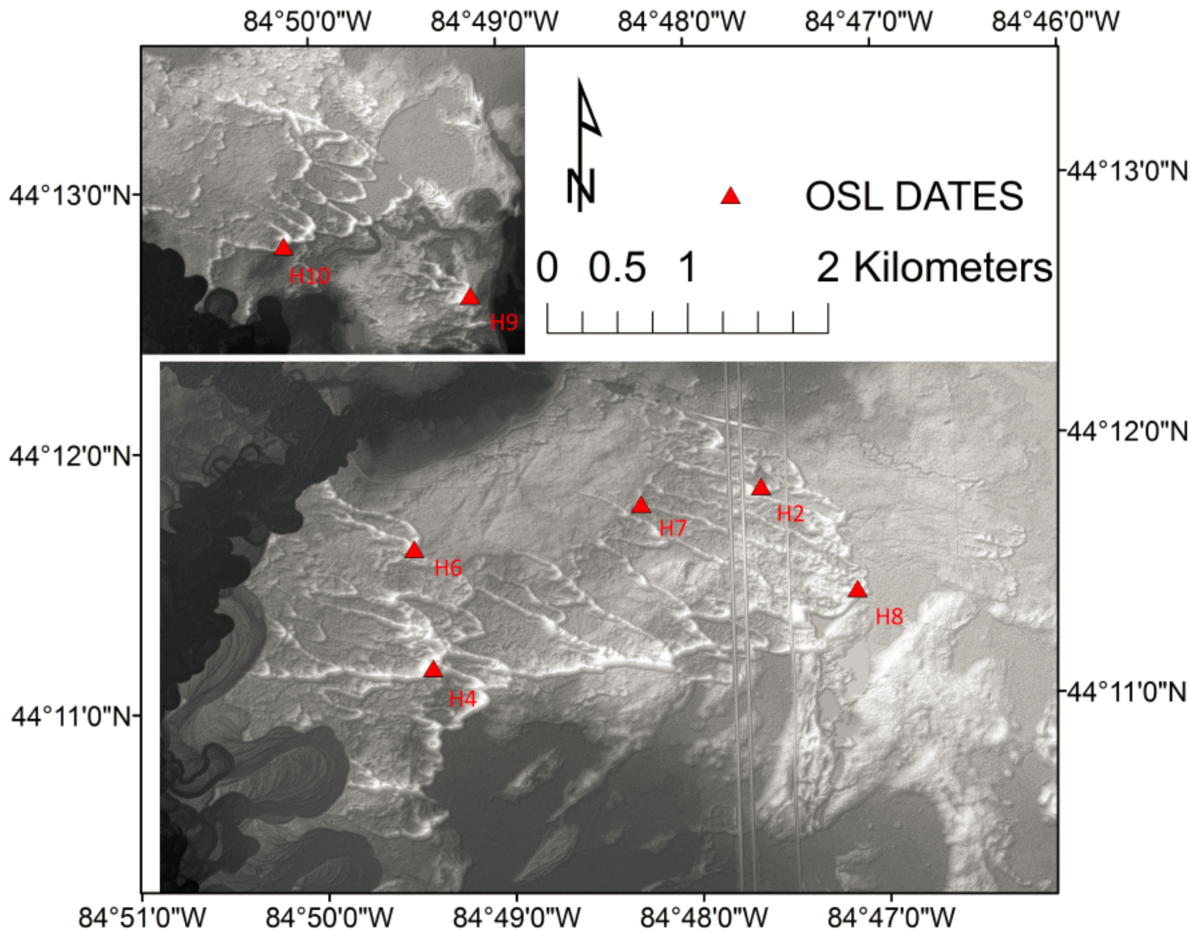

Figure 5 – Shows the approximate sample locations used for OSL dating by Arbogast et al. (2015) superimposed on analytical-hillshade images of the RW and RM complexes of the Rosco Dune Field. The estimated ages are compiled in Table 1 with the oldest corresponding to H10 in the extreme north and the youngest in the extreme southwest at H4. The RW and RM complexes are imaged at the same scale and in the proper spatial locations relative to one another.

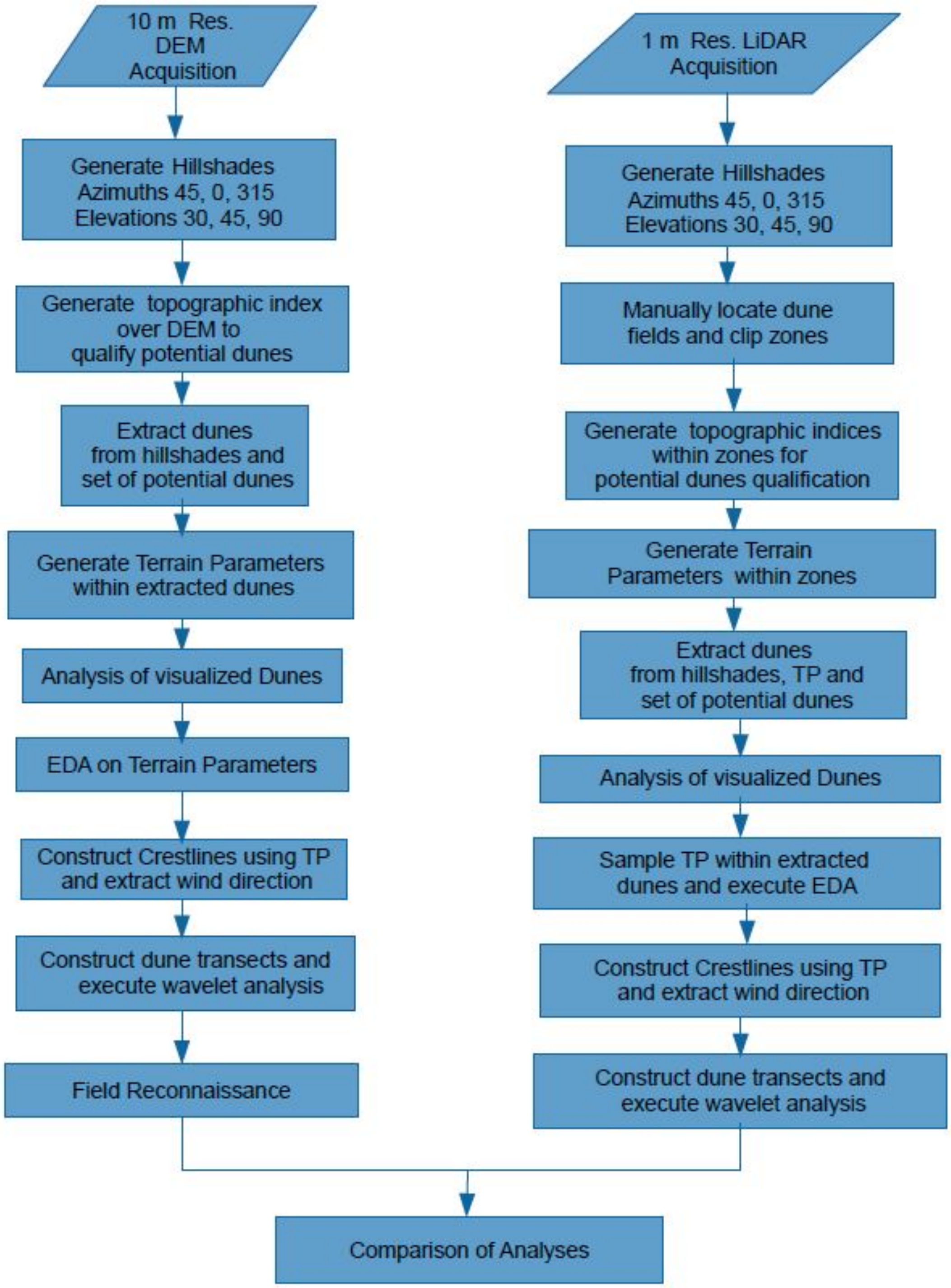

Figure 6 – The methodology workflow.

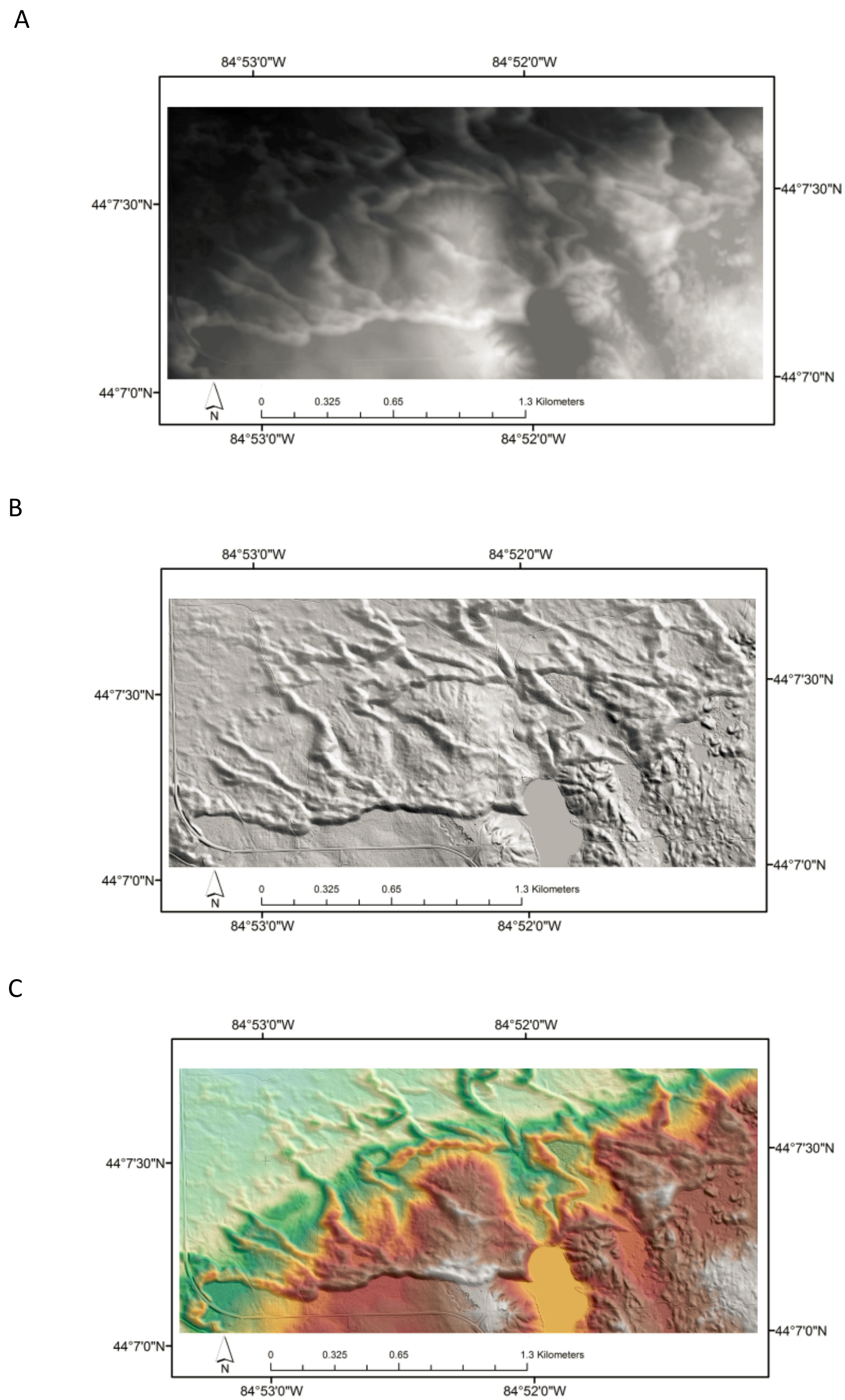

Figure 7 – A comparison of two dimensional visualizations generated from a digital elevation model of the Upper Clare lobe of the Clare Dune Field including: (A) A gray-scale image; (B) An analytical hillshade with vertical exaggeration; and, (C) Hypsometric color tinting blended with an analytical-hillshade.

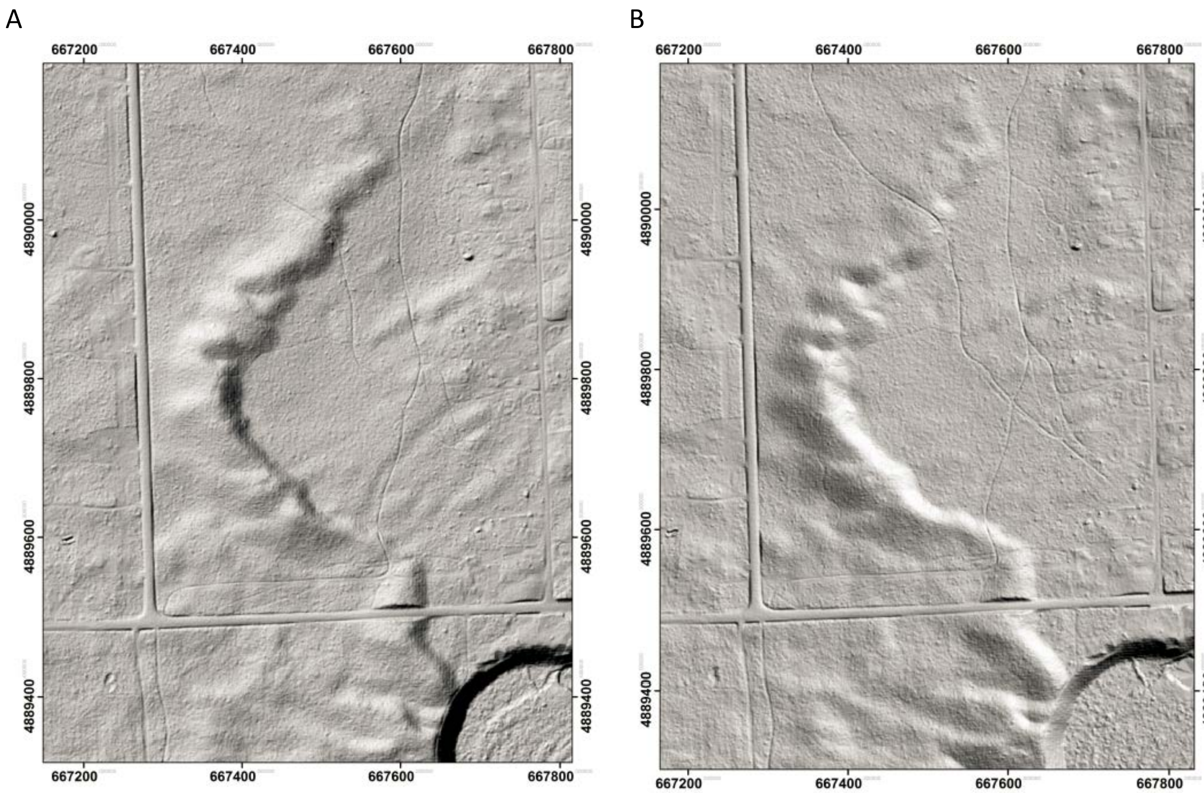

Figure 8 – Positioning of the illumination source in analytical-hillshade visualizations can be an important step in recognition of landforms. Image (A) is an analytical-hillshade visualization of a barchan dune west of the CDF. The illumination source is placed at azimuth 315°, an elevation of 45° and a vertical exaggeration of 4. (B) Another analytical-hillshade visualization of the same barchan dune, but with the illumination source positioned at azimuth 45°. Elevation and exaggeration are unchanged. The northern horn of the dune is twice as long as the southern horn, however, this is readily apparent only in image (A). Most hillshading in the present study used an azimuth of 45°. A second dune appears appended to the southern tip of the southern horn. A very faint, crescent-like bulge may be present in the southern horn, which if present, suggests that extension of the northern horn was the product of an off-center collision. Coordinates are for UTM Zone 16N with eastings across the horizontal axis.

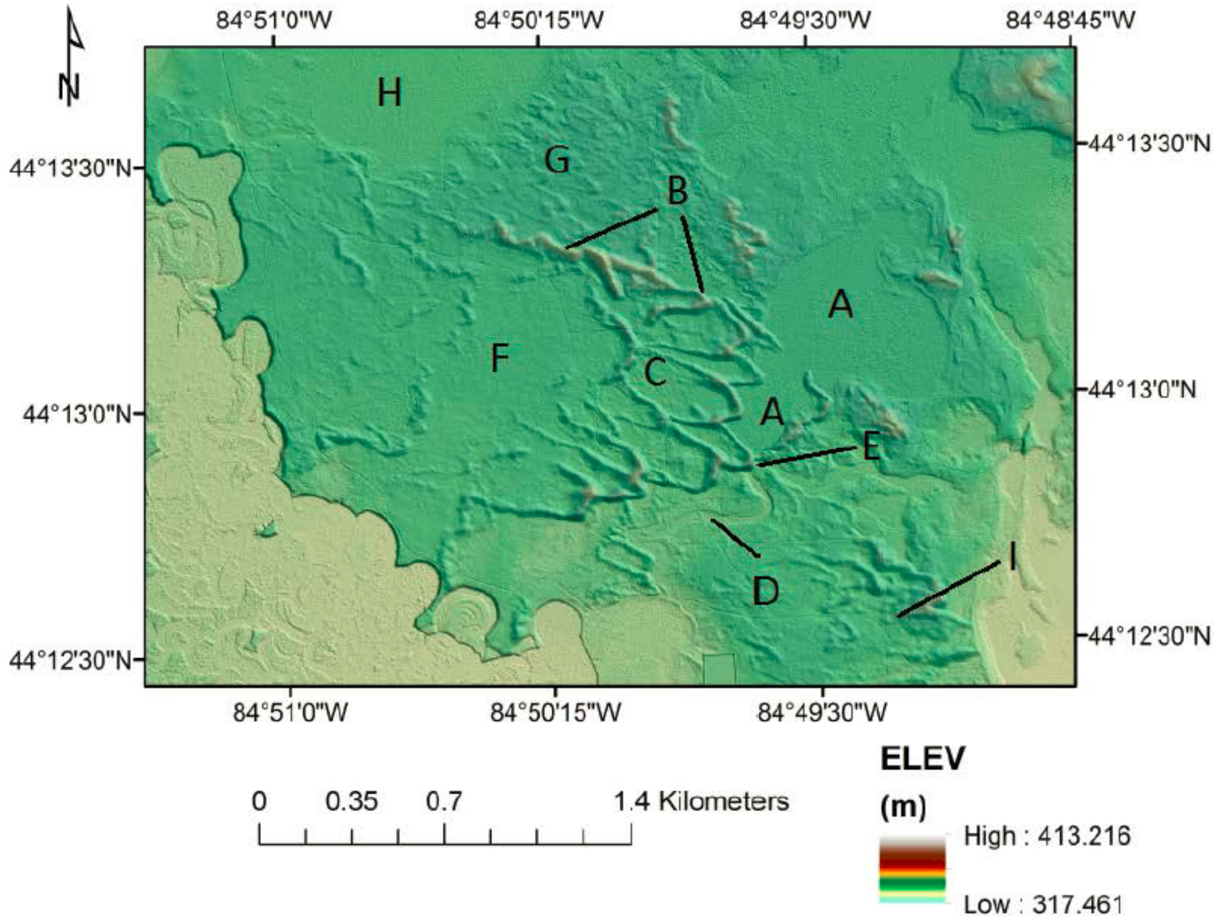

Figure 9 – The RW Complex includes a possible wetland "A", a ridge "B", compound parabolic dunes "C" with dunes superimposed on other dunes, a stream course "D" interdicted by a dune apex "E" and a possible deflation plain "F". Simple, smaller parabolic dunes "G" lie to the north of ridge "B" and to the southeast of a wetland "H". Wetland "H" may be a former lake bed. "I" are possible compound dunes.

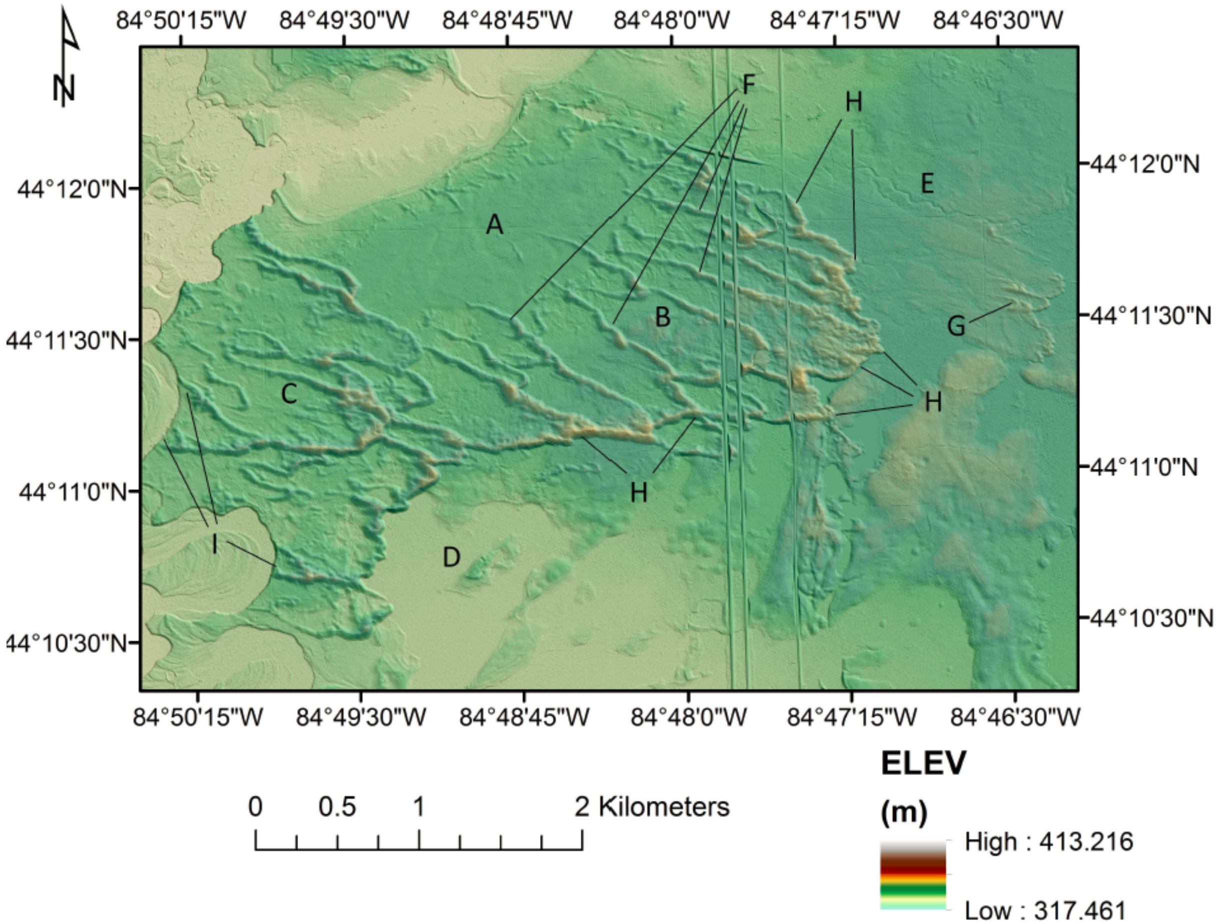

Figure 10 – The RM Complex is imaged with a hypsometrically-tinted layer, draped over an analytical-hillshade. Area "A" is interpreted as a deflation plane. The complex comprises two lobes, a "B" lobe located downwind from plain "A" and a "C" lobe to the southwest of lobe "B". The "C" lobe is located between the T-2 and T-3 terraces to the west and a wetland "D" to the southeast. The terraces crosscut dune arms of the "C" lobe suggesting that a possible deflation plain formerly existed to the west of this lobe. Lobe "B" extends onto uplands "E" and includes a plurality of elongated, sub-parallel ridges "F". The ridges "F" of lobe "B" join a dune complex or ridge line "H". A small group of parabolic dunes "G" lie about 1 km to the east of ridge "H". Crosscut dunes "I" are visible adjacent paleo-meanders of the T-3 terrace.

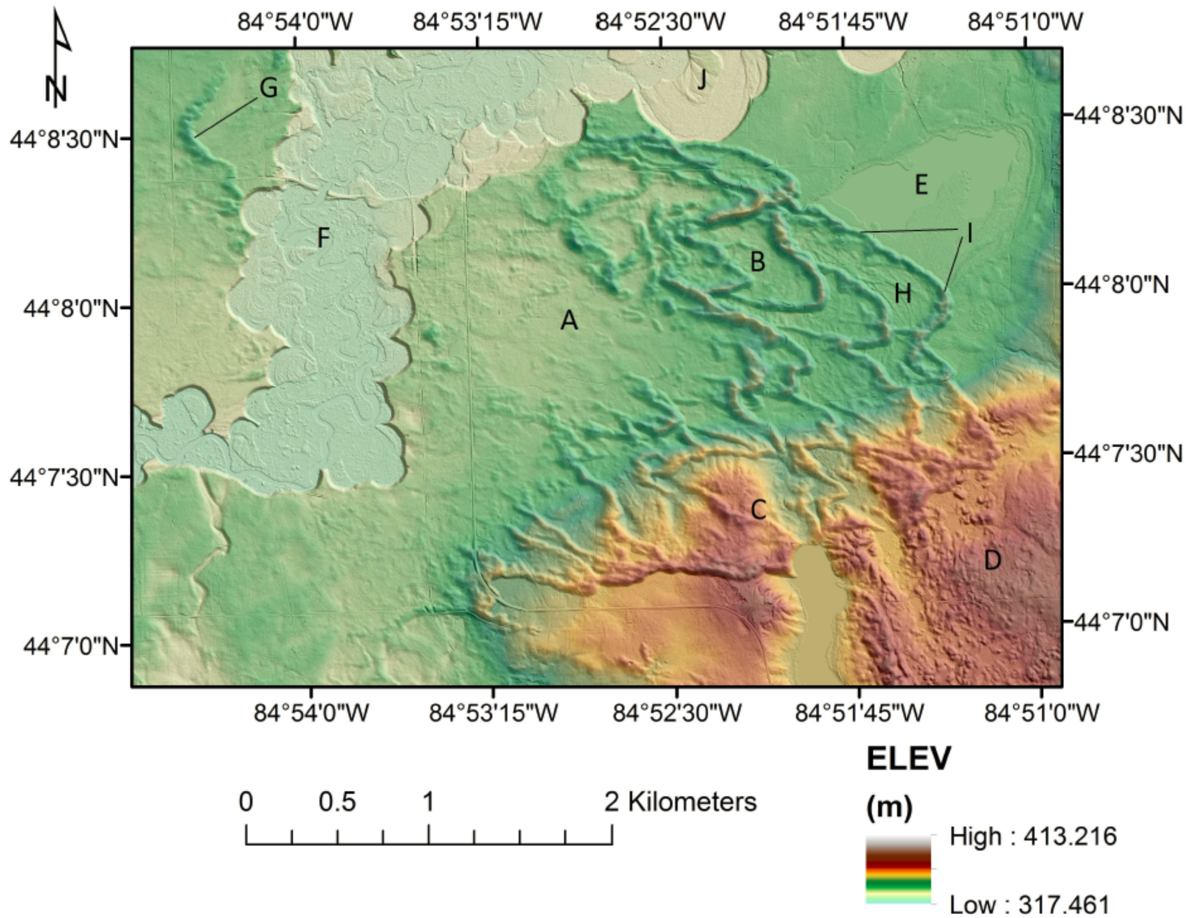

Figure 11 – The Clare Dune Field includes a possible deflation plain "A" west of the lower Clare "B" sub-unit and north of the upper Clare "C" sub-unit. Sub-unit "C" has climbed onto the Lake City-Harrison Ridges "D". Rice Pond and adjacent wetlands "E" border a ridge "I". The ridge, possibly formed by part or parts of one or more parabolic dunes, partially encloses a series of low relief ridges "H". The modern valley "F" of the Muskegon River separates the CDF from a possible barchan dune "G" to the west. A portion "J" of the T-3 terrace is visible at the upper center portion of the image.

A

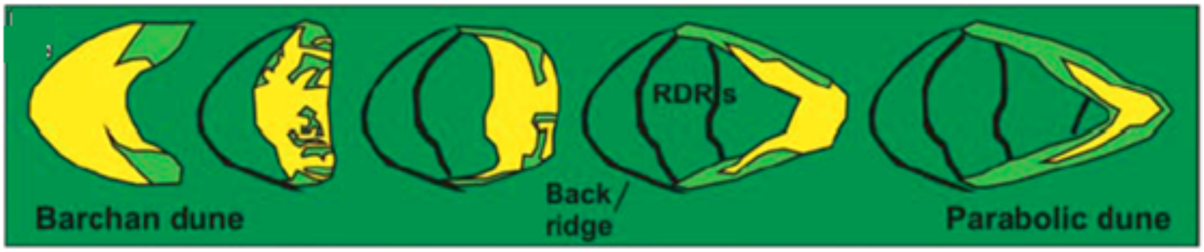

B

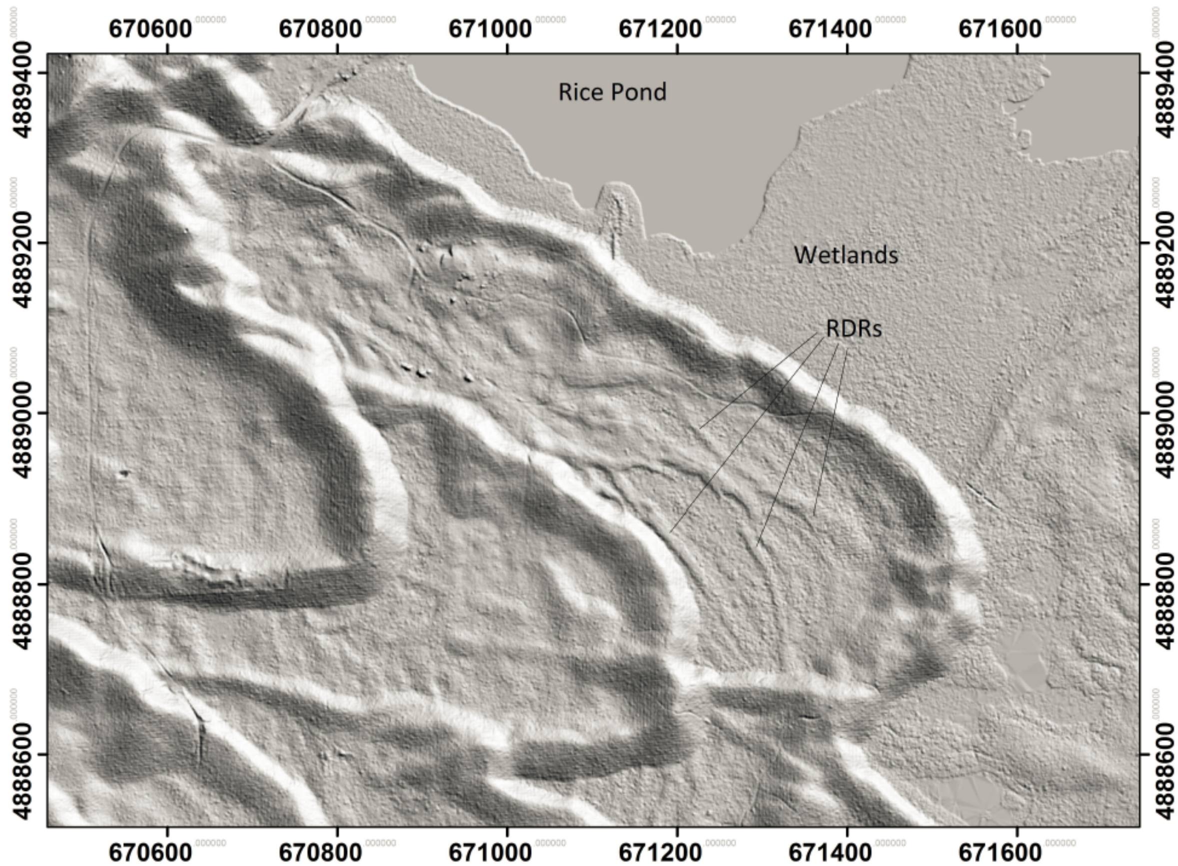

Figure 12 – (A) A cartoon model of residual dune ridges (RDR). RDR are low relief, elongated forms roughly extending from arm to arm within parabolic dunes. They can form as the dune evolves from a barchan form to a parabolic form. RDR have been interpreted as a series of preserved stabilized bases of stoss slopes of a migrating dune (Sources: Levin et al., 2009; Wolf and Hugenholtz, 2009). (B) Detail of the Clare Dune Field adjacent Rice Pond and nearby wetlands suggests possible RDRs within at least dune. A possible cause of these RDRs is seasonal flooding of the intradune area during periods when the dune was at least partially active, probably in a transitional state between a barchan and a parabolic form. Rising groundwater levels would have stabilized the bases of a series of stoss slopes marking former positions of the dune. Measurements are UTM Zone 16N coordinates.

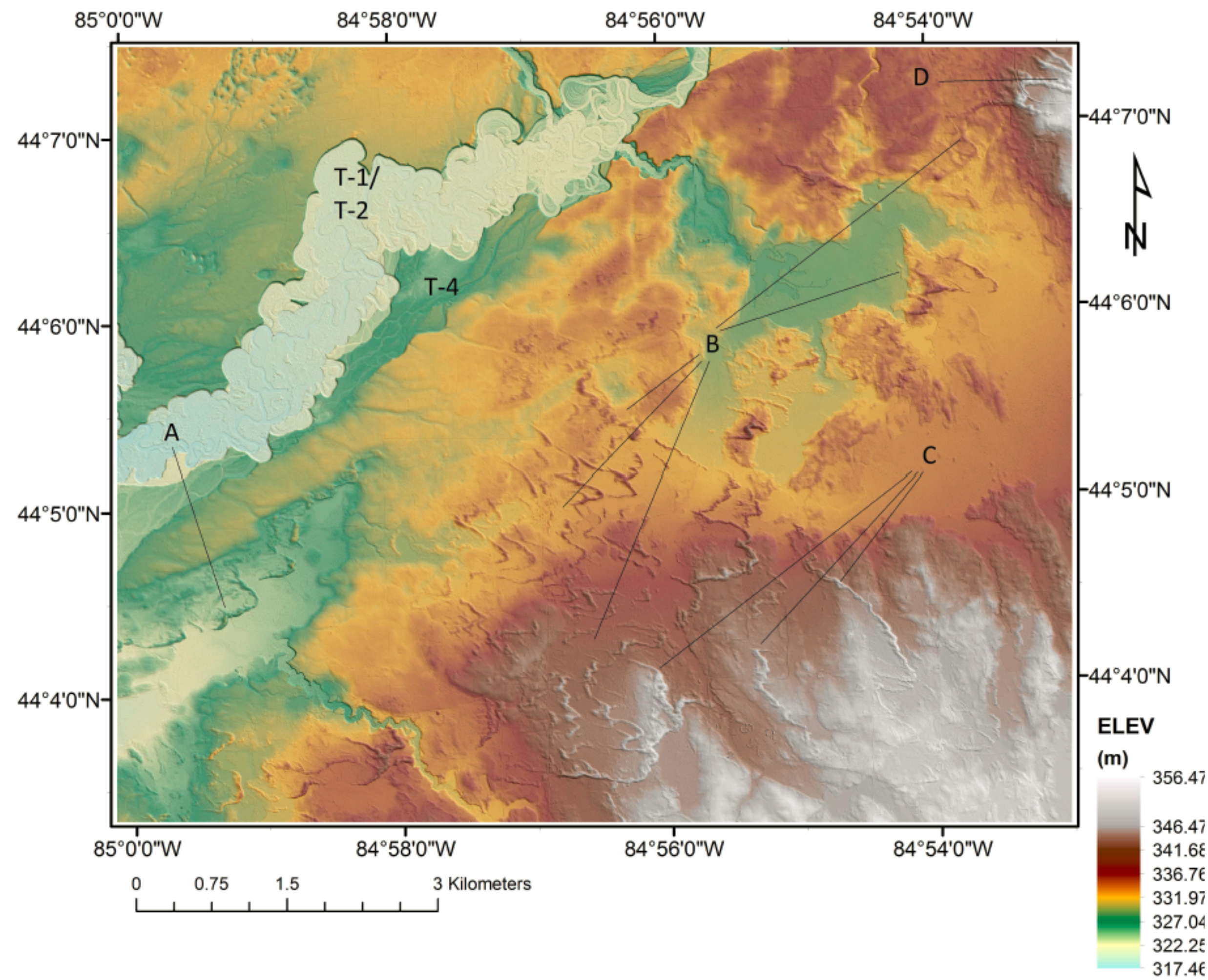

Figure 13 – The MRD is imaged in an analytical-hillshade (4x exaggeration) blended with hypsometric tinting (50% transparency). Only the "A" group dunes are within 2 km of the T-1/T-2 terraces. Dunes "B" and "C" range from ~ 2-7.5 km to the east of the modern Muskegon River Valley. Both the "B" and "C" groups are on uplands well above the T-4 terrace. The "B" group includes more parabolic forms than the "C" group, which includes more elongated forms. The "C" group tends to be at higher elevations than the "B" group and to be located at a greater distance from the modern river. At the extreme northeast corner of the view, dunes labled "D" are part of the Upper Clare sub-unit of the CDF. Relief among the MRD is predominantly in the ~ 2-3 m range, but in rare instances reaches 5 m.

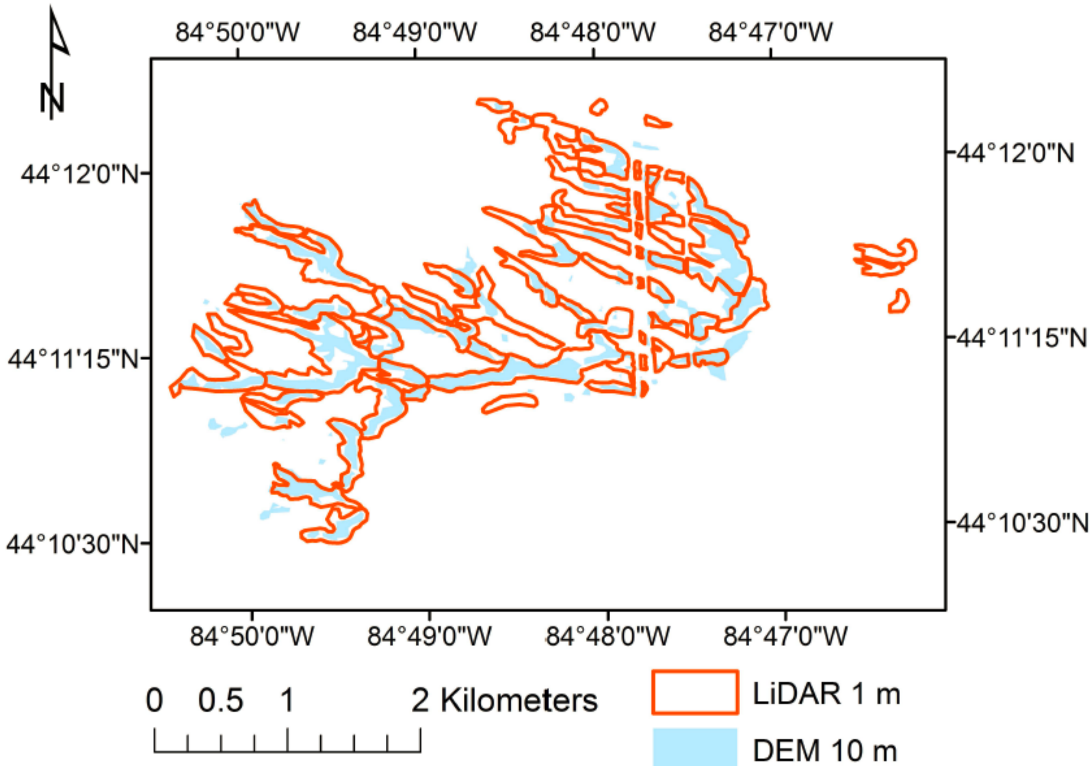

Figure 14 – A comparison of the dune polygons delineated from the LiDAR and DEM datasets for the Rosco Main Complex.

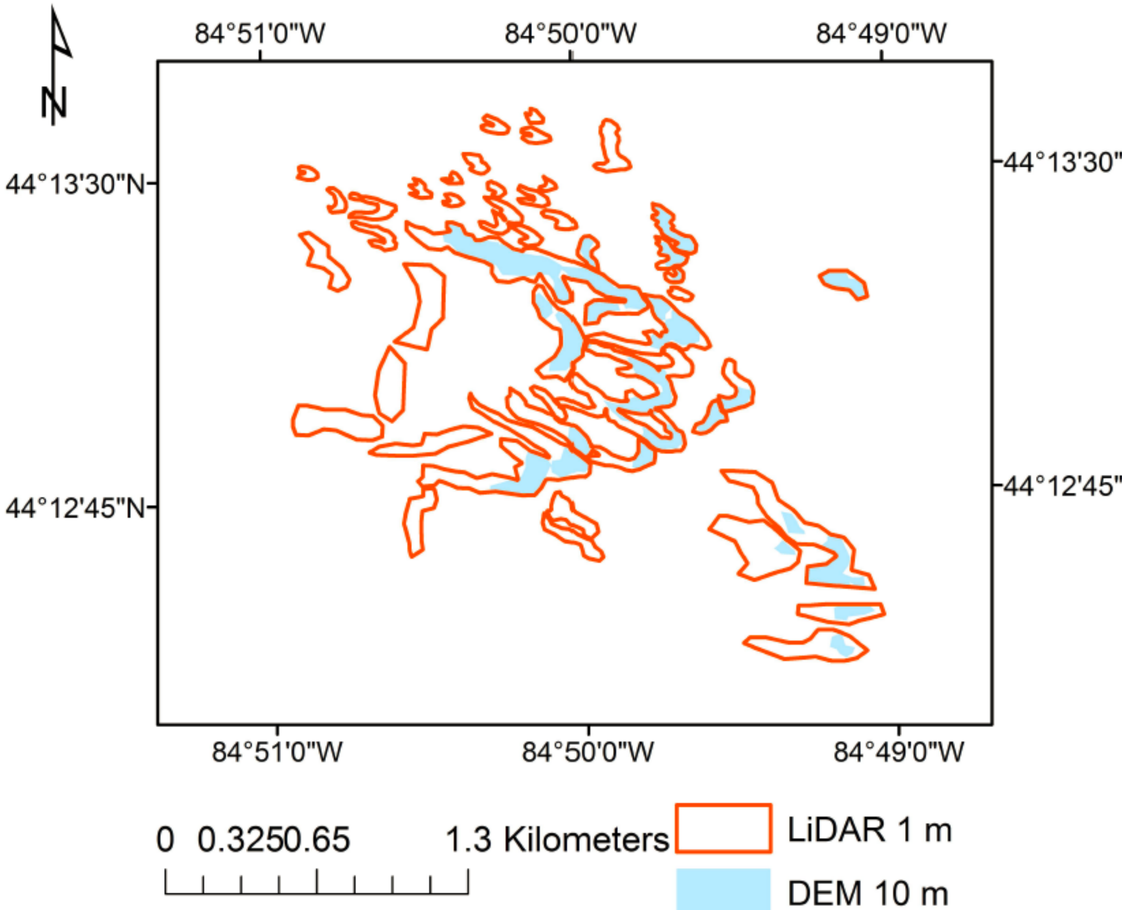

Figure 15 – Comparison of dune polygons derived from the DEM and the LiDAR datasets for Rosco Wolf.

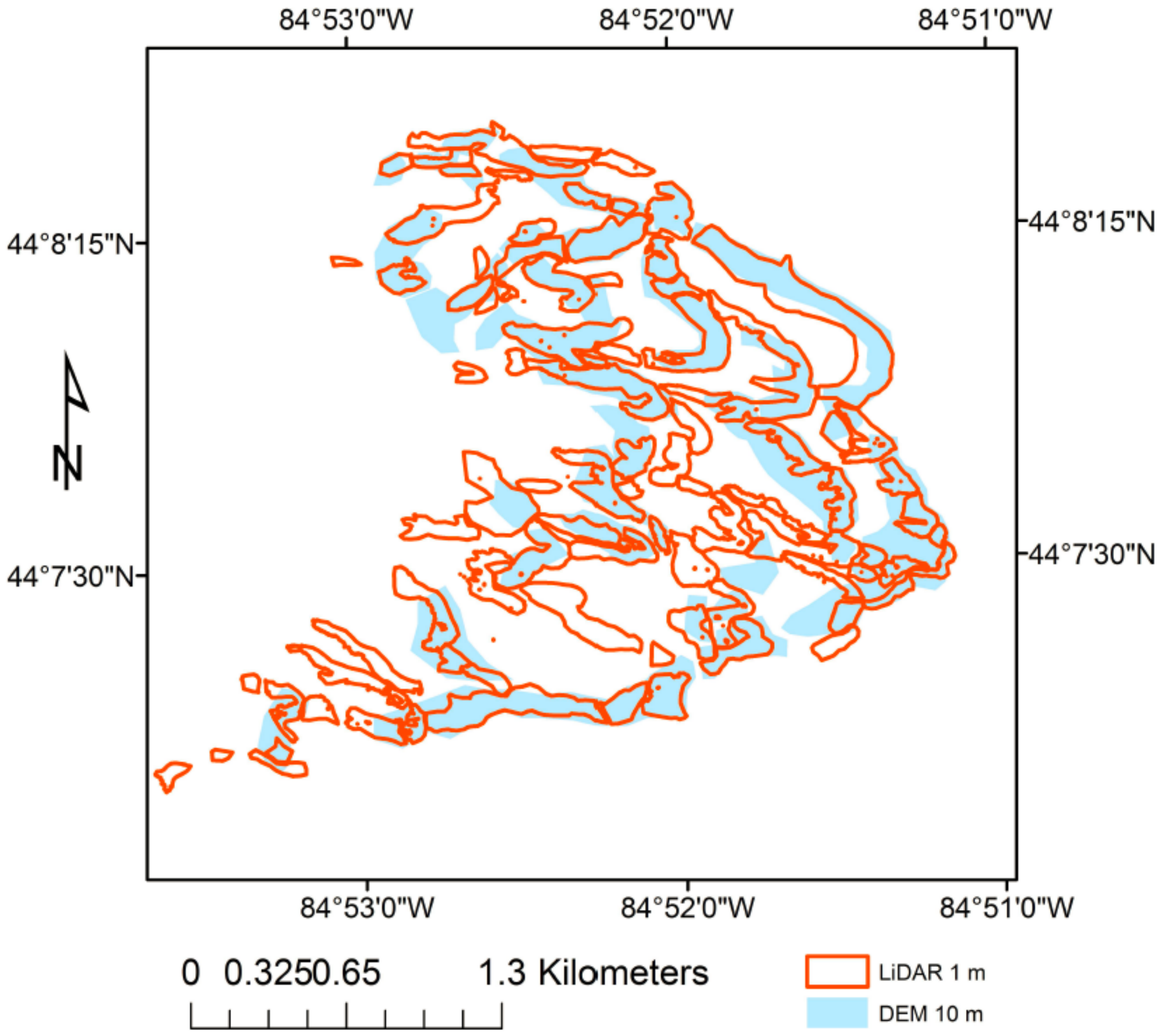

Figure 16 – Comparison of dune polygons derived from the DEM and LiDAR datasets for the Clare Dune Field.

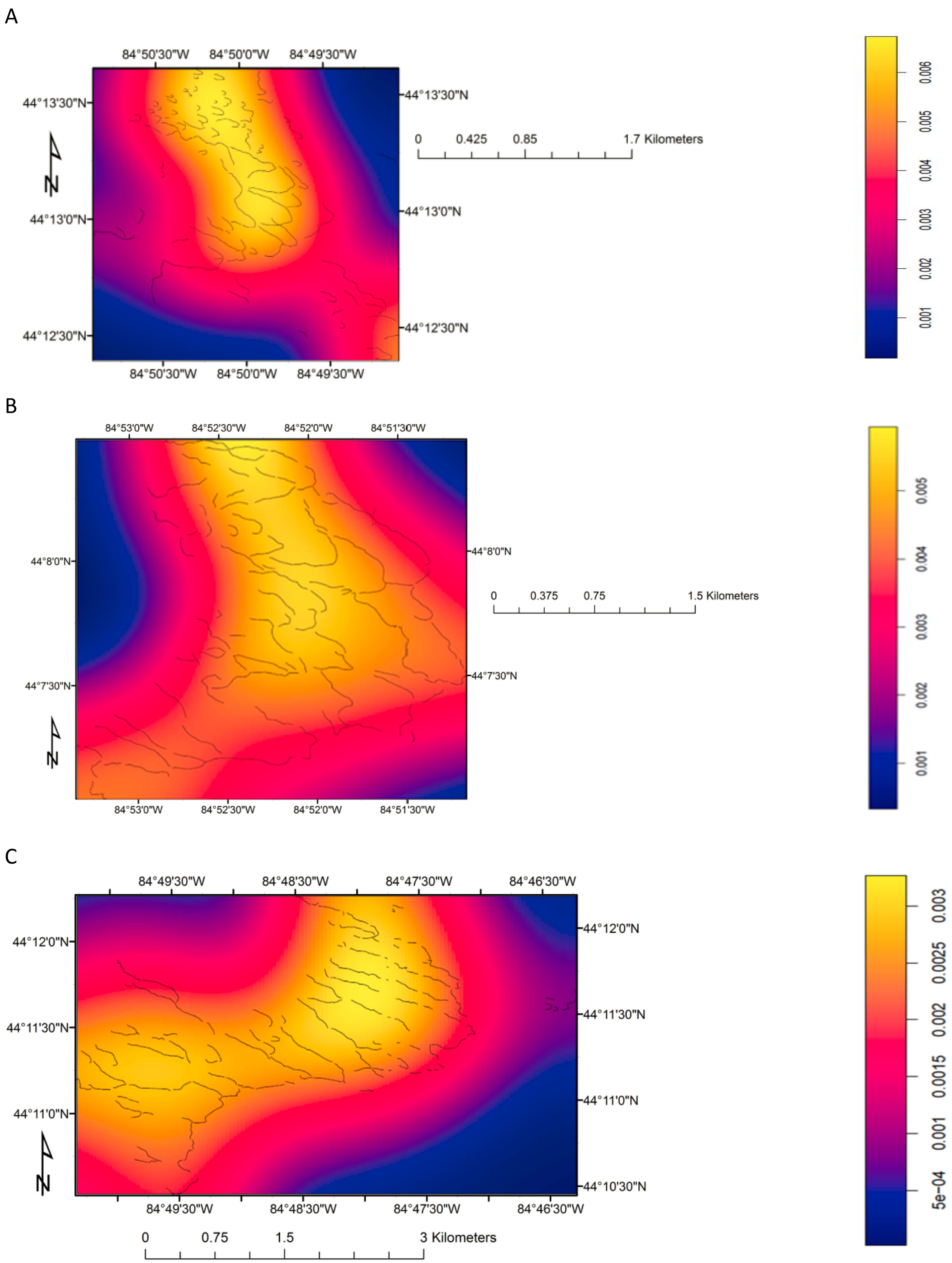

Figure 17 –Illustrates crest lines and crest heat density for the RW complex (A), the CDF (B), and the RM complex. RW and CDF exhibit substantially higher crest densities than does RM.

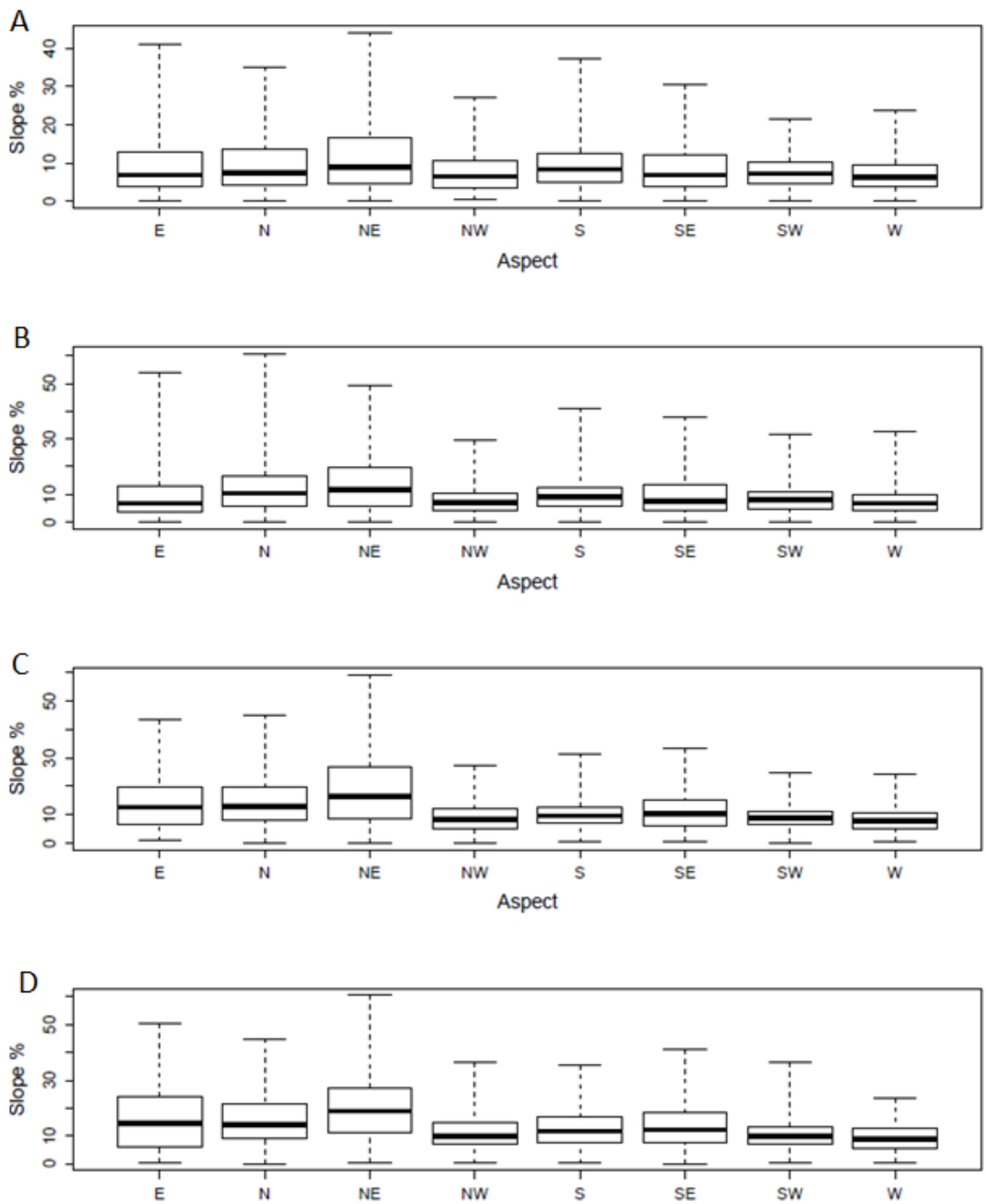

Figure 18 – Boxplot analysis of distribution of slopes by aspect for the LiDAR dataset for Rosco Wolf (A), Rosco Main (B), Lower Clare (C) and Upper Clare (D). The CDF has been divided into Lower and Upper sub-units. Steeper slopes exhibited a tendency to have northeasterly aspects for all divisions.

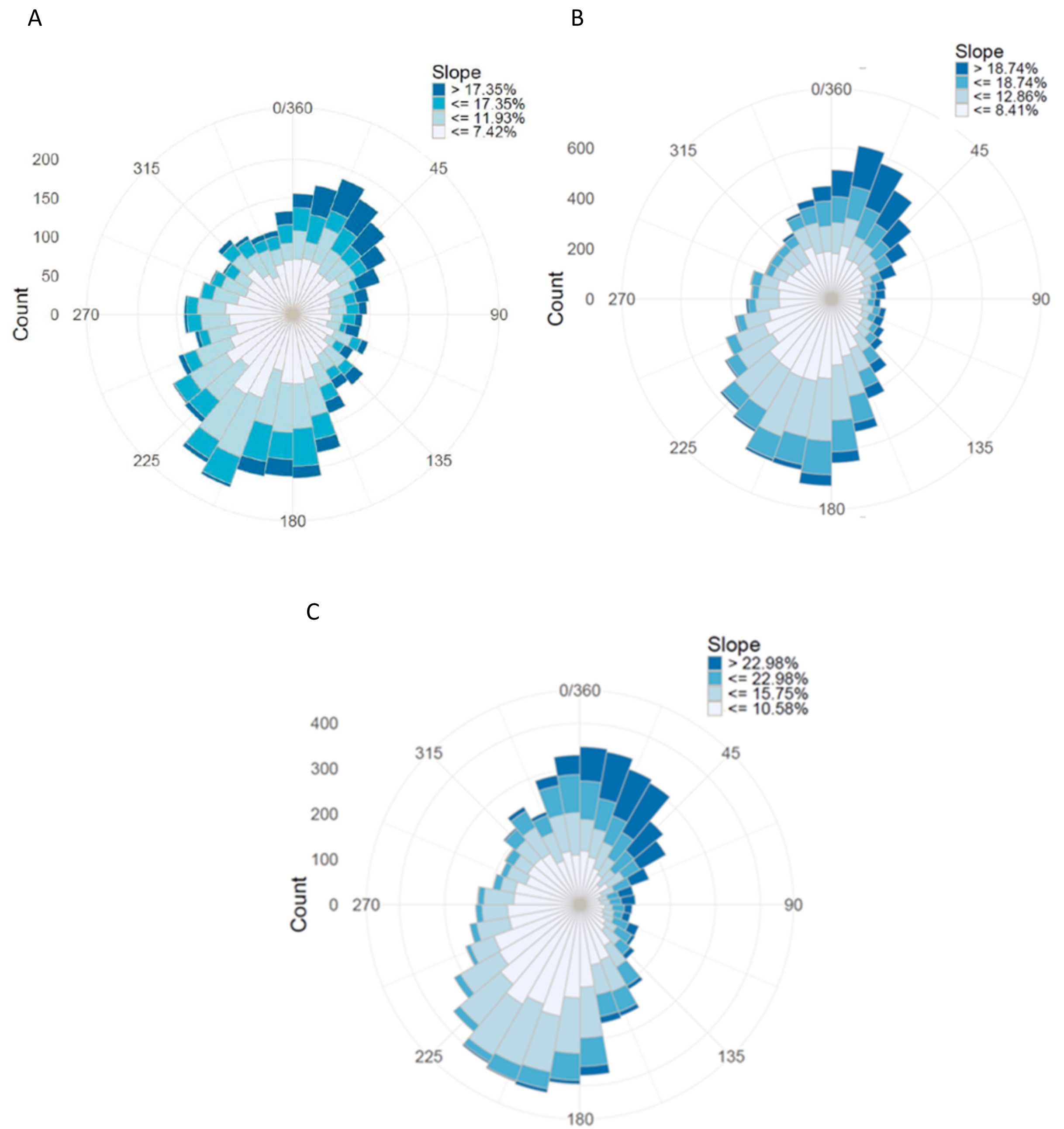

Figure 19 – The aspect distributions of slopes for 50th, 75th, and 90th percentile groups for Rosco Wolf (A), Rosco Main (B), and Clare (C) as derived from the LiDAR dataset. Based on the estimated prevailing wind regime it was expected that slope directions to the southwest and northeast would predominate, particularly for steeper slopes. The greatest area of slopes is oriented toward the southwest, but the distribution bias in the steepest slopes is strongly in favor of the northeastly aspects. This suggests a bimodal wind regime or a difference in preservation trends was at work.

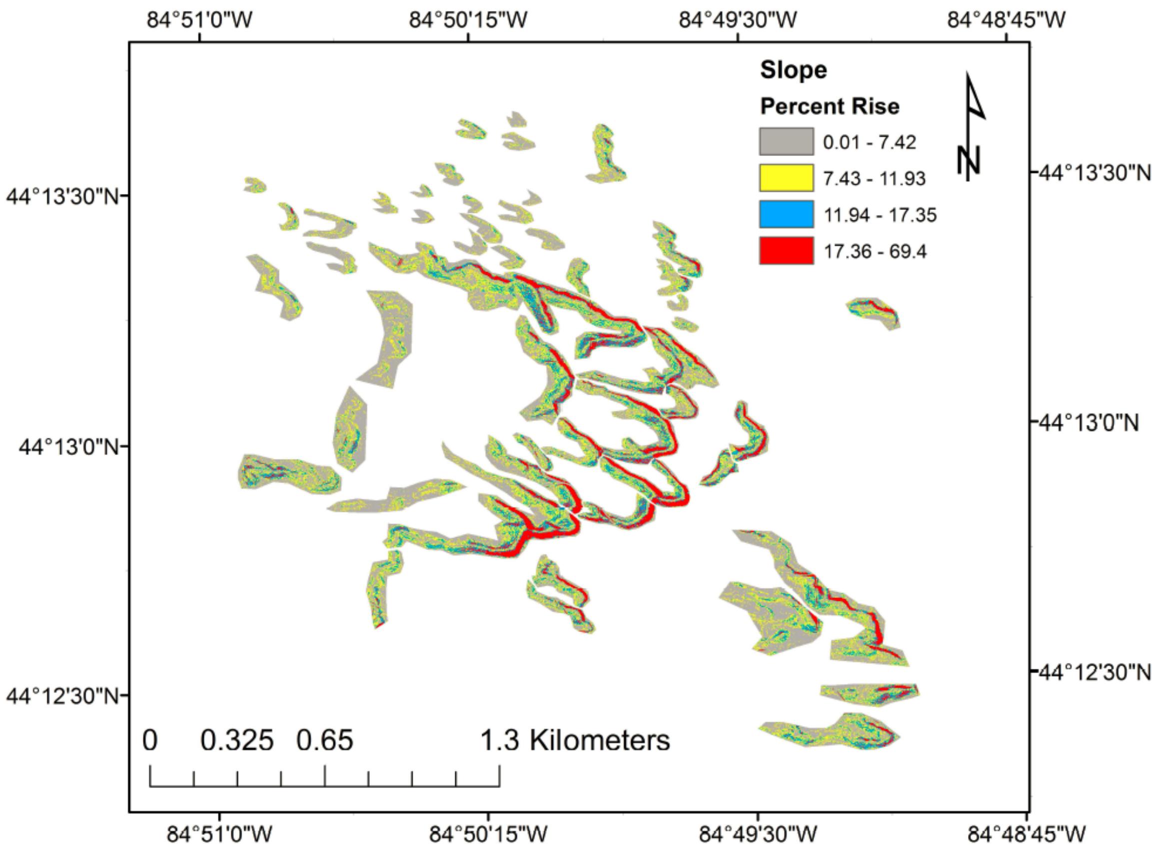

Figure 20 – The distribution of slopes in the RW Complex.

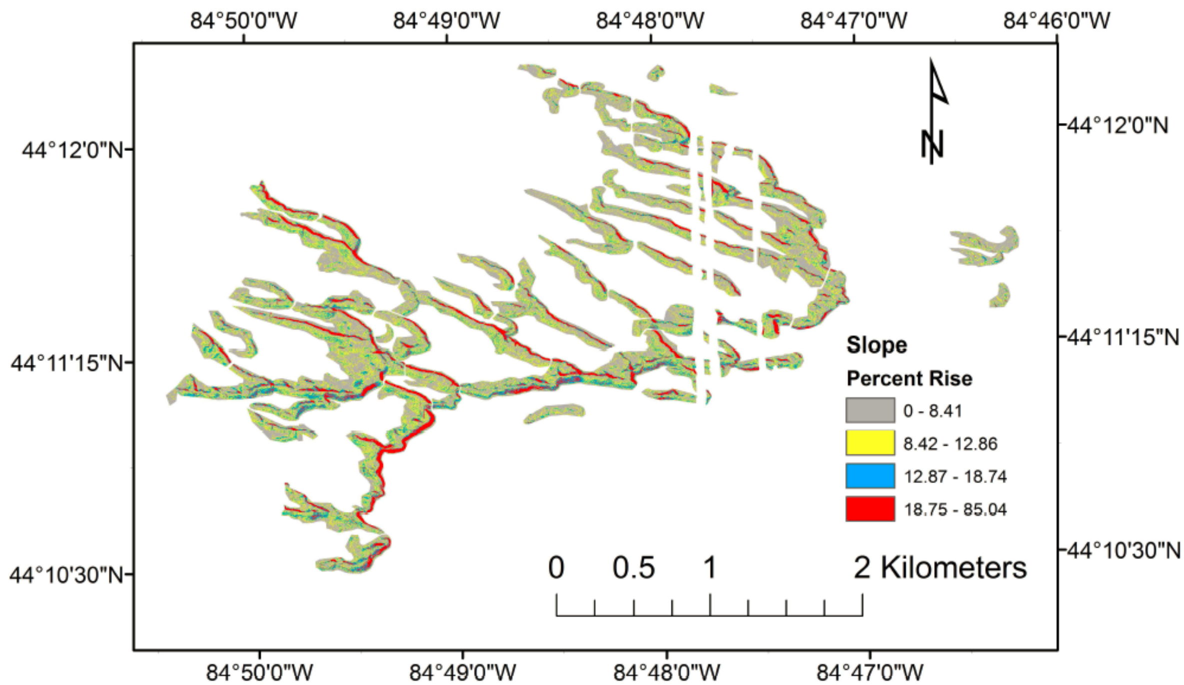

Figure 21 – The distribution of slopes in the RM complex

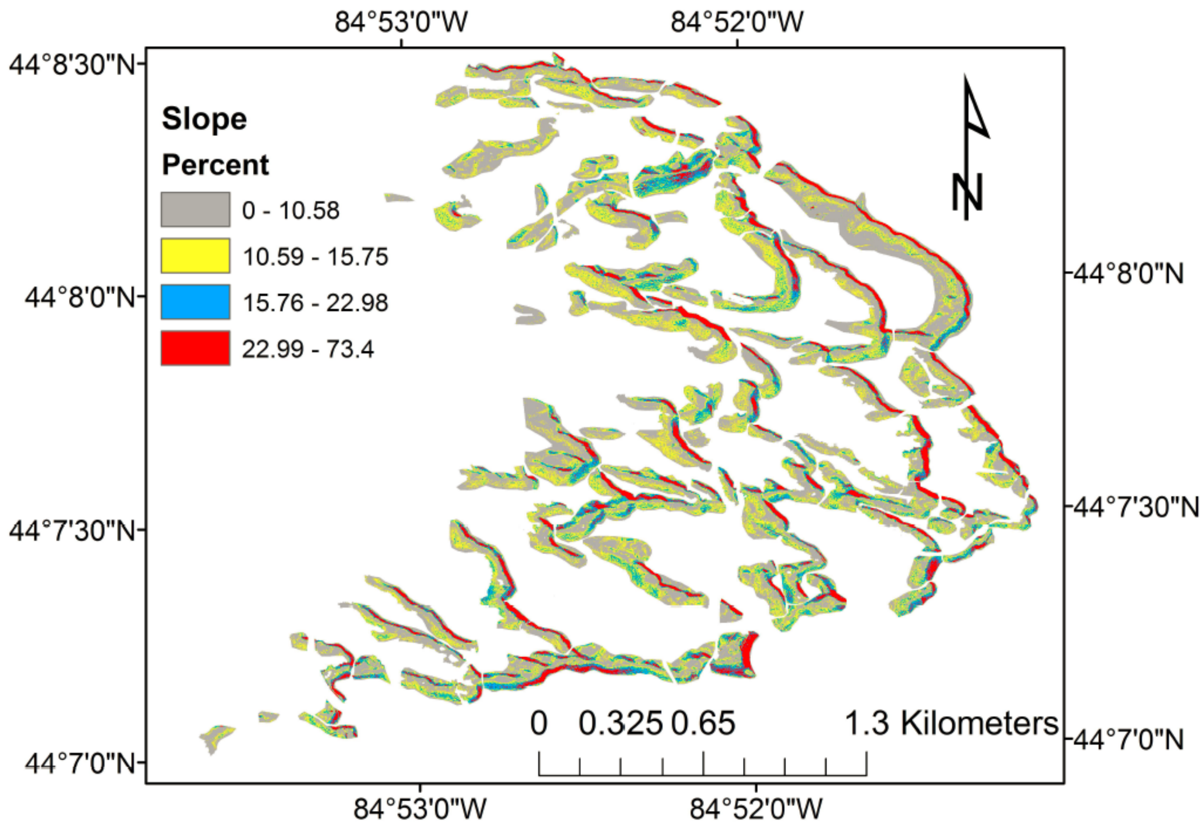

Figure 22 –The location of slopes by percent rise category for the CDF. Northeasterly and easterly orientations are predominant for the steepest category. Many of the parabolic dunes appear to have a fishhook like plan forms, with extensive northern arms and stunted southern arms.

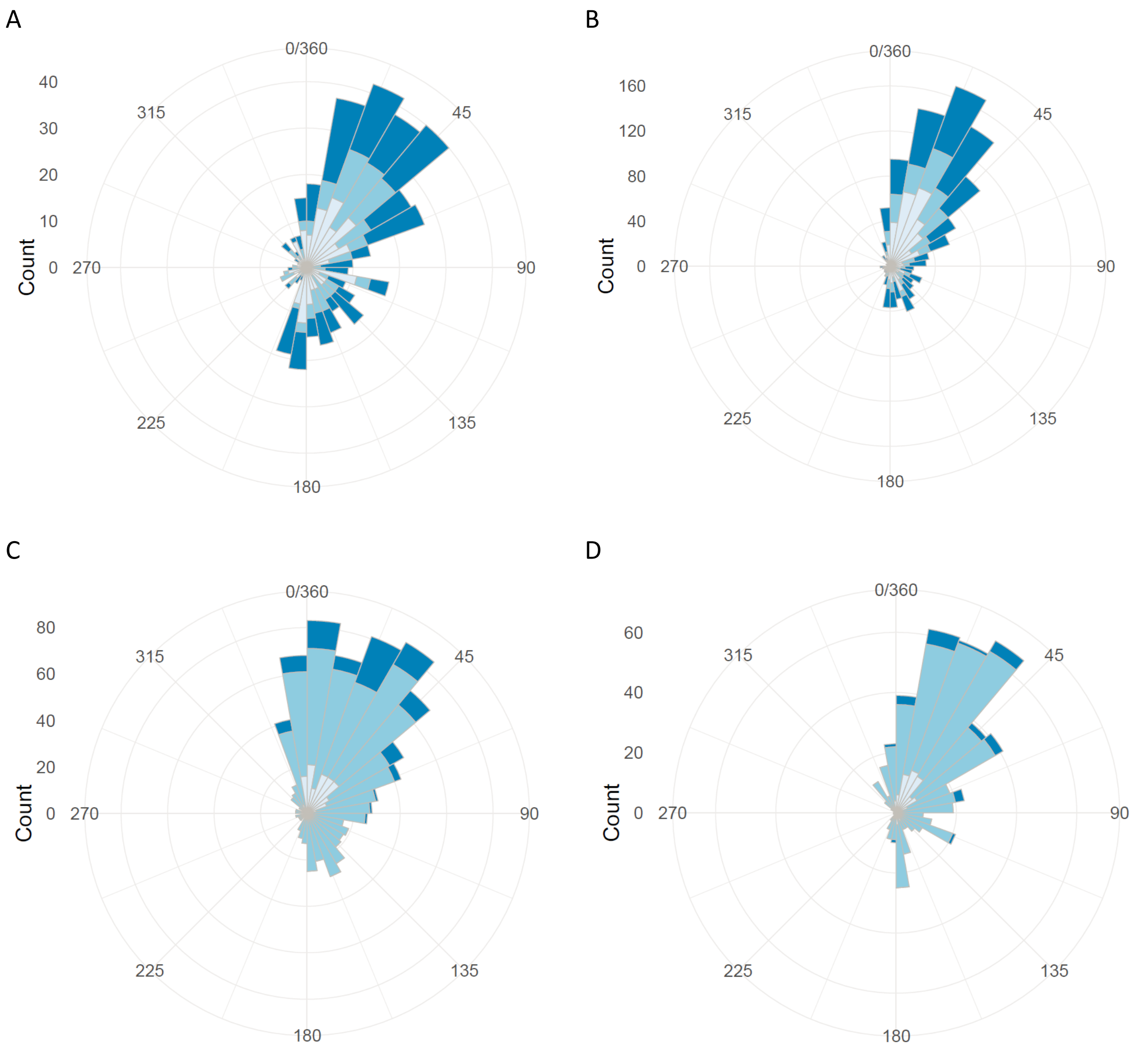

Figure 23 – Comparison of rose histograms for 10% of steepest slopes from the LiDAR dataset divided into three profile curvature (PC) classes (PC > 0.02 (Dark Blue); 0.02> PC > -0.02 (Light Blue); PC < -0.02 (Gray)): (A) Rosco Wolf (slopes > 17.4%); (B) Rosco-Main (slopes > 18.7%); (C) Lower Clare (slopes > 16.7%); and (D) Upper Clare (slopes > 23.0%). Straightness is taken as a proxy, in combination with grade, indicating a relic dune slip face. The prevalence of straighter slopes increasing with increasing slope was anticipated, however, the high proportion of straight slopes within the Lower Clare sub-unit (C) is somewhat surprising. This may be another indicator of a bi-modal wind regime.

A

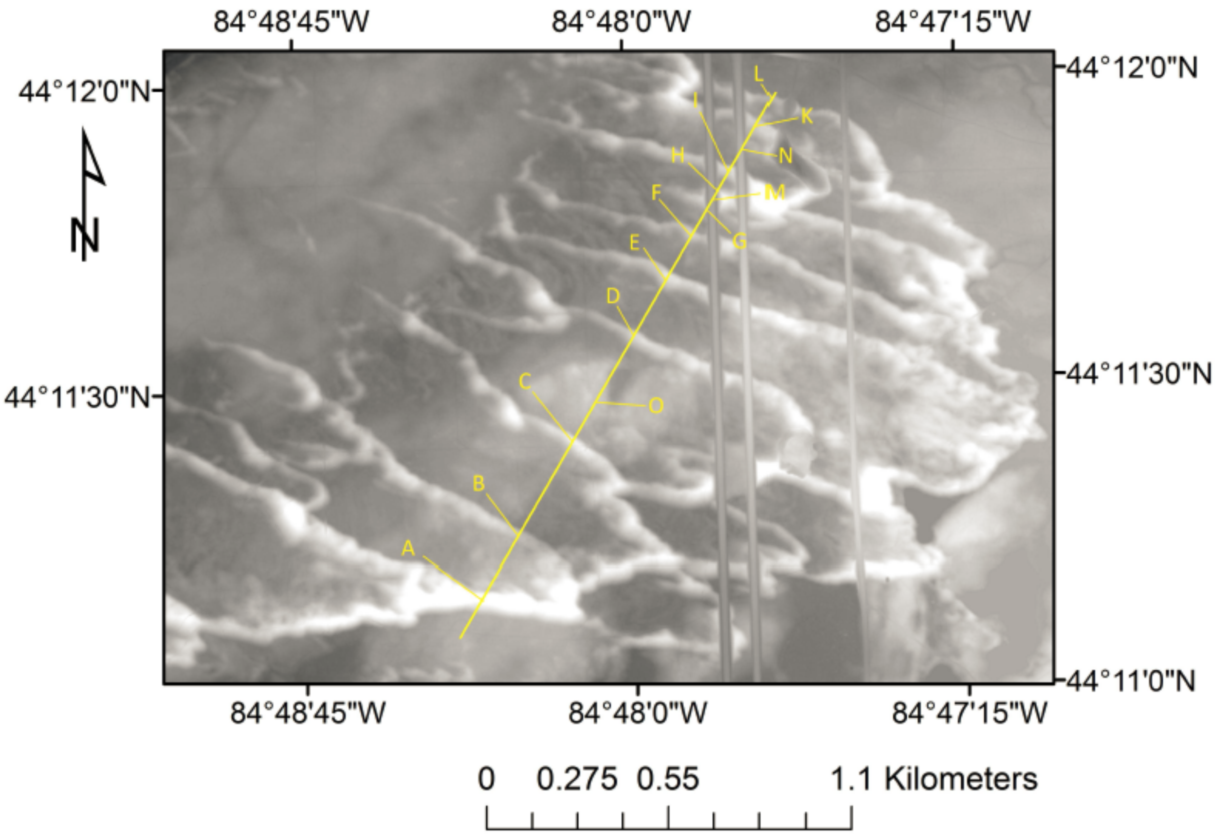

B

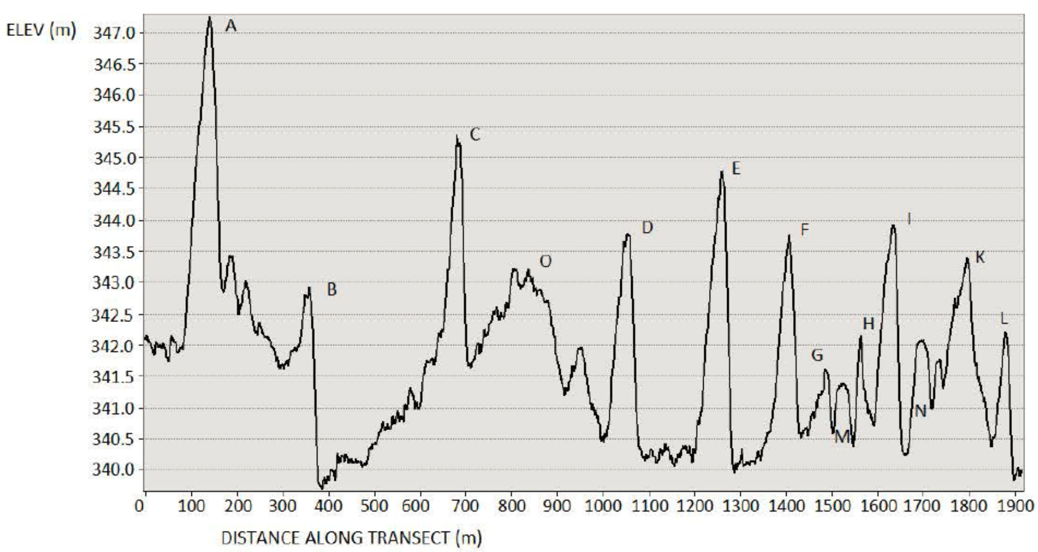

Figure 24 – (A) Shows the location of a transect running orthogonal to the crests of the elongated dunes of the RM complex. (B) An elevation profile along the transect from SW to NE. Corresponding locations between the image and the graph are marked.

A

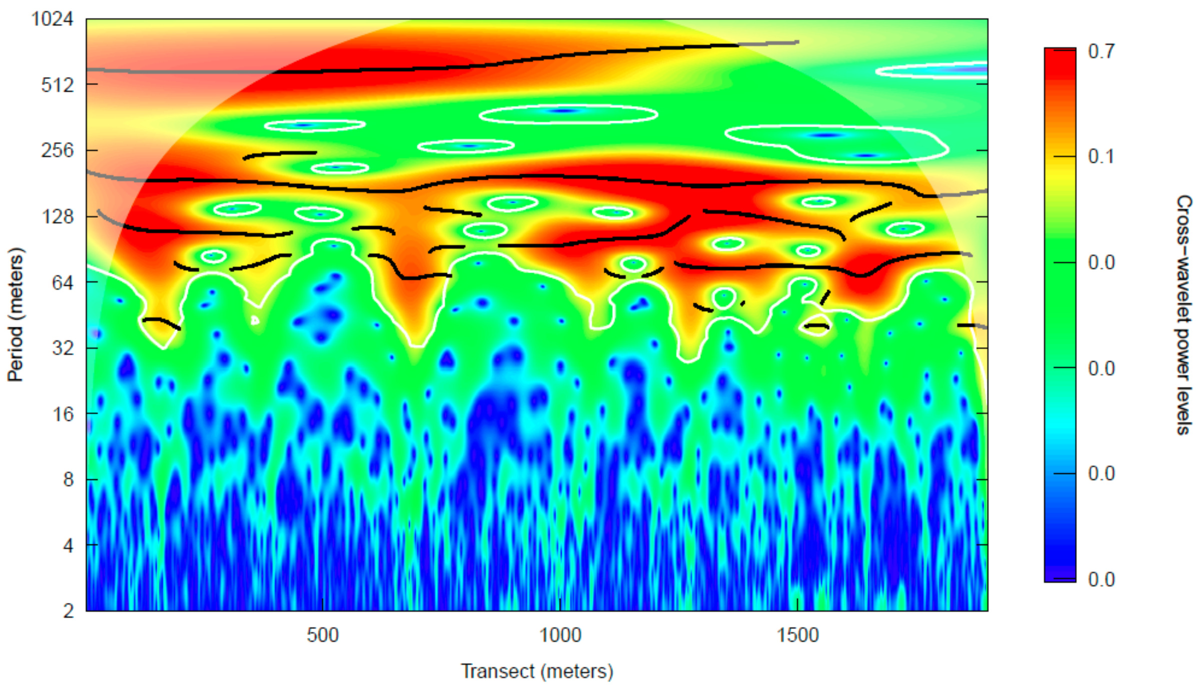

B

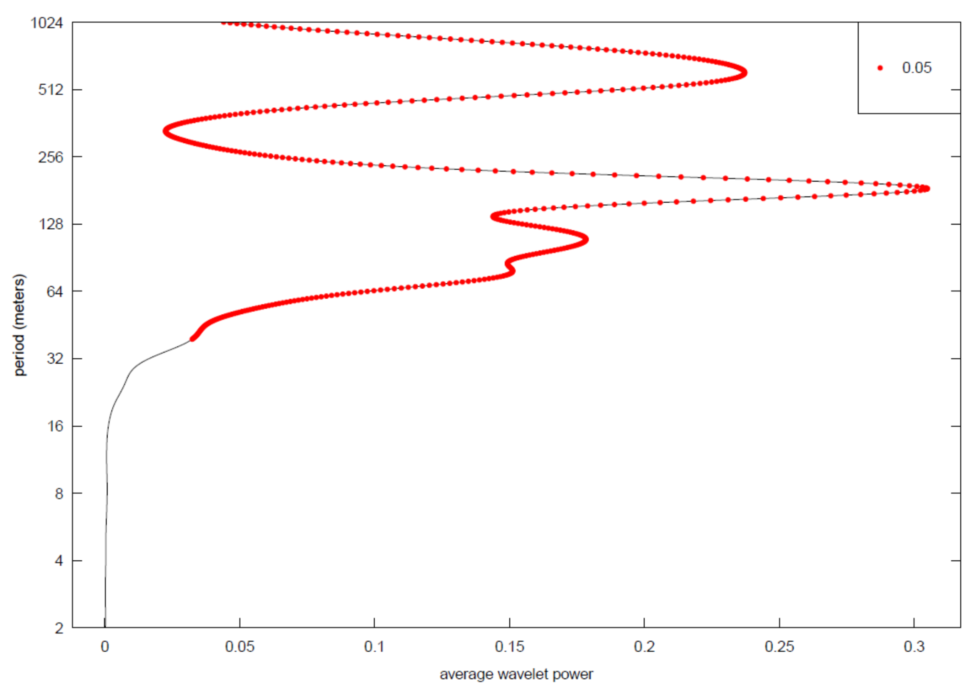

Figure 25 – (A) Univariate wavelet spectrum analysis of elevation along the transect in Plate A. The X-axis represents distance along the transect. The Y-axis represents crest to crest wavelengths. (B) Power to wavelength graph has peaks at ~70, 200 and 600 m.

A

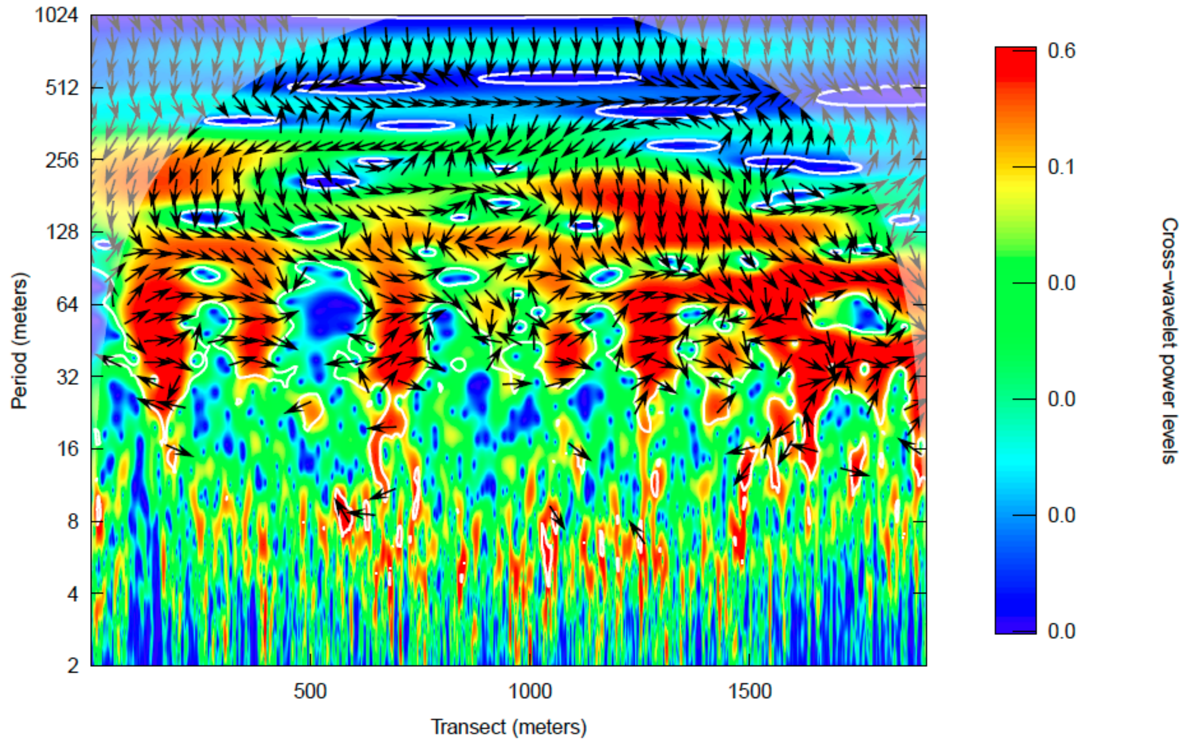

B

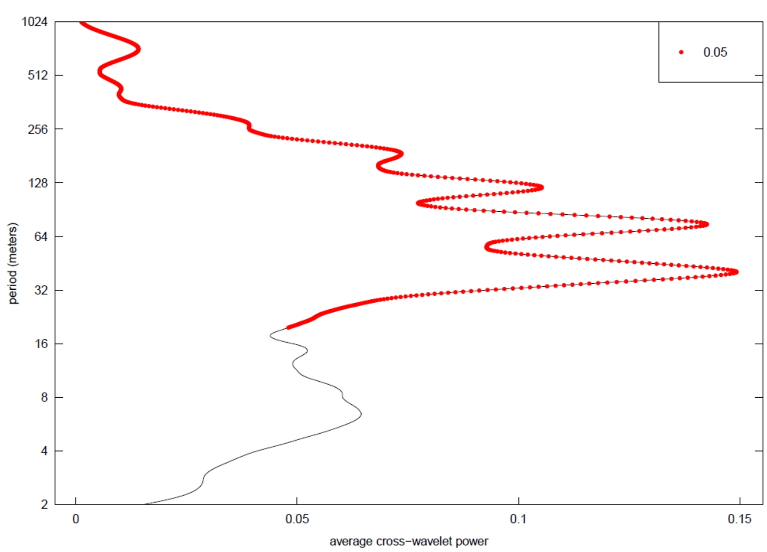

Figure 26 – (A) A heat map for the bivariate distance series for aspect over slope on the RM transect. Warmer colors represent wavelet coherence. The X-axis represents locations along the transect. The Y-axis represents correlation wavelengths. Arrow direction indicates positive (to the right) or negative (to the left) correlation. Up or down indicates a trailing or leading phase relationship. (B) Power to wavelength graph shows that the average cross-wavelet power has significant peaks at wavelengths of ~40 m, 80 m and 120 m.

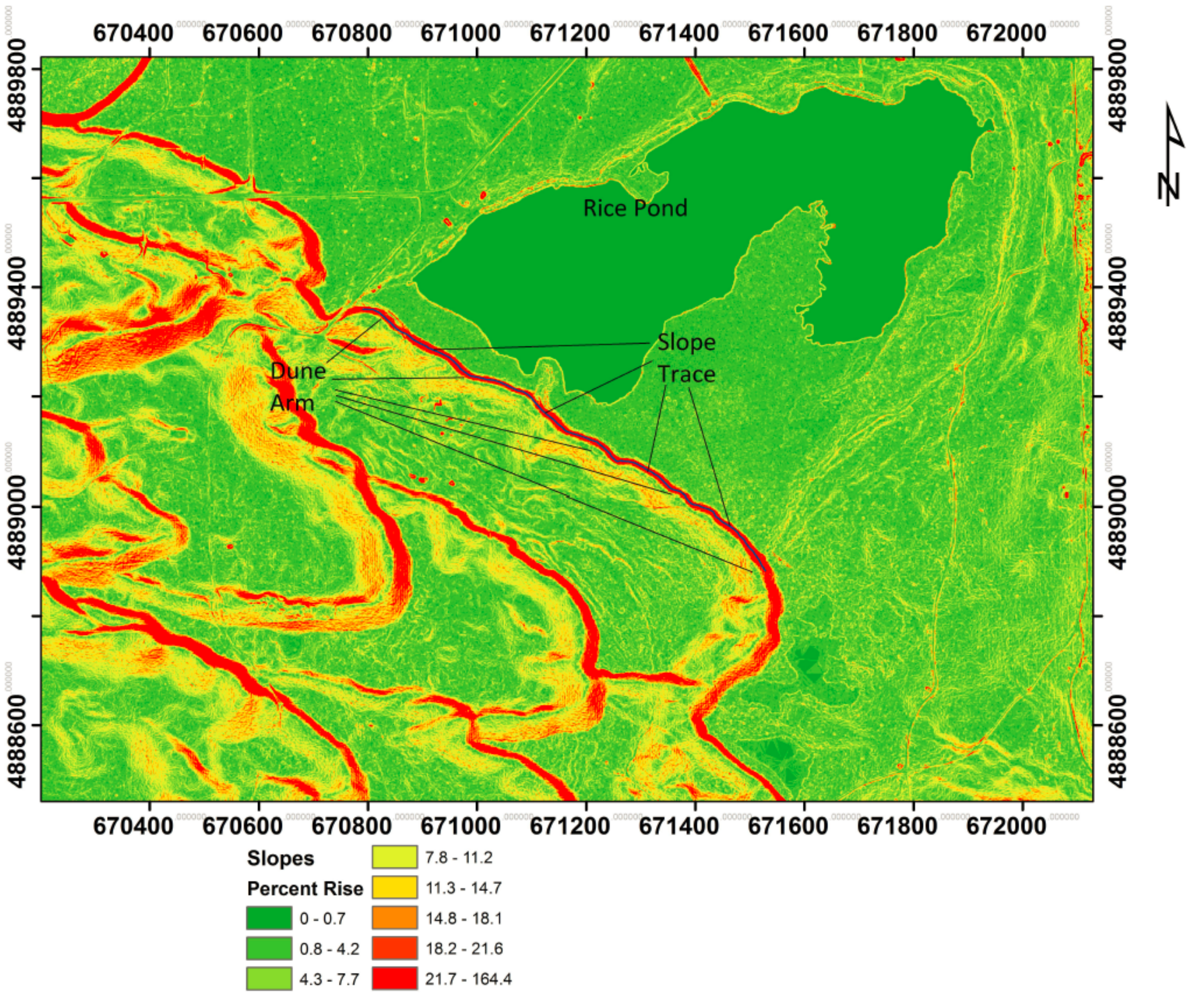

Figure 27 – The location of a 900 m long slope trace constructed along the steepest slope of a dune arm of the Clare Dune Field is shown. Aspect and profile curvature were sampled along the trace to the limit of resolution for the data set. Coordinates are UTM Zone 16N eastings and northings.

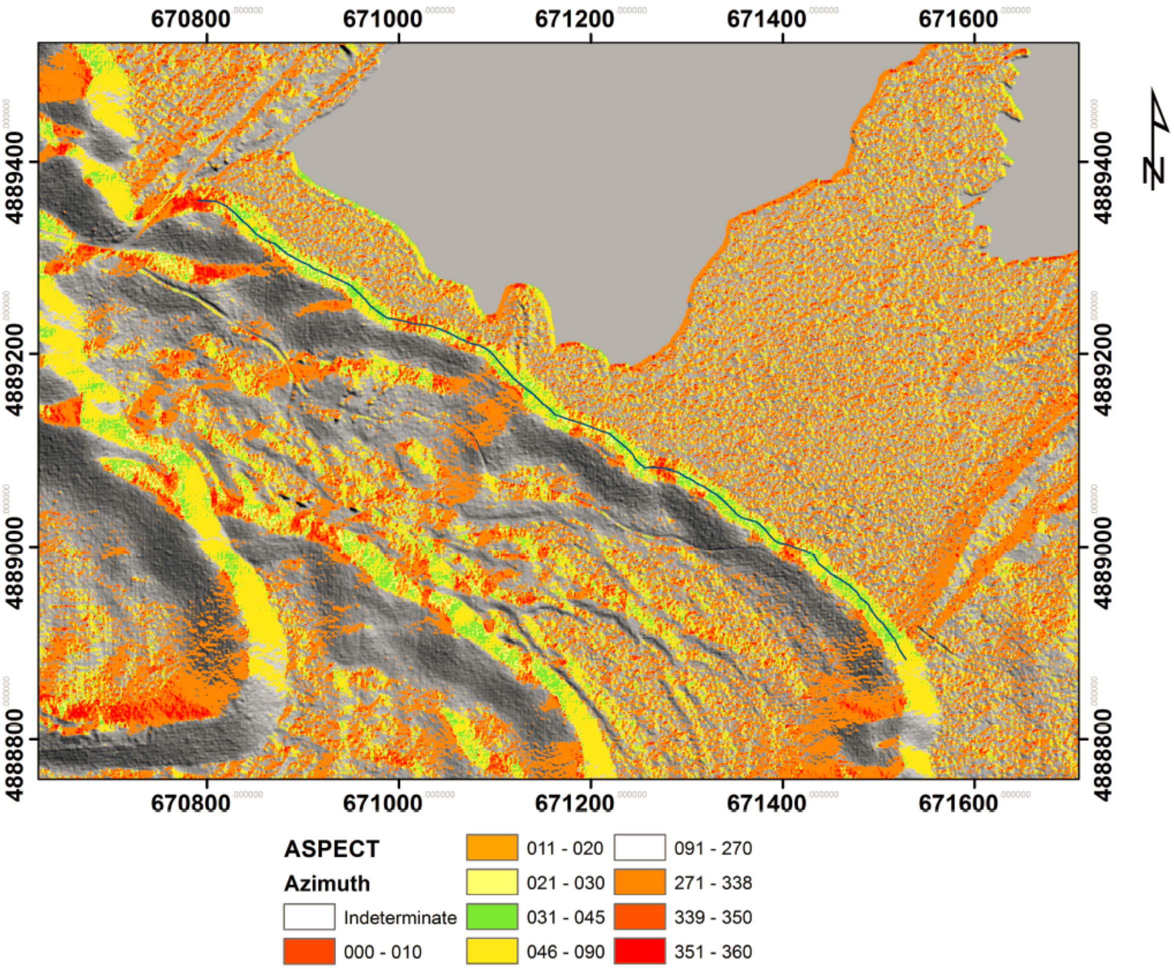

Figure 28 – Aspect change along NE face of the dune arm of Figure 24. Aspect along the trace varies from 350 to 074 along the trace.

A

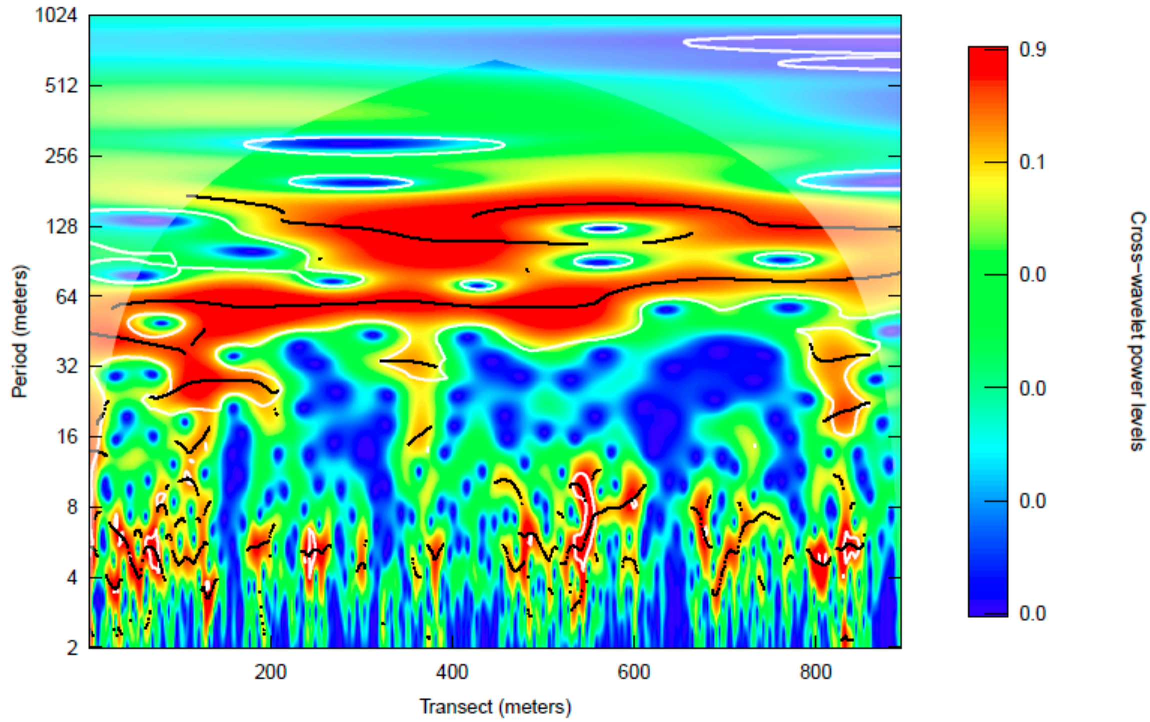

B

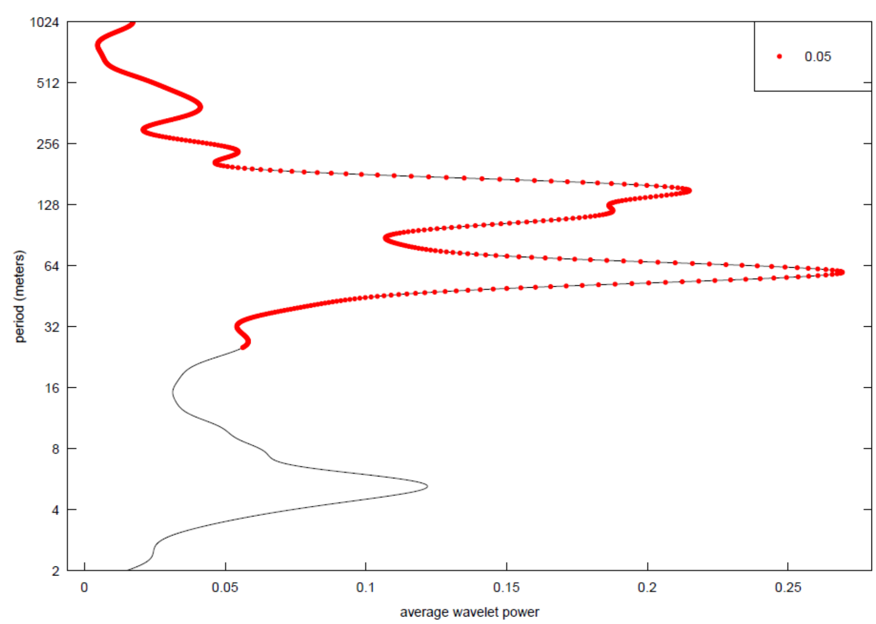

Figure 29 – (A) Depicts aspect wavelet power spectrum over the trace on the slope face for the dune of Figure 24. (B) Is the power graph for A. Statistically significant wavelengths of 64 m and just over 128 m are detected. The 64 m period extends the length of the trace. A 5 m signal is also present.

A

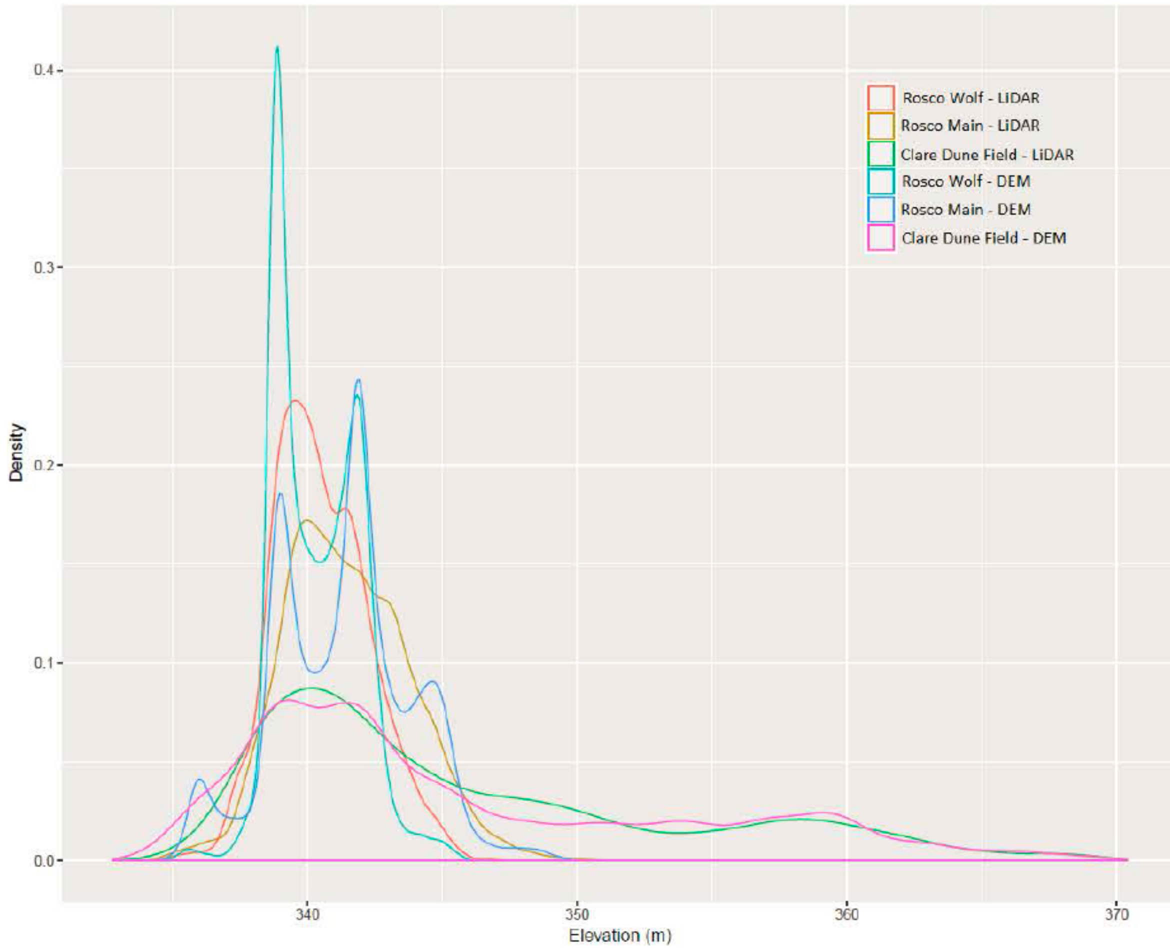

Figure 30 – (A) Is a comparison of elevation density within the dune polygons by field as derived from the LiDAR and DEM datasets. Bimodal elevation distributions are observed for Rosco Wolf and Rosco Main but not the Clare field from the DEM dataset. (B) Is a scatterplot of elevations within DEM dune polygons for Rosco Main against UTM eastings.

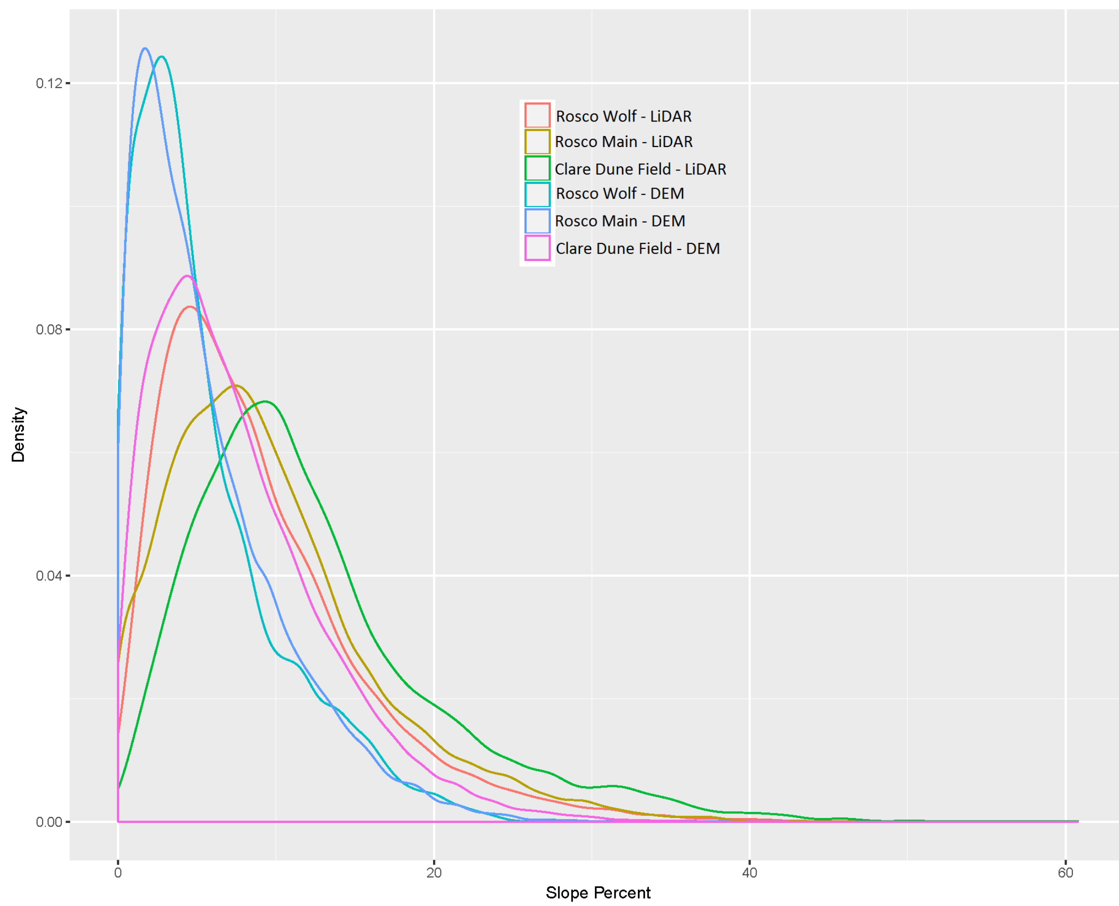

Figure 31 – Density function distributions for slopes derived using DEM and LiDAR dataset polygons for Rosco Wolf, Rosco Main and Clare Dune Field. The use of LiDAR data resulted in a distinct shift in peak density favoring steeper slopes for the Rosco Wolf and Rosco Main fields. However, this shift was far less pronounced for the Clare Dune Field than for Rosco Wolf and Rosco Main with the distribution for Clare derived using the DEM dataset resembling those derived from the LiDAR datasets and almost tracking the distribution for the Rosco Wolf Field.

A

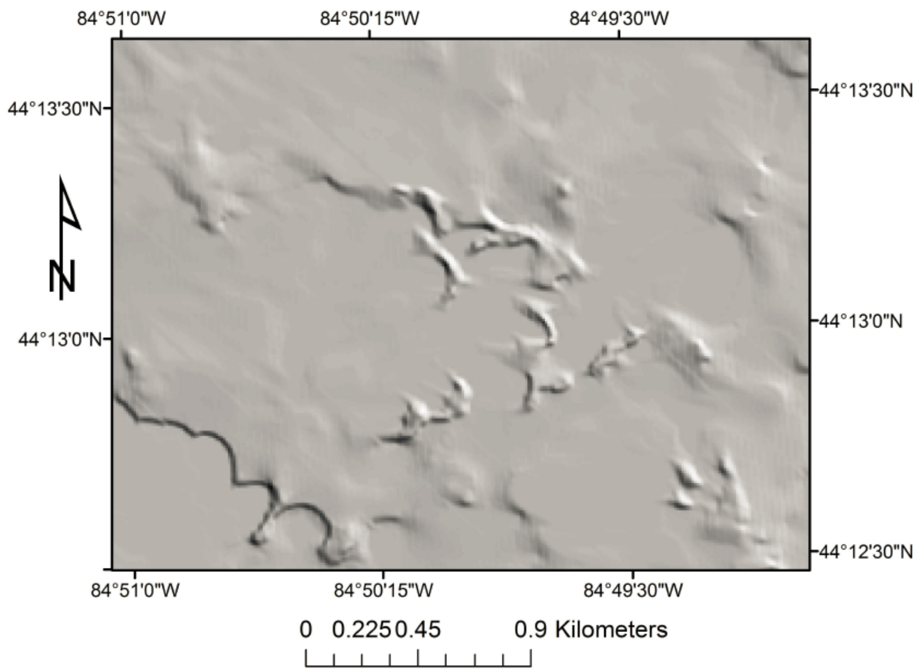

B

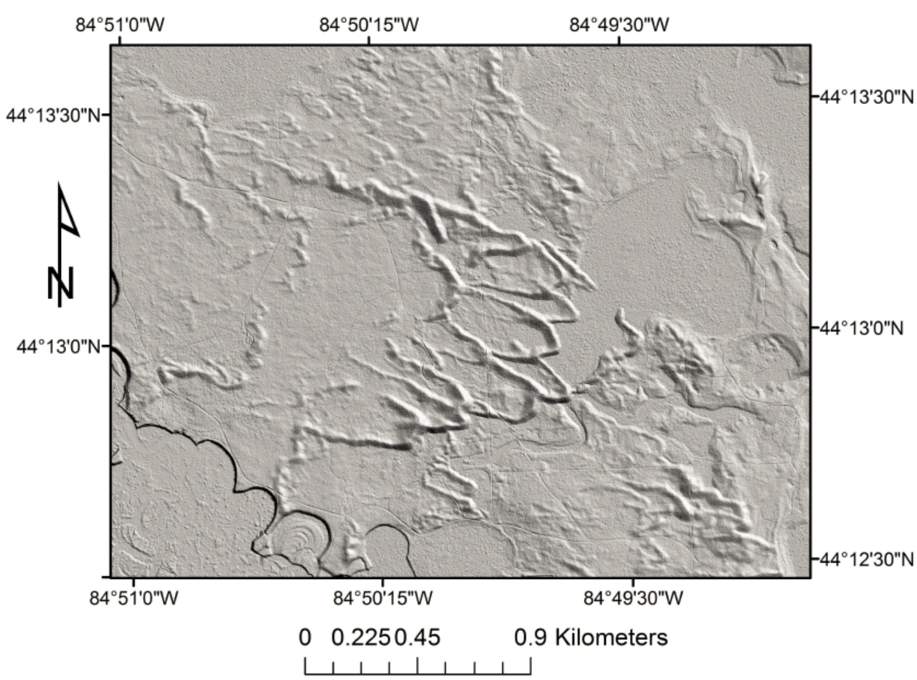

Figure 32 – A comparison of DEM (A) and LiDAR (B) datasets derived hillshades for RW complex. The increase in detail and extent of the field is marked for the LiDAR dataset. Compound parabolic forms, and all the northern dunes of the field are evident only in the finer resolution map. Stream burning appears to have been employed in generation of the DEM dataset.

A

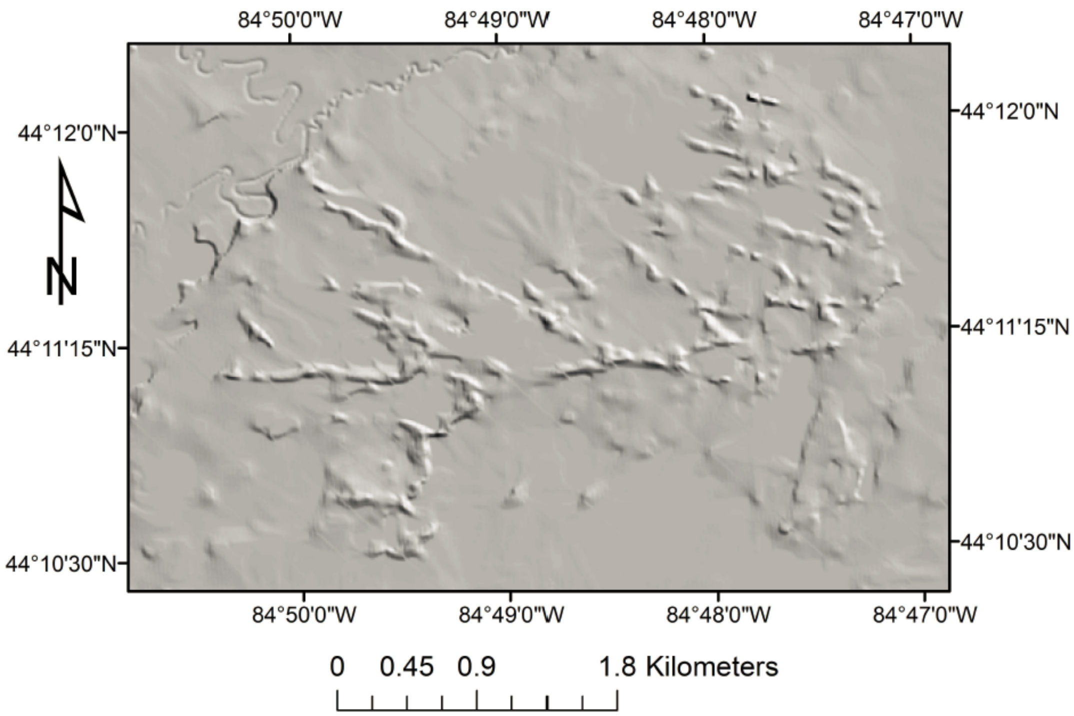

B

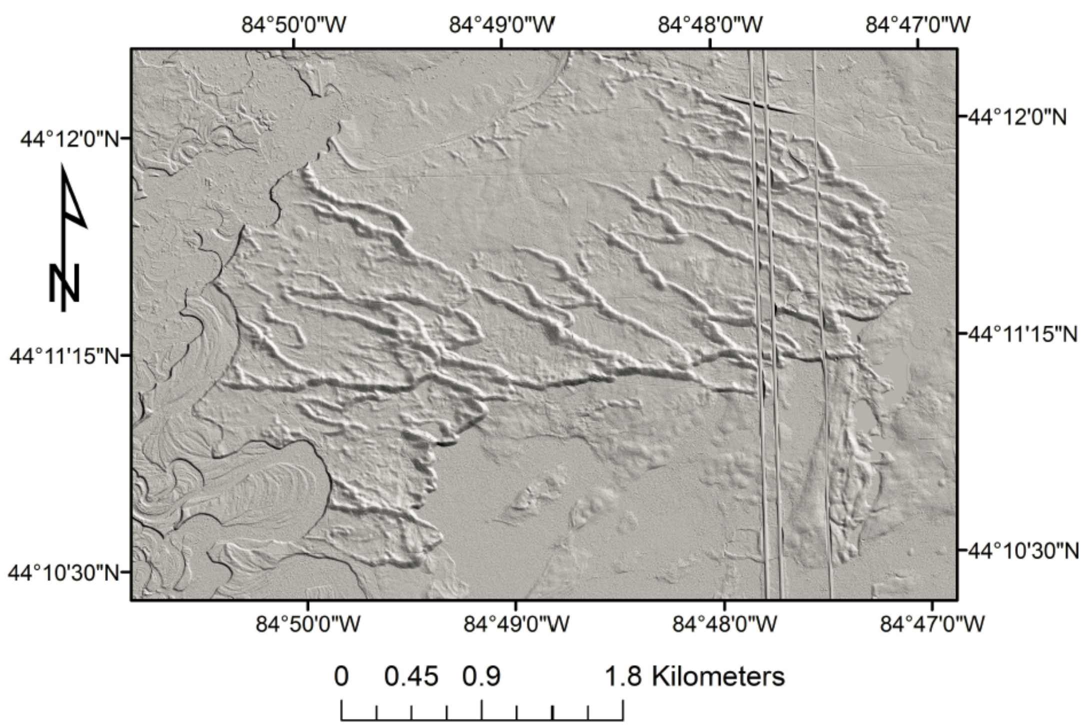

Figure 33 – Analytical hillshades of the Rosco Main Complex derived from (A) the DEM dataset and (B) the LiDAR dataset. Rayed features and elevated regions between dune arms seen in Plate (A) are gone in the visualization of the finer resolution dataset.

A

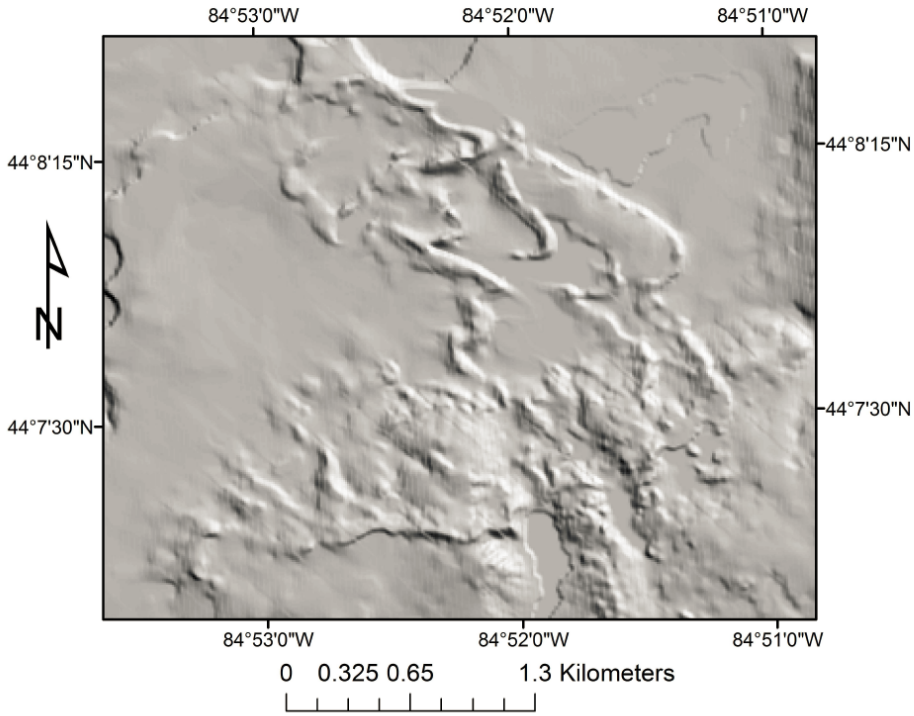

B

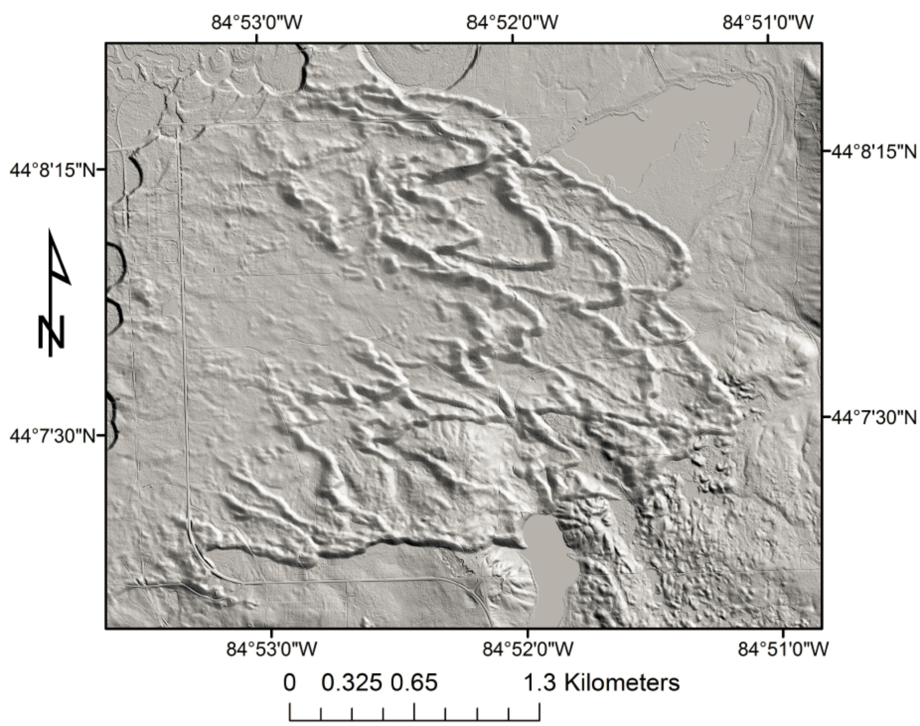

Figure 34 – (A) Hillshade from DEM dataset and (B) hillshade derived from LiDAR dataset for the CDF. The map derived from the DEM dataset was quite useful, though there was some tendency for inter-dune areas to be filled.

APPENDIX B. TABLES

TABLE 1. ARBOGAST ET AL. (2015) OSL DATES

LOCATION ID	DEPTH IN METERS	OPTICAL AGE +/- SD
H2_UPPER	1.0	11800 +/- 1300
H2_LOWER	5.1	11600 +/- 1100
H4_UPPER	1.0	9700 +/- 800
H4_LOWER	5.5	10100 +/- 1000
H6_UPPER	0.9	10800 +/- 900
H7_UPPER	1.0	11000 +/- 900
H8_UPPER	1.2	10200 +/- 800
H9_UPPER	1.2	10600 +/- 800
H10_UPPER	1.0	12400 +/- 1200
H10_LOWER	5.6	13000 +/- 1200

TABLE 2. TILES USED FOR DIGITAL ELEVATION MODELS

TILE IDENTIFIER	RESOLUTION	APPLICATION
USGS NED 1/3 arc-second n42w087 1 x 1 ArcGrid	1/3 ARC-SEC	DEM DATASET
USGS NED one meter x67y490 MI 16Co-Clare 2015 IMG 2018	1.0 METER	LIDAR DATASET
USGS NED one meter x67y489 MI 16Co-Clare 2015 IMG 2018	1.0 METER	LIDAR DATASET
USGS NED one meter x67y490 MI 16Co-Roscommon 2015 IMG 2018	1.0 METER	LIDAR DATASET
USGS NED one meter x67y490 MI 16Co-Missaukee 2015 IMG 2018	1.0 METER	LIDAR DATASET

TABLE 3. DUNE FIELD DESCRIPTIVE STATISTICS

		ROSCO WOLF	ROSCO MAIN	CLARE
DEM				
	Area of Dunes (m^2)	481,914	1,416,713	1,892,601
	Elevation Range (m)	10.5	16.9	35.9
	Mean Elevation (m)	340.3	341.4	345.7
	10^{th} Percentile Elev (m)	338.7	338.7	337.7
	25^{th} Percentile Elev (m)	338.9	339.4	339.4
	Median Elevation (m)	340.1	341.6	342.5
	75^{th} Percentile Elev (m)	341.6	342.9	351.2
	90^{th} Percentile Elev (m)	342.2	344.7	359.0
	Mean Slope (%)	5.48	5.60	7.60
	Median Slope (%)	4.08	4.29	6.46
	75^{th} Percentile Slope (%)	7.65	7.95	10.56
	90^{th} Percentile Slope (%)	13.50	12.32	15.09
LIDAR				
	Area of Dunes (m^2)	1,031,540	2,966,069	1,907,712
	Elevation Range (m)	12.1	16.2	36.2
	Mean Elevation (m)	340.5	341.5	345.9
	10^{th} Percentile Elev (m)	338.5	338.7	338.2
	25^{th} Percentile Elev (m)	339.2	339.8	340.0
	Median Elevation (m)	340.3	341.3	343.1
	75^{th} Percentile Elev (m)	341.7	343.1	350.0
	90^{th} Percentile Elev (m)	342.9	344.6	358.6
	Mean Slope (%)	8.92	9.64	12.35
	Median Slope (%)	7.42	8.41	10.58
	75^{th} Percentile Slope (%)	11.93	12.86	15.75
	90^{th} Percentile Slope (%)	17.35	18.74	22.98
	Mean Relief (m)	3.1	3.5	4.3
	Stnd. Dev. (95% Conf)	0.4	0.5	0.7
	Samples	22	43	37
	Max. Relief (m)	6.5	9.5	10.4
	Relief for the RW-Complex measured only for dunes south of ridge			

TABLE 4. SPATIAL PATTERN AND ORIENTATION ANGLES FOR CRESTS.

	Rosco Wolf	Rosco Main	Clare
Segment Lengths			
Total Length (m)	16,824	27,873	25,780
Mean Length (m)	16.3	26.2	18.5
25^{th} Percentile (m)	11.8	19.7	13.2
50^{th} Percentile (m)	15.1	25.6	17.5
75^{th} Percentile (m)	19.7	32.4	22.6
Orientations (degrees)			
Mean	102.2	117.5	104.0
25^{th} Percentile	42.5	88.6	39.8
50^{th} Percentile	123.6	142.2	127.4
75^{th} Percentile	153.4	159.8	154.8
Circular Variance (0-1)	0.45	0.38	0.47